Ring-laser tests of fundamental physics and geophysics

G E Stedman†

Department of Physics and Astronomy, University of Canterbury, Private Bag 4800, Christchurch, New Zealand

Abstract

HeNe ring-laser gyros are standard sensors in inertial guidance; mirror reflectances now reach 99.9999%. Present research instruments have an area of $\sim 1\ \mathrm{m}^2$, a passive quality factor of $\geqslant 10^{11}$, and a resolution of the frequency difference of counter-rotating optical beams approaching microhertz. In the Sagnac effect, this difference is proportional to the angular velocity. Present resolution is limited by thermal drifts in frequency pulling, itself reflecting mirror backscatter. The capability of ring lasers for measurements of geodesic interest, including seismometry and earth tides, and for detection of other sources of non-reciprocal refractive indices, including axions and CP violation, are discussed. In standard polarization geometries the observable is necessarily time-reversal odd. Scaling rules for dimensions, finesse etc summarizing past progress and suggesting future potential are given.

† E-mail address: g.stedman@phys.canterbury.ac.nz
www: http://www.phys.canterbury.ac.nz/~physges

Contents

1. Introduction

1.1. Rotation

Physical phenomena characteristic of rotation have a unique fascination at many levels. Elementary as well as advanced questions have an enduring attraction, as a few examples will illustrate. In mechanics, why is a telephone book relatively unstable when hand-spun about the axis associated with the *intermediate* moment of inertia (Hestenes 1990)? Why is the rate of nutation of a rotating plate removed by a factor of 2 from that of the plate rotation (Feynman 1989, Martinez 1992)? In optics, how could Michelson *et al* (1925) have measured the absolute value of the rotation rate of the Earth as a fringe *shift* in their mile long optical ring interferometer while it was fixed on the Earth when they could not check the zero of the fringe position by stopping the Earth's rotation (Telegdi 1990, Anderson *et al* 1994)? In electrodynamics, when a bar magnet is rotated, do the lines of magnetic flux rotate with it and could they so generate a Faraday emf in a suitable fixed circuit (Aono and Sugihara 1987)? If a merry-go-round with electric charge on the periphery is embedded in a changing axially symmetrical magnetic field, will the apparently unbalanced torque from the Lorentz force (and Faraday emf) make it rotate? If so, where does the mechanical angular momentum come from (Feynman *et al* 1968)? To what extent is it possible to rotate an atom—what are the available handles, and how strong are they (Woerdman *et al* 1992)? In relativity, why do the relativistic aspects of the composition rule for non-parallel Lorentz boosts induce a change in the classically expected spin–orbit coupling by a factor of 2, when the velocities involved are only fractions of c (Hirshfeld and Metzger 1986)? Since in a Machian context Foucault's emphasis on rotation with respect to 'absolute space' (see Tobin and Pippard 1994) is as meaningless as absolute linear motion, how can observations of a rotation, such as that of Michelson *et al* referred to above, which are confined to one frame of reference, be consistent with general relativity? How can the Lense–Thirring (frame-dragging) effect be an archetype of this observable, when such effects, expressing as they do the importance of some average of the rotation rates of distant and nearby matter, possibly be predicted from Mach's principle (Rindler 1972)?

Most of these are relevant to our topic in some way. Some low-frequency fluctuations in the direction of the Earth's rotation, for example, are partly due to the asymmetry of its moment of inertia ellipsoid (Goldstein 1950); the tidal effects of section 7 refer to half-day periodicities. But above all, the dramatic experiment of Michelson *et al* (1925) highlights the fact that it is possible to measure an absolute rotation rate by an experiment conducted entirely within the rotating frame. This experiment had been anticipated by Lodge in 1896 (Anderson *et al* 1994) as well as Michelson (1904), and unknowingly observed first by Harress (see section 2.4). Sagnac (1913) both predicted and observed (section 1.2) this effect, which then is properly named after him.

The demonstration of a related frequency splitting, rather than a phase shift, in a ring laser in the 1960s opened a new window for sensitivity. This has made the ring laser an accurate, durable and sensitive rotation-rate sensor, and has spawned a billion-dollar investment in ring-laser gyroscopes for inertial navigation. Commercial and military laboratories in the 1970s and 1980s made major improvements to supermirror manufacture, and reflectance losses have been reduced to one part per million (ppm) level. The geometry
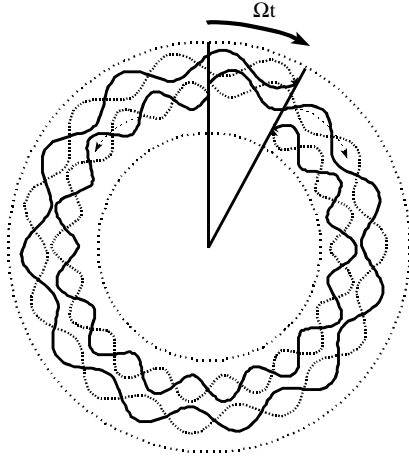
Figure 1. The Sagnac effect for two counterpropagating light beams in the same rotating cavity, here a circle for simplicity. The radial displacements of all beams are simply for clarity of separation. In the inertial frame, for an interferometer the corotating (counter-rotating) beam (outermost, innermost respectively) has a greater (lesser) phase shift on one circuit (section 1.2). In a laser (as depicted) these beams compensate for this by redshift (blueshift) (section 1.3); in this illustration each beam returns in phase, performing 12 full oscillations in going from the initial (12 o'clock) to final (1 o'clock) positions of a mirror. In the rotating frame, the difference frequency of laser beams is that of standing-wave antinodes (section 3.2).

constrains scientific applications normally to the measurement of a time-reversal violating parameter such as—but not only—the frame rotation rate.

1.2. Early history

Sagnac (1913) drew on purely classical ideas to predict the effect named after him. (Incidentally, the leading initial M often gratuitously added to G Sagnac in references is merely the customary Monsieur bestowed by *Comptes Rendus* on male authors.) Let a polygonal ring interferometer of area A (as defined by mirrors guiding two counterpropagating beams), rotate at an angular frequency Ω in an inertial frame. The round-trip (mirror-to-mirror) time difference between the two beams δt and their relative phase shift $\delta\phi$ is:

$$\delta t = \frac{4\boldsymbol{\Omega} \cdot \boldsymbol{A}}{v^2} \qquad \delta\phi = \frac{8\pi \boldsymbol{\Omega} \cdot \boldsymbol{A}}{\lambda v} \tag{1}$$

where v is the undragged velocity of the beam (for light, $v = c$). It is easiest to prove this for a circular interferometer (figure 1) with radius R and $A = \pi R^2$: the distance moved by a mirror during the transit time of the corotating beam $(+)$ and counter-rotating beam $(-)$ is $d_\pm = t_\pm \Omega R$ where $t_\pm = (P \pm d_\pm)/v$ and P is the perimeter of the ring (in this case $2\pi R$) so that $t_\pm = P/(v \mp \Omega R)$ and $\delta t = t_+ - t_-$, $\delta\phi = 2\pi v \delta t/\lambda$, which to first order in $\Omega R/v$ gives equation (1) for this case.

Again, for the special case of a circular ring, equation (1) can be written $\delta\phi = 4\pi(V/v)(P/\lambda)$ where V is the rotational speed of the periphery; the fact that $V \ll v$ especially for light is compensated by $P \gg \lambda$. It can also be written $\delta\phi = 4\pi(F/f)(P/\lambda)^2$ where $F = \Omega/2\pi$ and is the rotational frequency. The effect, therefore, is enhanced for small wavelengths and low particle speeds. Small wavelengths give bigger relative fringe

shifts for the same separation; lower speeds allow a greater separation of arrival times for a given rotation rate. This already indicates that matter interferometry, when possible, is likely to be of greater interest than optical interferometry. The recent explosive interest in atom optics, therefore, has some fascinating implications for Sagnac interferometry.

Sagnac's polygonal interferometer was mounted on a turntable. It had an area of 0.0860 m^2, a rotation rate of order 2 Hz, and the resulting fractional fringe shift 0.07 ± 0.01. Several interesting, if difficult, related experiments were also contemplated by Sagnac (1913, 1914) and it is of interest that he anticipated the use of the device on means of transport (ships in his case). Sagnac considered his experiment to be a direct manifestation of the ether, but this was quickly refuted (see Schleich and Scully 1984).

Harress's earlier observation was in fact a more accurate observation of the Sagnac effect (Anderson *et al* 1994). Moreover, it demonstrates, as first realized by Einstein (Zernike 1947), that the Sagnac fringe shift is unaffected by refraction (Post 1967). Harress was studying the effect of Fresnel drag in a glass. The area A appearing in equation (1) is the geometrical area, regardless of the presence of any homogeneous dielectric in the cavity, and hence the fringe shift is unaffected by the presence of dielectric in the cavity (see section 2.3).

The experiment of Michelson (1904) interestingly shows a variety of motivations. His discussion of the possibility of measurement of the one-way speed of light makes his paper an early contribution to a continuing debate (Anderson and Stedman 1992, 1994, Vetharaniam and Stedman 1993, Anderson *et al* 1997). In surprisingly modern style, Michelson (like Lodge) proposed an interferometer with an area of 1 km^2 to measure the Earth's rotation, another with an area of 100 km^2 to measure the rotation of the Earth around the Sun, and he even contemplated light beams traversing the equator in opposite directions as the ultimate terrestrial interferometric tool.

Michelson *et al* (1925) actually performed this 1 km^2 experiment (to be precise, 2010 × 1113 ft with a perimeter of 1.2 miles (1.9 km), giving an area of 0.21 km^2) in Clearing, Illinois, using 12-in diameter water pipes evacuated to 12 mm of mercury, as mentioned in their introduction. It successfully confirmed (with a result of 0.230 ± 0.005 fringe for the observed shift) his prediction of an interferometric fringe shift caused by the Earth's rotation in accordance with equation (1).

This experiment was motivated by the suggestion of Silberstein (1921) that relativistic or ether-theoretic frame dragging might affect the result, in that equation (1) might prove to be invalid for the action of the Earth's rotation: the ether might be entrained by the rotation of the Earth but not by that of a small laboratory mass.

Michelson embarked on his work with Gale in deference to the urgings of relativists such as Silberstein 'whose mathematical arguments he modestly professed he was unable to refute', and subsequently remarked that the experiment 'only shows that the earth rotates on its axis' (Lemon 1936, Shankland 1974). Its result agrees with Fresnel's old fixed ether theory, as well as the special and general theories of relativity.

For all that, Einstein also found the technique of the experiment of great interest, on account of one question posed in Michelson *et al*'s introduction: How does one calibrate a permanent bias? In a 1953 letter to Shankland (Shankland 1974), Einstein said: 'my admiration for Michelson's experiment is for the ingenious method to compare the location of the interference pattern with the location of the image of the light source. In this way he overcomes the difficulty that we are not able to change the direction of the earth's rotation'. Telegdi (1990) labelled this problem as 'the devil'. Before Michelson's work, Larmor taunted Lodge on his similar proposal: 'It is suggested that you are going to reverse the rotation of the earth in order to get an interference effect around your circuit'.

For each of the long and short ring interferometers two geometrical images of the source (independently of interference or rotation) are produced at the eyepiece from each sense of traverse. In practice these become separated as the result of (for example) the finite thickness of the beam splitter at the injection point. The interference pattern is found in the middle between these two images, with the zero-order fringe in the centre. These central fringes would be exactly halfway between the direct and reflected images if there were no effect due to the earth's rotation; Michelson measured the apparent relative displacement of the central fringes corrected by an amount equal to the difference in the mean positions of the two images of the two circuits.

Michelson's even more grandiose thought of an interferometer that encircled the Earth remained a pipedream until the last few decades. The Hafele–Keating experiment in which atomic clocks circumnavigated the Earth in commercial aircraft showed several relativistic effects. Hafele and Keating (1972) showed that their experiment demonstrated special relativistic time dilation and the twin paradox, also the general relativistic change of frequency with depth in a gravitational field. But the data produced also can be regarded as giving evidence for other (and related) relativistic effects, for example the accelerated clock hypothesis (Mainwaring and Stedman 1993). In particular, when the time dilation and gravitational field terms are taken into consideration it verifies (Schlegel 1973) the Sagnac time shift (equation (1)) as a direction-dependent change of synchronization of such a clock slowly transported around the Earth when compared to a clock at rest on (the rotating) Earth; a clock circumnavigating the world in an eastwards (westwards) direction loses (gains, respectively) 207.4 ns from the Sagnac effect. This was rendered more precise by the work of Allan *et al* (1985) who used a set of GPS satellites, whose timing was consistent to 2 parts in 10^{15}, to measure this Sagnac effect to an accuracy of 5 ns or 2% over the largest ring area yet achieved. Half of this error was attributable to the atomic clocks, and half to inaccuracies in the determination of the satellite ephemerides and other non-null time delays. The link between time delay and phase shift is proved in section 2.2, and an extension of this suggestion for the detection of gravitomagnetism is discussed in section 8.1.

1.3. Sagnac frequency splitting

Up till now only fringe shifts have been considered, and the optical frequency is taken as unchanged by rotation. However, even in a passive interferometer, the cavity modes have their frequencies modified as a result of the rotation, the phase shift being compensated by a wavelength change. This frequency splitting is derived from the original Sagnac effect. Within the circular model of section 1.2, the eigenmode requirement $f_\pm = N/t_\pm$ where N is an integer, and we have $f_\pm = N(v \mp \Omega R)/P$, $\delta f = f_+ - f_- = 2\Omega R/\lambda$ to first order. The corresponding equation for a general circuit has the form

$$\delta f = \frac{4\mathbf{A} \cdot \mathbf{\Omega}}{\lambda P} \tag{2}$$

where P is the optical path length and λ the wavelength in absence of rotation (Rosenthal 1962).

This increases the sensitivity of the device considerably in comparison with the Sagnac phase shift of equation (1); the large factors of c in the denominator are avoided. This frequency splitting can be revealed in a passive interferometer, and the ingenious Ezekiel–Balsamo technique has proved effective. Either passive or active frequency measurement has comparable intrinsic accuracy in principle; see Gea-Banacloche (1987), but the measurement of a frequency is more straightforward in an active device, since matching, injection and

feedback requirements are avoided. A laser amplifier within the cavity will allow both modes to oscillate independently. The conditions for self-oscillation require each phase shift of equation (1) to be compensated by a frequency shift so as to allow coherent amplification. The two counterpropagating lasing beams spontaneously shift in frquency so as to develop the splitting of equation (2), the corotating beam therefore becoming more red, and the counter-rotating beam more blue. The Sagnac frequency-splitting effect was first demonstrated for turntable experiments by Macek and Davies in a square ring with an area of 1 m^2 (see Heer 1984).

The Sagnac interferogram of the static device can be thought of as no longer stationary in an active device, but travelling past the detector as a whole. One may think of the counterpropagating waves as forming a standing wave of light or 'necklace', whose beads (say the antinodes) pass the mirrors and detectors at the rate δf (Schulz-duBois 1987). This is readily shown from the above. In the simplest circular case, $\delta\omega = 2\pi\,\delta f = [P/(\lambda/2)]\Omega$, so that the scale factor G, or ratio of mechanical to optical angular frequencies, is the number of half-wavelengths (or standing-wave antinodes) in the perimeter: $G = \delta\omega/\Omega = 2P/\lambda$. In the absence of a trigonometric projection factor, a complete revolution of the ring causes each antinode to pass the detector once. The presence of a trigonometric projection factor from the scalar product reduces this, as for a Foucault pendulum at low latitudes, in a manner which is not simply quantified in the necklace picture.

If a ring laser is scaled in size (as measured by a linear dimension, e.g. P) while retaining its shape and other properties, the Sagnac phase and time delay (equation (1)) and the Sagnac frequency splitting (equation (2)) both increase with P. The Sagnac phase scales as P^2, and the frequency splitting as P. This is the first and obvious reason why the use of as large a ring as possible is attractive; others are given later.

1.4. Sagnac effect for matter waves

As noted in section 1.2, slowing the particle speed (as for cold neutrons and atoms) enhances the Sagnac effect. The de Broglie relation may be used to write equation (1) as

$$\delta\phi = \frac{8\pi m\mathbf{\Omega}\cdot\mathbf{A}}{h}. \tag{3}$$

This in turn can be written for the case of a circular ring as $\delta\phi = 4\pi(V/c)(P/\lambda_c)$ where $\lambda_c = h/mc$ and is the Compton wavelength of the particle; as before V is the rotational speed of the periphery.

For a given rotation rate and interferometer geometry, then, the effect depends only on particle mass. Neutrons, and particularly atoms, have far greater mass than optical photons. Cooling the neutron before injection in a neutron interferometer has no direct benefit as far as the magnitude of the effect is concerned, but a neutron monochromator is nevertheless essential to tune the wavelength to be appropriate for Bragg reflection at the particle mirrors. Of many beautiful accounts of the capabilities of neutron interferometry, the account by Werner (1994) deserves special mention.

The fact that equation (3) involves Planck's constant has led to claims that matter interferometry is intrinsically quantum mechanical, while optical interferometry is intrinsically classical. The de Broglie relation is the quintessence of quantum mechanics. However, its relevance to equation (3) is to some extent a historical accident; a Newtonian believer in the particle nature of light might justifiably be perplexed by optical interference, as being a 'quantum', i.e. wave phenomenon. To some extent then it is a historical artefact to distinguish equations (1) and (3) as if one were 'classical' and the other 'quantum-mechanical'; after all, exactly the same observational effect is being described. Such

a distinction would have to make a fundamental distinction between the significance of experiments using particles with zero rest mass (as natural waves) from particles with non-zero rest mass (as natural particles). But this distinction itself is incompatible with the equivalence of all forms of mass for inertia and gravitation, and cannot be sustained within a unified theory which uses general relativity (Stedman 1986). Similarly, efforts to distinguish certain optical manifestations of Berry's phase or Josephson effects from gravity in superfluids as peculiarly quantum in character have not carried strong conviction.

Sagnac turntable-based experiments have been performed with Cooper pairs in superconducting interferometers (Zimmerman and Mercereau 1965) and with free electrons (Hasselbach and Nicklaus 1993).

The enormous potential of atomic interferometry discussed (for example) by Clauser (1988) is now beginning to be realized. A Sagnac effect for coherent beams of atoms was presented by Riehle *et al* (1991). The Sagnac effect of the Earth's rotation has been rendered visible in neutron interferometers (Werner *et al* 1979) and also in superfluid helium resonators (Avenel and Varoquaux 1996, Avenel *et al* 1997, Schwab *et al* 1977).

Gustavson *et al* (1997) report a Sagnac matter gyroscope using atomic de Broglie waves at microkelvin temperatures. They claim a short-term sensitivity of 2×10^{-8} rad s^{-1} Hz$^{-1/2}$, or 10^{-10} rad s^{-1} after $T = 10^4$ s. This is comparable to the sensitivity of 3×10^{-9} rad s^{-1} Hz$^{-1/2}$ corresponding to one existing large ring laser (see section 4 for the relevant theory and section 5.2 for details of that ring laser).

Lenef *et al* (1997) also describe an atom gyroscope, which reached 1% agreement with the predicted Sagnac effect in rotation rates up to $2\Omega_E$. These authors quote a measured sensitivity of 3×10^{-7} rad s^{-1} Hz$^{-1/2}$, agreeing with the atomic counterpart of equation (27) to within 9%.

Although the growth here is explosive and fascinating, it has not rendered optical methods obsolete. Neutron interferometers demand a nearby reactor. Low temperatures are vital for the superfluid systems, and altogether extremely low temperatures and highly sophisticated cooling and trapping conditions are mandatory for atom interferometers. The detection of the Earth's rotation is possible also with optical interferometers of similar overall dimensions (for example Spielman *et al* 1990; see section 1.5). Optical interferometers, even of the passive sort discussed in section 1.2, are not thereby obsolete; the use of multiple turns of optical fibre enhances the effective area.

1.5. Inertial guidance applications

Sagnac anticipated the navigational use of three mutually perpendicular interferometers. He postulated in Sagnac (1914) the use of three such rings, with areas of tens of square metres, in order to measure the roll, pitch and yaw of ships. Contrary to the supposed custom in research, the area of ring-laser performance has already proved its commercial and (unfortunately) its military usefulness; it is their scientific potential which has been neglected.

The history of the subsequent enormous development of this system for inertial guidance (Heer 1984, Chow *et al* 1985, Stedman 1985) is still obscured by commercial and military secrecy, and this account is only partially constructed from the existing, publicly available, information. Considerable emphasis remains on helium–neon lasers, which provide more power, better coherence, better beam quality, freedom from dielectric imperfections, lower price, more easily available and better quality accessories and components such as supermirrors and fuller overall development than obvious alternatives (Hecht 1992). In this review we shall concern ourselves almost exclusively with the helium–neon ring laser.

However, the fibre-optic gyro, even though normally a phase-shift measurement device, has dominated certain applications, including gyroscopic ones (Kim *et al* 1994). Honeywell (which had 1994 sales of $6.1 billion) has been a key player in the inertial guidance market; its ring-laser gyro systems and fibre-optic gyro systems (nowadays integrated with other approaches and strategies such as GPS) have revolutionized inertial navigation, and are now standard equipment. Honeywell certified the first ring-laser gyro (RLG)-based strapdown inertial system in 1981, and since then has supplied 19 000 RLG-based strapdown inertial reference systems to the commercial aviation industry. Specifications of their MCU4 unit include an attitude accuracy of $0.05°$ and heading accuracy of $0.4°$. Honeywell has produced nearly 100 000 ring-laser gyros and more than 6000 optical-gyro-based military navigation systems for commercial and military aircraft, missiles and land vehicles. The military applications are still major. As one example only, in the wake of the USA Gulf War operation (Desert Storm), Honeywell with McDonnell-Douglas has secured a $62 million contract to provide 'low-cost' Inertial Measurement Units (three-axis guidance packages including three ring-laser gyros, the package being 175 cm^3 and weighing 0.64 kg) for converting existing unguided free-falling bombs into precision-guided munitions, under the Joint Direct Attack Munition programme; sales are projected to reach 20 000 by 2002, and 100 000 by 2009. Another such contract relates to Stinger missile guidance.

Sperry (where Macek and Davies first demonstrated the ring laser in the early 1960s) is another company which also intensively developed the ring-laser gyro. Among current products we mention the MK39 unit for shipboard attitude measurement and the MK49 unit for inertial navigation†. These were the basis of the WSN-7 ring-laser gyro Shipboard Inertial Navigation System purchased by the US Navy in 1995. The specifications of the MK49 include: heading performance $±4.0$ arc min and stability 50 μrad s^{-1}, rms, roll and pitch performance $±1.75$ arc min rms, and stability of 15 μrad s^{-1}. Positional accuracy, determined by GPS and linear accelerometers, is to the performance of GPS, or (if GPS is lost) to 0.5 km h^{-1} in 4 h.

Raytheon were heavily involved in, for example, the production of ring-laser gyros for Patriot missiles, popularly celebrated for their role in Israeli and Saudi defence in the Gulf War. The use of a non-planar gyro in one Raytheon model has interest in that the non-planarity splits beams of opposite sense of circular polarization, and the availability of four frequencies allows certain biases to be eliminated on taking appropriate differences (Statz *et al* 1985). Litton Sys. has bought out the Raytheon gyro development operation. As with Honeywell, one strong market is in fighter aircraft. Honeywell's H-423 ring-laser gyro-based Inertial Navigation System (INS) and the Litton LTN-92 ring-laser gyro based Inertial Reference Unit feature in relation to (for example) an F-15E Eagle. Though not as accurate as GPS (after an 1100 km sortie the INS is usually no more than 1 km out of register), it is independent of outside electronic jamming or other interference.

Ring-laser-based guidance systems are being developed by Toyota for example (in its Mark-II navigation system) as the basis of an automobile navigation system of the future, with the intention of making road maps obsolete (Kersey and Burns 1993).

Fibre-optic gyros have proved useful in a very wide variety of fields, such as oil prospecting. The Sagnac signal generated by the Earth's rotation is sensitive to the orientation of the device, and if the orientation is defined by the ring laser being totally embedded in an oil-well drill bit, the alignment of exploratory bores can be monitored deep underground. Thanks to advanced technological tricks including dither, such small gyros monitor the projection of the Earth's rotation to an accuracy of $0.01° h^{-1}$ or 5×10^{-8} rad s^{-1},

† See http://www.sperry-marine.com/pages/products_nf.htm

a fraction 7×10^{-4} of the Earth's rotation rate Ω_E (Kim and Shaw 1986).

Incidentally, the effect of the Earth's rotation on small to medium ring-laser systems has been routine in the aviation gyro industry for 15 years, although largely undocumented (as unremarkable); it has been noted as a bias in a variety of ring-laser or ring-interferometer set-ups (Aronowitz 1971, Bilger and Stowell 1977, Spielman *et al* 1990, Bretenaker *et al* 1993a).

1.6. Mirror manufacture

Mirror quality may be specified by the power reflectance R. One key result of the commercial and military development has been a vast improvement in mirror quality, 'five-9s quality' ($R = 99.999\%$) and now even 'six-9s' (1 ppm total loss of power in reflection) characterizing the 'supermirrors' now available. In improving the quality factor of the cavity, the operation with regard to lock-in, frequency resolution, signal/noise, backscatter-induced pulling of the frequency etc is improved at least in proportion. Therefore, the manufacture of mirrors has become a critically important art, and largely defines the gyro performance. The chief source of imperfections are scattering at the many surfaces and absorption in the mirror materials. Transmission, vital for the function of any laser for at least one mirror, also reduces reflectance.

This has made totally non-magnetic thin-film dielectric mirrors of major importance, although magnetic mirrors play an important part in certain applications, partly through their electronically controllable bias (for example Andrews and King 1996).

Such mirrors involve say 22 pairs of quarter-wavelength layers of materials such as SiO_2 and either TiO_2 or TaO_5 with differing refractive indices. These are sequentially evaporated onto a well-prepared substrate (often fused silica or Zerodur) by ion deposition. A surface half-wavelength coating of SiO_2 helps protect the supermirror, which is then surprisingly robust. It is critically important that the substrate be ultrasmooth, since any 'hill' will make its presence felt throughout the superimposed layers and so limit the mirror finesse regardless of the reflectivity of a small section. With controlled ion bombardment by argon and nitrogen for example, substrate surfaces can be prepared with an rms roughness well below the molecular diameter; one supermirror in our possession was measured to have an 'rms surface roughness' of 0.016 Å (Bilger *et al* 1994). Obviously, the ion deposition process is also quite critically important. The uniformity of thickness of each layer is not so critical (and is specified only to a few per cent), since when the absorption of the bulk material and non-specular reflection at the many interfaces is minimized, what light is not reflected at one layer can survive to be reflected at a deeper point. The bulk absorption of the coating material is critical, and methods of surface preparation, and above all the adjustment of the characteristics of the interfaces between the materials by such things as controlled interpenetration and the judicious use of chemical reagents, are areas where state-of-the-art technology is not shared publicly. However, the standard Fresnel relations suffice to explain many important properties.

An example of the commercial pressures is given in the award by a USA jury in 1993 of US\$1.2 billion in damages in a lawsuit, *Litton Systems v. Honeywell Inc.*, in connection with the ion-beam mirror-coating technology. In March 1996 this jury verdict was reversed by a judge because, the patent being declared invalid, the licence agreement became unenforceable because 'there is a total absence of evidence that the mirror manufacturer ever actually used any Litton trade secret in manufacturing a mirror for Honeywell. The mere existence of an agreement not to use plaintiff's trade secrets does not relieve plaintiff of the burden to prove that the defendant accused of appropriating the trade secrets did in

fact make use of them, and that the use was prohibited by the agreement'. A mere recitation that the licence also covers know-how and was not sufficient to save the agreement.

Present commercial methods could still be improved; we are still several orders of magnitude from the limits set by the intrinsic absorption of the mirror-coating materials (Bilger *et al* 1994). Commercial development has had a habit of finding ingenious ways to push such limits, for example in dramatically lowering the losses and minimizing other defects of fibre-optic cables many orders of magnitude towards fundamental limits. It is therefore reasonable to speculate about 'parts per billion' and not merely 'parts per million' supermirrors. Development work at the present time appears to be initiating progress towards this ultimate limit.

Derived parameters from the mirror reflectance R include the finesse $F = 2\pi/(1 - R^4)$ and the (cavity-length dependent) quality factor $Q = PF/\lambda$. (As with a Fabry–Perot, these define frequency resolution etc; for example, the cavity decay time is $\tau = Q/(2\pi f_0)$. P is the perimeter, and f_0 the laser frequency.) The finesse of an 'n-nines' mirror is therefore 1.7×10^n, and a HeNe laser built from such will have a quality factor $\sim 2.7 \times 10^{n+6}P$.

The method used to measure the quality factor in our work has been a simple ringdown measurement, namely to shorten rapidly (in microseconds) the radio-frequency excitation of the lasing plasma and study the exponential decay of the light. In our earlier work we fitted the ringing response curve of the cavity as an externally injected laser frequency drifted through the cavity resonance (Li *et al* 1991). This method was very successful, but was more complicated in practice. A careful analysis of such methods is given by Poirson *et al* (1996).

Another mirror parameter of interest in ring-laser applications is that of the anisotropy in phase change on reflection, or 'birefringence'. Even at normal incidence for linear lasers, this affects the performance of a laser (Winkler *et al* 1994, Jacob *et al* 1995). In a ring laser birefringence can play an all-important role in the transition behaviour and scale as the polarization of the ring eigenmodes changes from linear to circular as the ring becomes aplanar (Martin 1984, Bilger *et al* 1990). Its magnitude can be minimized in manufacture through adjusting the thickness of the top layer (Bilger *et al* 1990).

1.7. Some unusual interferometers and gyroscopes

Earth's rotation might be detected in principle by studying the associated Coriolis effects on atoms via induced optical activity (Silverman 1992, Stedman 1990a), or magnetic effects (Papini 1967, Ljubičić and Logan 1992). It has been seen in NMR splittings of atomic mercury eigenstates (Venema *et al* 1992, Mashhoon 1995). As noted above the Sagnac effect can be viewed as the Coriolis effect on photons or de Broglie particles.

A large ring laser such as G (see section 5.5) would represent a major and decisive step on the way towards realizing old proposals for measuring various effects at the 'general relativistic' level of $10^{-10}\Omega_E$ using ring lasers. This includes the ideas of Scully *et al* (1981) for an Earthbound ring either locked onto the stars to sense the Lense–Thirring frame dragging from the Earth's rotation, or alternatively, if rotating with the Earth, and at a similar level of precision, to pin down more precisely than the available (astrometric) experiments the preferred frame parameter α of the parametrized post-Newtonian (PPN, local Lorentz- and metric-preserving) alternative family of theories of gravity.

Ranganathan (1992) considered a folded geometry for a light beam in two-mirror resonators as a rotation sensor. Forder (1986) has investigated the use of a loop of transmission line as a system for investigating the interaction of electromagnetic and gravitational fields. An orbiting ring laser has been proposed for gravitational wave detection

(Chaboyer and Henriksen 1988). Percival and Strunz (1997) suggest the use of a matter interferometer to explore Planck-scale phenomena in the laboratory, in particular space-time fluctuations; it is necessary in their proposal to use particles of finite rest mass, so that proper time changes on the interferometer path. Silverman (1991) suggests a search for an Aharonov–Bohm effect for photons from the virtual excitations of QED (see section 9.3).

1.8. Scope of this review

Many specific matters which have been the subject of considerable and often intense research in ring lasers since the 1970s, and which are discussed in standard works (e.g. Aronowitz and Collins 1970, Aronowitz 1971, Haus *et al* 1985, Chow *et al* 1985, Statz *et al* 1985, Wilkinson 1987), are not reviewed here; for example, we do not discuss fibre-optic gyros or pulsed lasers.

The sections immediately following give some background to those particular effects which could be particularly important in limiting the potential application of large ring lasers as a tool for fundamental studies, with priorities and emphases being determined by experience with one large ring (C-I, section 5.2). The gyroscopic use is still a major one, for example in discussing the potential of large rings to contribute to the measurement of seismic effects and of lunar tides (see section 7), but others are discussed in sections 8 and 9.

The Sagnac measurement pertains to phase and its time-derivative frequency, and not directly to amplitude. Hence sources of inaccuracy in maintaining a constant amplitude are not of concern, at least at first order, when studying the limitations of a ring-laser gyroscope. Anything which affects the interferometric phase is of critical importance. The next two sections look at two major limitations of this.

2. Fuller theory of the Sagnac effect

2.1. Range of interpretation

The history and interpretation of the Sagnac effect is reviewed by Post (1967), Heer (1984), Schleich *et al* (1984), Chow *et al* (1985), Stedman (1985), Hasselbach and Nicklaus (1993), MacKenzie (1993); see also Dieks (1991b) and Anderson *et al* (1994). The theoretical associations of the Sagnac effect are ubiquitous. It is a defect of the present work that the references and insights of such papers as Hasselbach and Nicklaus (1993) are not included here.

The extent to which the original derivations of the Sagnac effect endorse an ether-theoretic model has been debated, for example, by Post (1967), Dieks (1991b) and Hasselbach and Nicklaus (1993), but it is now generally recognized that the prediction of equation (1) is remarkably robust to the assumed theoretical framework, at least for spinless particles. The Sagnac effect can be derived from the special relativistic Doppler effect at the mirrors (Dresden and Yang 1979) or (as below) from general relativity (Post 1967, 1972a, b, Anandan 1981, Statz *et al* 1985). The Sagnac effect can be set in analogy with the Aharonov–Bohm effect through the analogy between the Coriolis force in a rotating frame and the Lorentz force from a magnetic field (Sakurai 1980, Opat 1990, 1991) or equivalently the Larmor relationship. It can also be regarded as one optical manifestation of the Berry phase (Hendriks and Nienhuis 1990, Hasselbach and Nicklaus 1993) and (hence or otherwise) as a consequence of time-reversal violation (Stedman *et al* 1995a, see section 9.2). It can be regarded as a prototype of the need for an anholonomic coordinate system, in which clocks slowly transported around different paths do not agree when next

coinciding; it can raise questions on the relation between various historical concepts of time (Dieks and Nienhuis 1990, Dieks 1991a, b).

2.2. *Method of derivation*

Analyses of the Sagnac effect using general relativity are given for example by Dresden and Yang (1979), Schulz-duBois (1987), Post (1967), Anandan (1981), Ashtekar and Magnon (1975), Scully *et al* (1981), Schleich and Scully (1984), Opat (1995), Landau and Liftshitz (1987), Forder (1984, 1985), Møller (1972), Harris (1996), and Scorgie (1990a, b, 1991, 1993a, b).

In the nature of the case, none of the general relativistic derivations even of the simplest Sagnac formula such as equation (1) is particularly easy to follow, and a significant number do not avoid inadequacies and inconsistencies. General relativity is proverbially liable to misuse. The consistent use of a coordinate choice is critical; the geodetic precession (section 2.3) can be represented as a Lense–Thirring or gravitomagnetic effect (Ashby and Shahid-Saless 1990) despite the association of the latter with an invariant (Ciufolini and Wheeler 1995). The last word is not attempted in this review. Rather, it is hoped that the following comments will stimulate a more careful comparison of methods and results than seems to exist at this time.

One may categorize all credible approaches to deriving the Sagnac effect according to their use of an inertial or of a rotating frame. Most proofs use the non-inertial frame of the Sagnac device, with the process stationary in time. Alternatively, one may use an inertial frame, with all world lines being helical, and all optical components changing frequencies and wavevectors, e.g. by the Doppler effect (Dresden and Yang 1979). In an elegant analysis, Opat (1995) comments that 'hybridising the two approaches is fraught with pitfalls': this categorization is exclusive.

Another possible categorization, though less exclusive in principle, is as to whether a transit time or snapshot approach is used in the evaluation of phase changes in an interferometer (Neutze *et al* 1996). In general (Post 1967, Opat 1995) the phase change associated with a space-time contour is evaluated allowing for both temporal and spatial change: $\Delta\Phi = \oint (\boldsymbol{k} \cdot \mathrm{d}\boldsymbol{x} - \omega\,\mathrm{d}t)$ where $\boldsymbol{k}$ is the wavevector and ω the angular frequency of the wave. In the snapshot approach, all times are set identically in some frame and $\oint \boldsymbol{k}\cdot\mathrm{d}\boldsymbol{x}$ is calculated around the closed loop of the interferometer; in the transit-time approach, $\oint \omega\,\mathrm{d}t$ is calculated over the time of flight of a wavefront around the interferometer. Dresden and Yang (1979), Schulz-duBois (1987) and Hasselbach and Nicklaus (1993) for example take a snapshot picture; in this approach one takes a snapshot of an extended wave at a particular time in one frame and applies a suitable wave equation. One must then impose boundary conditions very carefully, and particularly so if they are time dependent. The interferometer path cannot correspond to that of a classical particle, since its velocity is not infinite. In passing we note that Dresden and Yang (1979) give an impressive first-order special-relativistic proof based on Doppler shifts at moving mirrors, valid for neutrons or photons, and that Schulz-duBois (1987) gives an ingenious description based on an inertial analogy; his statement that the velocity of light is c in any reference frame cannot be sustained (Peres 1987). By contrast, Dieks and Nienhuis (1990), Møller (1972) and Neutze (1995) for example use a transit-time picture; this approach is prone to misuse when dispersive and accelerating media are considered.

Many approaches to the Sagnac effect (too numerous to reference here) are implied by or based on a derivation and application of Maxwell's equations in a rotating frame in a manner supposedly compatible with general relativity; from the Maxwell's equations so generalized,

the calculation of the non-reciprocity of the speed of light is straightforward. Such a derivation is always done in the coordinate systems preferred by the authors; however, formal complications such as the anholonomicity arising from any particular coordinate choice need care, different coordinate systems give very different formulations, and the results do not clearly manifest (coordinate) gauge invariance. Indeed, sometimes they appear to be clearly incompatible with gauge invariance, as in Post's (1967) otherwise helpful review; Tyler and Mysak (1995) note a related problem with Post (1967). A full account should ideally reconcile various choices of metric and tetrad. These include the 'natural' Grøn–Møller approach (Grøn 1975, 1977, 1979, 1984), where the object of anholonomicity vanishes but the coordinates are oblique, the instantaneous frames approach (Corum 1977), which uses oblique axes with a non-vanishing object of anholonomicity, and the anholonomic frames approach (Corum 1977, 1980) where also the tetrad is orthogonal. Kichenassamy and Krikorian (1994) claim that their approach is superior to any of these.

The fact that the same Sagnac formula is involved for slow clock transport as for light propagation in all situations reflects the fact that synchronization of a remote clock using light beams sent to and fro on a given path between the master and remote clock gives the same result within general relativity as slow clock transport along that path, even when each result is path dependent. This was noted first by Eddington (1924); see also Peres (1978), Soffel *et al* (1986), Rosenblum and Treber (1988) and Anderson *et al* (1997). The change in the reading of a standard clock at the beginning and end of a journey $1 \to 2$ is the change in proper time τ, where for any metric the infinitesimal interval $ds^2 = -c^2\,d\tau^2 = g_{00}c^2\,dt^2 + O(dx)$. Under slow transport ($dx/dt \to 0$), then, $d\tau = \sqrt{-g_{00}}\,dt$. This interval (and proper time change) is independent of coordinate choice, and we may estimate it piece by piece using the Minkowski metric of the local Lorentz frame LLF relevant for each infinitesimal part of the journey. In this local frame, the Einstein synchronization convention of special relativity holds (Anderson *et al* 1997), according to which coordinate time t_{LLF} at all points is established by equalizing the one-way ($1 \to 2$ and $2 \to 1$) apparent flight times of light in a round-trip journey on a given path. In this convention $g_{00} = -1$, and we derive $\tau = \int dt_{\mathrm{LLF}}$. Hence slow clock transport time τ along a given path always agrees with the change in a particular global coordinatization of time which itself is based on equalizing the one-way parts of round-trip light travel times over a sequence of infinitesimal steps on that path (and therefore over its full extent).

2.3. Corrections to the standard formula

A Feynman path integral approach to the Sagnac effect (minimization of the action $S = \int_P L\,d\lambda = \hbar\Delta\Phi$) has been used by Opat (1995) in a neutron interferometer. Hasselbach and Nicklaus (1993) also use the action to consider the effect of rotation on electron phase in their discussion of electron Sagnac effects. It is useful that first-order corrections arising from perturbation of the classical path cancel in an action calculation; however, one should distinguish the classical path in an inertial frame from the rotationally perturbed classical path, and a more complete story has some interesting twists (Neutze and Hasselbach 1997).

Scully *et al* (1981) show that, in the rest frame of the interferometer and a coordinate system in which $g_{\mu\nu}$ is equal to the Minkowski metric at the centre of the ring, to first order equation (2) becomes

$$\delta f = \frac{2}{\lambda P} \int \nabla \times \boldsymbol{h} \cdot d\boldsymbol{S} \tag{4}$$

where $h_i = g_{0i}$ are the mixed space-time components of the metric. In popular choices of rotating frame coordinates and metrics $\nabla \times \boldsymbol{h} = 2\boldsymbol{\Omega}$, given equation (2). As for

Schulz-duBois (1987), Dresden and Yang (1979) and most general-relativistic proofs, this demonstration explicitly allows for arbitrary (non-circular and non-planar) geometry.

Most derivations of the Sagnac effect in the literature, however elaborate, including those just mentioned, are similarly content to use a linear approximation to derive the standard formulae of equations (1) and (2), even though the former was known to Lodge and Larmor in 1896 (Anderson *et al* 1994). Certainly terms beyond those linear in Ω need to be evaluated in a fully relativistic theory. These terms are often stated to involve a factor of the form $(1 - \Omega^2 R^2/c^2)^n$ for some power n. Anandan (1981) and Scorgie (1991) give $n = -\frac{1}{2}$, and Landau and Liftshitz (1987) $n = -1$. Post's (1967) problem with gauge invariance leads to his vacillating between these, to the point of suggesting a resolution from experiment; others such as Soares and Tiomno (1996) imply that there is no such higher-order correction ($n = 0$). This literature still awaits resolution. Admittedly there is no prospect of practical interest in this term for photons.

Michelson (1904) suggested that the orbital motion of the Earth around the Sun might be detectable in a sufficiently gargantuan ring interferometer. This raises a question which remains interesting and could become amenable to experiment (section 8.1). Such an 'orbital Sagnac effect' might seem not to be consistent with general relativity: the centre of the Earth is in free fall, and if we ignore the rotation of the Sun on its axis no Lense–Thirring term (section 8.1; Mashhoon *et al* 1984) exists to rotate the axes of the local inertial frame. However, precession occurs for a gyroscope satellite in the Schwarzschild metric. In coordinates fixed with respect to the stars, Hamilton (1981) gives a free-fall torque-free gyroscope a precession rate

$$\mathbf{\Omega} = \tfrac{1}{2}\nabla \times \mathbf{h} - \tfrac{3}{2}\mathbf{v} \times \nabla\phi. \tag{5}$$

The first term is recognizable as the standard 'Sagnac' term of equation (4). This is, however, now augmented by the second term, which is variously known as the geodetic, Fokker or de Sitter term (Hamilton 1981); $\mathbf{v}$ is the orbital speed and ϕ the Newtonian gravitational potential. The geodetic term carries centrifugal and Coriolis effects, which must affect an optical interferometer as much as a mechanical gyroscope, when properly treated (Hamilton 1981), and may be recognized as inducing an orbital Sagnac effect. It has been measured, if indirectly, in lunar laser ranging (Williams *et al* 1996). Incidentally, the geodetic term is not to be thought of as a Thomas rotation $\beta\mathbf{v} \times \mathbf{a}/(1 + \beta)$, in that the proper acceleration $\mathbf{a}$ of a free-fall gyroscope is zero (Hamilton 1981). A Thomas rotation term indeed enters the analysis when the ring laser is on the surface of the rotating Earth (Scully *et al* 1981). It may be noted that a geodetic term up to 25 times the magnitude of the geodetic term from solar gravity is also associated with the effect of this rotational motion of a ring laser in Earth's gravity.

The occurrence of the geodetic term may be seen explicitly. Those derivations which relate the Sagnac effect to the line integral or curl of $\mathbf{h}$ often refer to a particular coordinate frame. Møller (1972) gives the formula

$$\Delta t = \oint 2\mathbf{h} \cdot \hat{\mathbf{w}}\, d\sigma/\sqrt{-g_{00}} \tag{6}$$

for the transit-time difference between counterpropagating beams, where $\mathbf{w}$ is the light velocity $\hat{\mathbf{w}}\, d\sigma/dt$ in a coordinate system with $d\sigma^2$ as the spatial metric ($d\sigma^2 = dx^i\, \gamma_{ij}\, dx^j$, $\gamma_{ij} = g_{ij} - g_{i0}g_{j0}/g_{00}$). Equation (6) of Scorgie (1993a) shows more generally that

$$\Delta t = \oint \frac{2n\, d\rho}{cg_{00}}\sqrt{|g_{00}| + (\mathbf{h} \cdot \hat{\mathbf{v}})^2} \tag{7}$$

where $\hat{v}$ is the unit tangent $dx/d\rho$, n is the refractive index and $d\rho^2 = dx^i\, g_{ij}\, dx^j$. Such derivations clearly include the effects of g_{00} and so the Newtonian potential. As mentioned, Scully *et al* (1981) use a special coordinate system to derive equation (4), and show explicitly that the necessary change from Schwarzschild coordinates includes the effects of the geodetic term of equation (5) in equation (4).

The effect of intrinsic spin has been debated. Partly in this connection, Soares and Tiomno (1996) take on all comers: 'with the exception of Dresden and Yang, all derivations of the Sagnac–Mashhoon effect are incorrect or incomplete'. Their exception seems partial since Dresden and Yang's analysis (for neutrons as well as photons) did not yield the Mashhoon effect (a spin-rotation coupling term $\sigma \cdot \Omega$ in the Hamiltonian for the rotating frame) which Soares and Tiomno regard as an additive correction to equation (1) for spin-$\frac{1}{2}$ particles. Earlier controversy over this term (Anandan 1992) is best redirected to the relativistic hypotheses regarding rotating frames (Hehl and Ni 1990, Mainwaring and Stedman 1993). Several formulations of the quantum mechanics of a spin-$\frac{1}{2}$ particle in a rotating frame are available (Hehl and Ni 1990, Lalak *et al* 1995). Intrinsic spin couples to curvature only (Harris 1996) and a force-free torque-free intrinsic spin vector is simply parallel-transported, rotating as a gyroscope axis. The spin–rotation coupling makes the equivalent statement from the viewpoint of the rotating frame, and is merely the kinematic results of the transformation to the rotating frame (Hannam 1997).

To a good approximation, neither linear velocity nor linear acceleration affect the result or indeed are detectable by a ring laser (Kuriyagawa *et al* 1975, Kuriyagawa and Mori 1979); this has been verified experimentally (Aronowitz 1971). The effects of space-time curvature in matter interferometry have been discussed (Anandan 1984). Scorgie (1993a) finds very small terms in the Sagnac signal which depend on accelerations and gravitational fields. Neutze (1995) gives an improved formulation for the effect of angular acceleration on the Sagnac effect in ring lasers.

The scale factor of a gyroscope (the ratio of the mechanical rotational frequency to the Sagnac frequency) is calculated above assuming an infinitely thin optical path. However the Gaussian modes have a finite beam diameter d (defined by the exact cavity geometry and not simply scaling with the perimeter) typically of 0.5 mm, a fraction of the diameter commensurate with the required sensitivity, and corrections might in principle be expected by incorporating the beam diameter. One might expect corrections at the level $(d/R)^2$, i.e. above ppm in C-I. However, there is evidence that this is a pessimistic assessment (Prade and Vinet 1988) and this matter has not been of concern.

The dispersion of mirror birefringence (section 1.6) could in principle affect the Sagnac formula in a practical system in that counter-rotating beams, because of their differing frequency, might have different characteristics at the mirrors and so different optical path lengths. However, this effect is itself maximal only when reflectance varies maximally with frequency (Schwider 1992), i.e. away from the design value.

2.4. Corrections from the media; drag effects

Zernike (1947) gives an interesting expansion of his theme that 'the subject of the propagation of light in moving media has a curious history full of controversies and errors'. A number of further controversies have occurred since 1947. Several component debates on the role of dispersion in the Sagnac effect with reference to electron and neutron as well as photon experiments are reviewed by Hasselbach and Nicklaus (1993).

For the optical Sagnac effect, if a dielectric is present in the cavity, at rest with respect to it, and dispersion is ignored, it seems plausible from an elementary perspective that a

correction is needed to all formulae on account of the change in time delay in one circuit of the ring. However, it was recognized by Einstein (Zernike 1947) in connection with the experiment of Harress (see below) that the area factor A should not be so 'corrected'. To first order throughout, the speed of light within the inertial frame is $c/n + \varepsilon v$ where n is the refractive index, v the speed of the medium (parallel to the light) and ε the drag coefficient, or fraction by which the velocity of a medium shifts the light speed within it. With respect to the ring this speed is $c/n + \varepsilon v - v$. Hence the v-dependent part of the light travel time of equation (1) over a path l in the rotating frame is $vln^2(1 - \varepsilon)/c^2$. Since no Doppler effect exists when the medium is stationary with respect to the source, the frequency dependence of n is irrelevant and the drag coefficient has the classical value $1 - 1/n^2$ making the light travel time independent of n. Hence the expressions of equation (1) for time delay and phase shift are not affected by the presence of a dielectric in this case. This holds provided the refractive index is independent of time, and a function of position only (Scorgie 1993a).

The story is different for the Sagnac frequency-splitting formula of equation (2) for two reasons. First, the optical path length which appears in this equation, unlike the area, must be corrected for the refractive effects of any medium (including the gain medium in an active device). The experiment of Privatov and Filatov (1977) confirms the analysis of Post (1967) over several alternative formulae; the P of equation (2) is the optical path length $\oint n \, dl$ of the ring, and this emerges from careful theory (for example Scorgie 1993a). In addition, the frequencies now are different, and dispersion can have a dominant effect (Scorgie 1993b).

When the medium is moving with respect to the rotating frame, light-speed drag affects the result. The role of moving and accelerated dispersive media in the beam path has been the focus of some theoretical discussion (Scorgie 1993a) and also of some remarkable and increasingly accurate experiments over many years in ring interferometry (Post 1967, Kowalski *et al* 1993a, b).

Indeed, light drag in moving media assumed great importance at the turn of this century (Neutze *et al* 1996). Drag measurements directly disprove the Newtonian velocity addition law (Holton 1969). The ether drag experiment of Michelson and Morley (1887) had only an indirect influence on Einstein's thinking, and Einstein has stated (Holton 1969) that the key results which led to special relativity were his conviction that the electromotive force induced in a body in motion in a magnetic field was nothing other than an electric field, the phenomenon of aberration and the results of the Fizeau (1851) light-drag experiment. Another Nobel laureate, Zeeman, performed a *tour de force* in his drag experiments of 1916–1922 (Zeeman 1916, Zeeman and Snethlage 1920, Zeeman *et al* 1920a, b, 1922a, b). These experiments still set a formidable goal in the laser era, to distinguish unambiguously by experiment the magnitudes of the different dragging coefficients when dispersive moving media are subject to different boundary conditions.

Within special relativity, consider a dielectric sample with rest frame I' moving with velocity v relative to the laboratory frame I; the sample has a phase-refractive index (with respect to a vacuum) $n \equiv n(\omega)$ at the frequency ω (as measured in I) of an electromagnetic wave. In the sample frame I', the phase velocity is $v'_p \equiv \omega'/|k'| = c/n'$ where in dispersive media the refractive index changes with the Doppler frequency shift induced by frame change: $n' \equiv n(\omega')$. To first order, a Lorentz boost from I' to I gives $\omega = \omega' + v \cdot k' = \omega'\{1 + n'v \cdot \hat{k}'/c\}$, $|k| = |k' + \omega'v/c^2| = |k'|(1 + v \cdot \hat{k}'/cn')$ so that the phase velocity in I is, to first order in the velocity,

$$v_p \equiv \frac{\omega}{|k|} = \frac{c}{n'} + v \cdot \hat{k}\left(1 - \frac{1}{n'^2}\right). \tag{8}$$

The second term is the dragging effect; the light velocity is altered because of the sample velocity v. When $v \parallel k$, $v_p = c/n' + v\epsilon_{\text{Fresnel}}$, where the Fresnel drag coefficient is $\epsilon_{\text{Fresnel}} \equiv 1 - 1/n'^2$. This expression was first derived by Fresnel (1818) on the basis of an elastic ether theory.

If the boundary of the dragging medium is stationary in I and if the medium velocity is both parallel to the incident beam and normal to the boundary, $\omega' = \omega\{1 - n'v/c\}$ so that $n' = n - \omega n(\mathrm{d}n/\mathrm{d}\omega)(v/c)$. Therefore, again to first order, $v_p = c/n + v\epsilon_{\text{Lorentz}}$ where the Lorentz (1895) drag coefficient is $\epsilon_{\text{Lorentz}} \equiv 1 - 1/n^2 + (\omega/n)\,\mathrm{d}n/\mathrm{d}\omega$. However, if the media boundary is the surface of a rigidly moving sample and the incident beam propagates through a vacuum, we find $\omega' = \omega(1 - v/c)$ such that $v_p = c/n + v\epsilon_{\text{Laub}}$. The drag coefficient in this context is $\epsilon_{\text{Laub}} \equiv 1 - 1/n^2 + (\omega/n^2)\,\mathrm{d}n/\mathrm{d}\omega$, and was first obtained by Laub (1908); see also Parks and Dowell (1974). Landsberg (1961) has discussed these different coefficients in a unified form.

The first quantitative measurement of Fresnel (actually Lorentz) drag was that of Fizeau (1851). In his optical ring interferometer the counter-propagating light beams followed the same optical path, making their relative phase insensitive to variations in the refractive index of the medium (water) and of the surrounding air. Fizeau confirmed the Lorentz drag coefficient to 16% accuracy. Thirty-five years later, using wider flow tubes and a more reliable light source, Michelson and Morley (1886) obtained the drag coefficient in water to 5% accuracy. In 1887, Michelson could compare his measured drag coefficient only with Fresnel's (1818) theory, which ignored dispersive corrections. His results are compatible with the necessary dispersion corrections, provided by Lorentz (1895). Harress (Knopf 1920, Zernike 1947, Anderson *et al* 1994) studied Fresnel drag in glass, using a rotating polygonal ring interferometer constructed from adjacent glass prisms. Although this experiment was intended to show dispersion effects, no such effects could be detected, the results being independent of refractive index. There was an unexpected bias which was identified as the Sagnac effect only after Harress's early death; if this bias is subtracted, Harress's data gives an uncertainty of 2% for the drag coefficient at the wavelength $\lambda = 535$ nm, and 3% for $\lambda = 625$ nm. Zeeman and co-workers further refined the passive optical interferometer, obtaining a drag coefficient with an accuracy of 5% for quartz (Zeeman and Snethlage 1920), and an accuracy of 1.7% with flint glass (Zeeman *et al* 1922a, b). These accuracies demanded the inclusion of the dispersion term in the Laub drag coefficient and provided the first clear experimental distinction between the Lorentz and Laub drag coefficients $\epsilon_{\text{Lorentz}}$, ϵ_{Laub}.

The ring laser facilitated high-precision measurements of drag because the measurable quantity was a beat frequency rather than a phase shift between counterpropagating modes. Macek *et al* (1964) first introduced drag effects via a rotating disk into a ring laser. Bilger and Zavodny (1972) and Bilger and Stowell (1977) placed a rotating fused silica disk along one arm of a ring laser at the HeNe wavelength of 633 nm. Light entered the plane face of the disk off centre and at an oblique angle of incidence. The experiment had the advantages of using a stationary interface between media, of using a large dynamic range (almost two decades of velocity range, and a factor of 65 in the beat frequency, which permitted a very accurate verification of the linear dependence on velocity), and of using two different analysis techniques (plotting the beat frequency versus radius and versus rotation rate). Together with the synchronization of the gating of the rotation rate counter and of the beat frequency counter, these design features greatly reduced systematic errors. Bilger and Zavodny (1972) took the drag coefficients to have the Lorentz form; Parks and Dowell (1974) confirmed this and generalized the drag formula to arbitrary angles between the sample velocity and the incident light beam. The derived drag coefficients differed from

the theoretical predictions by the relative amounts -2400 ± 5500 ppm (Bilger and Zavodny 1972) and 1060 ± 780 ppm (Bilger and Stowell 1977) respectively. If the experiment of Kowalski *et al* (1993a), in which a fused silica sample was longitudinally accelerated, is interpreted as a measurement of the Laub drag coefficient, the value obtained has an uncertainty $\sim$ 2000 ppm. Sanders and Ezekiel (1988) subsequently employed a passive ring resonator, also at the HeNe wavelength of 633 nm. They oscillated their glass samples longitudinally, as did Zeeman, and so measured a modified Laub drag coefficient; Laub, because the boundary of the sample moved with the medium, and modified because the beam direction and the velocity are non-parallel in the sample. Although their velocity range, 19.9–29.9 cm s^{-1}, and dynamic range, 266 Hz–3.042 kHz, were relatively small, Sanders and Ezekiel used four different materials with very different refractive indices and dispersions. They assigned their measured drag coefficient an absolute experimental error of 280 ppm, commensurate with the standard deviation of the relative deviations of 480 ppm implied by their data. Their reported result agrees best with theory, differing from their theoretical estimate by 60 ppm, and motivated their claim (echoed for example by Cook *et al* 1995) to the most accurate verification of a Fresnel drag coefficient in moving media to date. This agreement is fortuitous; Neutze *et al* (1996) give a revised analysis of the theoretical prediction. The Sanders–Ezekiel arrangement is more vulnerable to previously unanalysed systematic effects than is the Bilger–Stowell arrangement; a variety of geometrical and relativistic complications significantly affect the observed frequency difference in such an experiment. Corrections include the identification of a quoted refractive index in air rather than a vacuum, the choice of frame in calculating angular deviations, and the deviation of the beam path from the optical axis. This revised theory deviates from the Sanders–Ezekiel experimental results with a mean and standard deviation of -1290 and 620 ppm respectively. The experiment of Bilger and Stowell (1977) is less prone to unanalysed systematic effects, and the relative deviations in the drag coefficient have mean and standard deviations of $+1060$ and 780 ppm respectively. Hence, although present drag measurements give direct manifestations of relativity, these have achieved an accuracy only of order 1000 ppm.

If in a neutron interferometric experiment, the boundary does not move with the medium (as for Fizeau drag), and the medium has no nuclear resonance at thermal energies, Horne *et al* (1983) predicted, and Arif *et al* (1985) confirmed, that a null-phase shift results. Klein *et al* (1981) experimentally verified the drag coefficient in a Laub-like experiment to an accuracy of 9%; Bonse and Rumpf (1986) achieved an accuracy of 1.5%. Arif *et al* (1988, 1989) obtained a Fizeau-like phase shift for fixed boundaries which was non-vanishing because of the vicinity of a nuclear resonance. The associated drag coefficient was measured to an accuracy of 18%.

3. Frequency pulling and locking

3.1. Basic pulling theory

We discuss here one topic which in our experience is of especial significance in limiting the accuracy of large rings for the applications considered later: the effects of frequency pulling (including the associated locking). Pulling remains important in the large ring, despite the fact that (as shown in section 3.9) it is dramatically reduced in large rings.

A principal source of frequency error in the gyroscopic systems considered here is that of mode coupling due to backscatter. In the 1600s, Christiaan Huygens noticed during an illness that two pendulum clocks on his bedroom wall kept exactly in time. He recognized that wall motion coupled these, and deduced that when two oscillators are coupled, their

frequencies are affected, being pulled together or even exactly the same when without coupling a difference exists. The same effect is well known for adjacent tuned circuits, and Adler's (1973) theory has been a watershed for this and other applications.

What is true for mechanical and electronic oscillators is equally true for optical oscillators. Anything such as backscattering at impurities which allows light from one ring-laser beam to affect the other beam will degrade the Sagnac frequency splitting. In the worst case (worst, that is, from the perspective of a wished-for gyroscopic application), the splitting collapses; the oscillators lock as in Huygens' case, and the effect of rotation is to change only the relative phase of the eigenmode oscillations. This occurs within the so-called lock-in band, when the frequencies are sufficiently close. Locking phenomena in ring lasers have been studied extensively on account of their critical importance for the development of optical gyroscopes and the insight they give into laser dynamics (Aronowitz and Collins 1970, Aronowitz 1971, Haus *et al* 1985, Chow *et al* 1985, Statz *et al* 1985, Wilkinson 1987, Christian and Mandel 1986, 1988, Etrich *et al* 1992, Bretenaker *et al* 1993a, b).

An elementary analysis suffices to show several important features of this (Wilkinson 1987). We label the beams $+$ for anticlockwise (CCW), and $-$ for clockwise (CW). Let the electric field at any point $z_\pm$ in each beam $\pm$ have a complex amplitude phasor $\tilde{E}_\pm = E_\pm \exp i\phi_\pm$. Its phase $\phi_\pm = \omega_\pm(t - z_\pm/c)$; $\omega_\pm$ are the corresponding actual mode frequencies (including corrections for dispersion etc) and $z_+(z_-)$ is the optical path length around the ring from a reference point A in a CCW (CW) sense. We take $P_\pm$ as the total optical path lengths, so that $\omega_\pm P_\pm = 2\pi cN$. The Sagnac frequency (derived from optical path non-reciprocity and ultimately from time-reversal violation) is written in this subsection as $f = (\omega_+ - \omega_-)/2\pi$ (rather than δf, to simplify the equations).

On the simple Adler-type model of the above references, at any point the phasor $\tilde{E}_\pm$ obeys the equation

$$\frac{d\tilde{E}_\pm}{dt} = i\omega_\pm \tilde{E}_\pm + r\tilde{E}_\mp \tag{9}$$

where r is the fractional amplitude backscatter rate, and the phase difference $\psi = \phi_+ - \phi_-$ obeys

$$\frac{1}{2\pi}\frac{d\psi}{dt} = f - l\sin\psi. \tag{10}$$

(The physics of this is illustrated in section 3.2.) The parameter $l \equiv r/\pi$ and has the significance of a lock-in threshold frequency. For $f < l$, equation (10) yields a static or locked phase relation $\psi = \sin^{-1}(f/l)$. The Sagnac effect is completely suppressed; there is no frequency difference. The relative beam phase varies with the applied mechanical frequency and the noise in this determination has been studied by Rozanov (1970). For $f > l$, the differential equation has the solution

$$\psi = \frac{1}{\pi}\tan^{-1}\left(\frac{l + p\tan\pi pt}{f}\right) \tag{11}$$

where the pulled frequency is

$$p = \sqrt{f^2 - l^2}. \tag{12}$$

In equation (11) the phase advances in a periodic but inconstant fashion with time, having an Airy function profile (figure 2(*a*)), the net frequency p being reduced, or pulled, below the desired Sagnac frequency f. Equation (12) shows that the amount of pulling depends on the proximity of the lock-in threshold frequency l (figure 2(*b*)), and the fractional effect for small l/f is a quadratic function of this ratio.
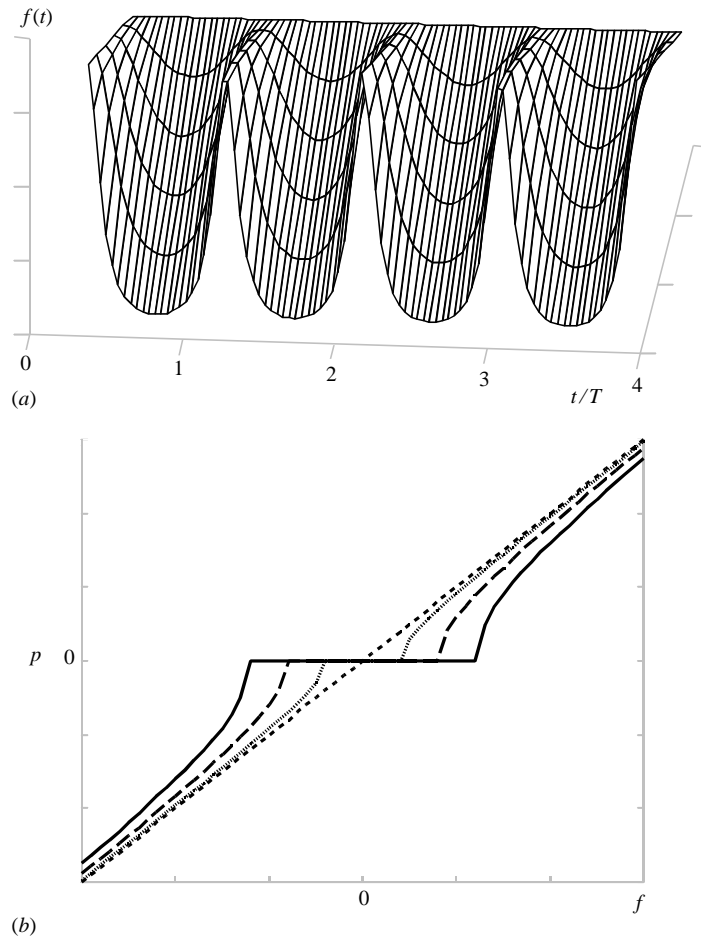
Figure 2. Effects of pulling. (*a*) Instantaneous frequency (equation (16)) as a function of time (scaled to give four periods T). The ratios l/f of the lock-in to nominal Sagnac frequency are $n/6$ for $n = 0$ (no variation: $p = f$), 1, 2, 3, 4 (maximal frequency excursion). (*b*) Pulled frequency p as a function of applied frequency f (equation (12)). The ratio of l to the maximum value of f ranges from 0 to 0.4.

3.2. Analogies

3.2.1. Necklace model. In the necklace model (section 1.3), backscatter has the effect of constraining the movement of the beads of the necklace, which responds as far as is practicable by altering the bead positions so as to minimize losses (Haus *et al* 1985, Wilkinson 1987); as Bretenaker *et al* (1993a, b) have shown, vignetting gives similar effects. If an imperfect output mirror is only slowly dragged along the necklace, the beads on the latter are carried along with it; the laser is locked. At faster speeds the laser unlocks, and the beads 'slip' periodically on the mirrors, thus undoing some of their enforced motion in between the more 'frictional' parts of the interaction. The first effect of this is that the necklace is moved in a sawing motion, thus giving the Airy profile of equation (11) as a manifestation of the 'jerking' motion of the necklace.

The laser beams lose energy when the antinodes of the necklace are over lossy scatter

sites, and recover lost energy through laser gain when not so placed. Therefore, backscatter makes the intensity of each beam fluctuate accordingly (section 3.6); the difference in this dynamic behaviour of the instantaneous frequency (the bead position) and the beam or interferogram intensity (the bead size) is a direct reflection of the importance of laser gain on the timescale of all related effects (the inverse of the pulled frequency).

3.2.2. Mechanics. Of several possible mechanical analogies (see for example Cresser *et al* 1982a) we give a somewhat novel one here.

If we think of $d\psi/(\pi \sqrt{m} \, dt)$ as a mechanical speed v, where m is the mass of some test particle, we derive from equation (10)

$$\tfrac{1}{2}mv^2 + V(\psi) = f^2 \qquad V(\psi) \equiv 2lf \sin \psi - l^2 \sin^2 \psi \qquad (13)$$

which may be regarded as an energy conservation equation, with $V(\psi)$ the analogue and position- (ψ-)dependent potential energy. For $l = 0$, there is no potential energy, and the particle speed (phase evolution) is set by the unpulled frequency f. In the lock-in limit ($f < l$), the total 'energy' f^2 is less than the maximum of the potential, and the analogue particle will oscillate within one well of the potential. However, if $f > l$, the particle can perform a 'roller-coaster' ride across the periodic potential, slowing on the hills and speeding up in the valleys (figure 3). Though the valleys are relatively deep and quickly traversed, the constant spacing of the zeros makes the hills more effective in limiting progress, and the particle's average speed is reduced, to the pulled frequency p.

Another model of pulling is deferred to section 3.7 so as to allow for a more full discussion.
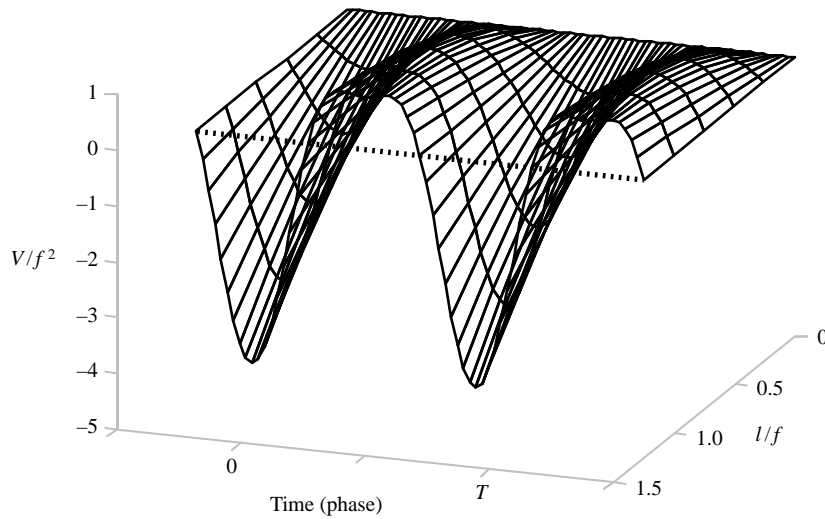

Figure 3. Analogue potential surface V (normalized by the total analogue energy f^2) to describe pulling. For a given applied rotational frequency (with Sagnac freqency f), the particle undergoes one-dimensional motion parallel to the time (or phase) axis. The cross-section that is relevant depends on the frequency ratio l/f, which is varied from 0 to 1.25.

3.3. Magnitudes of pulling effects

The magnitude of the lock-in threshold frequency l is of critical interest; we follow Aronowitz (1971) and Stedman *et al* (1995c) with some variations. A fraction s of the amplitude (and so a fraction s^2 of the intensity) of any beam will be scattered at each reflection; for a clean supermirror, s^2 is of order 10^{-6} (ppm). We assume for simplicity that the scattering is uniform in angle, so that a fraction $d\Omega/4\pi$ of this intensity is scattered into the other beam, where $d\Omega$ is the acceptance solid angle of that beam. (This should also be a 'worst-case' choice; to the extent that the mirror imperfections are Lambert scatterers, they will be much less effective in scattering at $90°$ and so will induce a relatively low lock-in threshold for a square ring.) The angle θ over which scattered light is captured by the other beam (and which gives $d\Omega \sim \pi\theta^2$) is a typical diffraction angle $\theta = \lambda/d$. d is a beam diameter, of order 0.5 mm and a relatively weak function of ring dimensions; $d \propto P^{1/2}$ (because set in part by the wavelength); we ignore this dependence below. The fractional intensity backscatter then is $(s\lambda/2d)^2$. In a cavity of perimeter P and with four mirrors, these reflections occur for one beam at the rate of $4c/P$. Hence the fractional amplitude backscatter rate $r \sim cs\lambda/(dP)$, and the lock-in threshold (half the range, i.e. $-l$ to l) becomes

$$l \sim \frac{cs\lambda}{\pi dP}. \tag{14}$$

The lock-in threshold is therefore minimized by having better mirrors (decreasing the total scattering amplitude s) and bigger rings (increasing the perimeter P). At the He–Ne wavelength and for modern supermirrors, $l \sim 10^2/P$ Hz, so reducing to the hertz level in large rings.

3.4. Spectral harmonic content

The above approximations are adequate to display many features of a full solution. In particular, a more full study (Stedman *et al* 1995b) supports the form of equations (10)–(12) and the formal consequences we now outline. Equation (11) may be written

$$\psi(t) = 2 \arctan \frac{v}{f} = 2 \arctan \frac{\sin(\pi pt + \chi)}{\cos \pi pt} \tag{15}$$

where $v \equiv l + p \tan \pi pt$, $\chi \equiv \tan^{-1}(l/p)$, p being the pulled frequency $\sqrt{f^2 - l^2}$. The observed instantaneous frequency $d\psi/(2\pi\,dt)$ is

$$f_o = \frac{p^2}{f - l \cos 2\pi pt}. \tag{16}$$

The period of the frequency excursions $T = 1/p$. From equation (16), the observed frequency varies between $f + l$ and $f - l$ (the denominator varies between these values, and the numerator is the product). However (as section 3.2 suggested), it is not symmetrical in between so that its average value, or pulled frequency $\overline{f_o}$—that determined from gyro output counts—is not f but the reduced value p.

Fourier analysis of the instantaneous frequency gives a geometric progression of harmonics whose ratio r is given by

$$r = \left(\frac{f - p}{l}\right) = R(q) \qquad R(q) \equiv q - \sqrt{q^2 - 1} \qquad q \equiv f/l. \tag{17}$$

Hence for progressively lower lock-in thresholds, $r \to 0$ linearly with l, and harmonics (as opposed to the fundamental signal) of the instantaneous frequency exist only because of the existence of backscatter, pulling and a lock-in threshold.

In the representation $\psi = \arg[(1 - r \exp 2\pi \mathrm{i} pt)^{-1}]$, the argument of Ψ is the analytic signal Z, whose form is the Airy function familiar from Fabry–Pérot theory:

$$Z(t) = C' \sum_{n=0}^{\infty} (r \exp 2\pi \mathrm{i} pt)^n = \frac{C}{1 - r \exp 2\pi \mathrm{i} pt}. \tag{18}$$

This same general behaviour is found whenever the harmonics of a signal are in geometric progression.

In experiment, a small fraction of each counterrotating beam exits by transmission at a mirror, and these emergent beams are guided so as to interfere at a beam-combining prism. This produces an interferogram whose fringes travel past a detector (also fixed in the rotating frame) at the rate p. The time-dependent light intensity monitored by the detector gives the gyroscope output signal, and this signal is closely related to the real part of $Z(t)$. The analytic signal may then be reconstructed numerically from the interferogram (the unobserved imaginary part is the Hilbert transform of the real part) so as to infer the phase ψ. The equivalence of this to the above is discussed in Stedman *et al* (1995b).

3.5. Backscatter phases

Two important generalizations of the above theory, apparent in the expanded theory of Stedman *et al* (1995b), deserve special mention. The first, covered in this subsection, is that the phase of the backscattered light has a dramatic effect on the lock-in threshold (Privatov and Filatov 1977) which fluctuates between zero and the value of equations (10) and (14) as the dimensions of the ring change over the scale of a wavelength. This is a major source of Sagnac frequency drift in large rings.

Backscattering contributes to the time evolution of each beam's phasor at a reference point A in the ring (say the region of amplification, or the position of the output mirror leading to the beam combiner). At the nth centre of backscatter, at the optical path length $z_{n\pm}$ from A in the appropriate direction, each phasor $\tilde{E}_\pm$ has a distance-induced phase shift relative to A of $\exp(-\mathrm{i}\omega_\pm z_{n\pm}/c)$. Let the centre contribute a complex backscattering amplitude factor $\tilde{A}_{n\pm}$ to the phasor; propagation back to A has the effect of adding a further phase factor $\exp(\mathrm{i}\omega_\pm z_{n\mp})$, and the phasor accumulates a distance-dependent phase shift at A of $\tilde{A}_{n\pm} \exp -\mathrm{i}\omega_\pm(z_{n\pm} - z_{n\mp} + P_\mp)/c$. To a very good approximation we may take average values in this phase, also $z_{n+} \simeq P - z_{n-} \equiv z_n$, $\omega P = 2\pi cN$, to show that the return journey doubles the distance-dependent phase (Rodloff 1987). The effect of backscattering at A is then to inject per unit time a complex fraction

$$R_\mp = \sum_n \tilde{A}_{n\mp} \exp(2\mathrm{i}\omega z_n/c) \tag{19}$$

of one amplitude $\tilde{E}_\mp$ into the other, $\tilde{E}_\pm$. Note that the distance-dependent phase is identical for both beams; the backscatter fractions R_+, R_- differ only through the the non-reciprocity of local backscattering amplitudes $A_{n\pm}$ (Rodloff 1987). We define amplitudes and phases of these fractions and the local scattering amplitudes by $R_\mp = r_\mp \exp \mathrm{i}\epsilon_\mp$, $\tilde{A}_{n\pm} = A_{n\pm} \exp \mathrm{i}\epsilon_{n\pm}$. The net phases ϵ_+, ϵ_- are critically dependent not only on the phases $\epsilon_{n\pm}$ of the backscatter at each centre but also on the separation z_n between the centres through the common factor $\exp(\mathrm{i}2\omega z_n/c)$.

When laser pumping, saturation and cross-saturation (parametrized by a, β, ξ respectively) are included as well as backscatter, the phasor differential equations generalize to the form (Stedman *et al* 1995b)

$$\frac{1}{E_\pm} \frac{\mathrm{d}E_\pm}{\mathrm{d}t} = (\pi a - \beta E_\pm^2 - \xi E_\mp^2) + \rho_\mp \cos(\psi \mp \zeta) \tag{20}$$

$$\frac{\mathrm{d}\psi}{\mathrm{d}t} = 2\pi f - \rho_- \sin(\psi - \zeta) - \rho_+ \sin(\psi + \zeta). \tag{21}$$

where $\rho_\pm \equiv r_\pm E_\pm / E_\mp$, the relative beam phase is now $\psi \equiv \phi_+ - \phi_- + (\epsilon_+ - \epsilon_-)/2$, and the net backscatter phase $\zeta \equiv (\epsilon_+ + \epsilon_-)/2$. If we suppose that $\rho_+ = \rho_- \equiv \rho$ (the otherwise critical phase dependence does not appear in these parameters), equation (10) generalizes to

$$\frac{1}{2\pi} \frac{\mathrm{d}\psi}{\mathrm{d}t} = f - l_\zeta \sin \psi \qquad l_\zeta \equiv \frac{\rho}{\pi} \cos \zeta. \tag{22}$$

Two special cases are of interest. In the conservative case, $\zeta = \pi/2 \bmod \pi$, and $l_\zeta = 0$; in this model backscattering does not affect the relative phase ψ whose measurement is of interest for gyroscopic purposes. This is equivalent (Christian and Mandel 1986) to the condition $R_+ + R_-^* = 0$. In the dissipative case, $\zeta = 0 \bmod \pi$, l_0 and is maximal (and equal to l), and the phase ψ is maximally affected.

The effects, therefore, are critically dependent on the net backscatter phase $\zeta \equiv (\epsilon_+ + \epsilon_-)/2$. The nth scatterer contributes $\epsilon_{n\mp} + 2\omega z_n/c$ to $\epsilon_\mp$, and so $\frac{1}{2}(\epsilon_{n+} + \epsilon_{n-}) + 2\omega z_n/c$ to ζ. Hence the effects are strongly distance-dependent, and a change in z_n (by thermal expansion or compression under changes in ambient pressure) by an eighth of a wavelength will transmute a situation with conservative backscatter (and negligible pulling) into dissipative backscatter (and maximal pulling).

The additional term $\epsilon_{n+} + \epsilon_{n-}$ is associated with the sum of local backscatter-phases scales. Time-reversal symmetry of a response tensor such as the susceptibility or polarizability is sufficient to guarantee conservative coupling at the local level for each scatterer (Haus *et al* 1985, Stedman *et al* 1995b) though the distance factor makes this merely an arbitrary initial value in practice.

3.6. Intensity variations

The other major generalization is to the inclusion of backscatter-induced intensity variations in each beam. These have the periodicity of the pulled frequency p (so that the Sagnac effect can be seen from a study of the intensity of one beam only) and a relative phase related to the net backscatter phase ζ (Stedman *et al* 1995b). This has considerable practical potential; monitoring this relative phase and re-injecting a suitably tailored signal has enabled a method of backscatter stabilization (Privatov and Filatov 1977).

As shown by equation (20), the backscattering rates $r_\pm$ directly affect the time variations of the magnitudes of the intensities, and the $\rho_\pm$ are not constants. For small variations, both intensities are simple sinusoidal functions of the pulled phase, and equation (20) shows directly that, as far as the trigonometric factor in the backscattering is concerned, the phase difference between these beam intensity variations is itself 2ζ (Wilkinson 1987, Christian and Mandel 1986, 1988, Stedman *et al* 1995b). Hence in the dissipative (conservative) case, the beam intensity variations are in phase (antiphase, respectively).
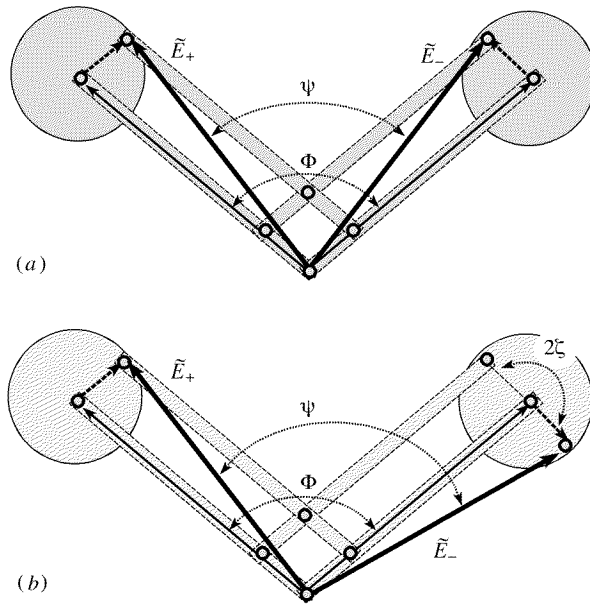
Figure 4. Phasor diagrams for describing pulling, based on equations (9) and (10). One may regard the broken lines as a mechanical framework with the indicated pivots. A proportion (dashed vector) of one beam phasor (thin solid vector) is added to the other, indicating the time development of the final phasors $\tilde{E}_+$, $\tilde{E}_-$ (thick solid vectors). In the absence of pulling, Φ would be $(\omega_+ - \omega_-)t$ and increase in time linearly; $\psi(t)$ is this phase adjusted for pulling, and itself reacts on the dynamics of Φ. (*a*) Dissipative coupling ($\zeta = 0$). $\psi(t)$ is alternately smaller and larger than $\Phi(t)$ as the latter varies from 0 to π and from π to 2π respectively. On average, it is less, hence the frequency is pulled down. (*b*) Conservative coupling ($\zeta = \pi/2$). In the approximations used here, the geometry ensures that $\psi(t)$ is equal to $\Phi(t)$ and is a linear function of t.

3.7. Phasor diagrams

Equation (9), with the inclusion of the backscatter phases of section 3.5, lends itself to modelling with a simple perspex model on an overhead projector, displaying the major predictions (figure 4); the phasor diagrams follow Wilkinson (1987) and Dennis and Diels (1994). Two phasors represent the beam amplitudes, and rotate with respect to each other since $\omega_+ - \omega_- \neq 0$. A proportion r (assumed constant) of one phasor is added to the other, affecting the time dependence of the magnitude and angle of each phasor in a way which is characteristic of the additional phases generated by the backscattering factors $\exp i\epsilon_\mp$ through the sum $\zeta = (\epsilon_+ + \epsilon_-)/2$. If $\zeta = 0 \bmod \pi$, corresponding to a symmetrical pattern of phasor addition (figure 4(*a*)) it is readily perceived from the diagram (or better, from a model) that the phasors have the same length at any instant (i.e. beam intensities are the same function of time) but that their relative angle (frequency pulling) is maximally affected by backscatter. This corresponds to dissipative coupling. If $\zeta = \pi/2 \bmod \pi$, phasor addition has an antisymmetrical character (figure 4(*b*)) and the phasor length variations are in antiphase, while their relative angle is a constant, so that the instantaneous phase shows no pulling effects in the approximations used here. This corresponds to conservative coupling.

3.8. Avoiding pulling and locking

The traditional methods of diminishing the effects of pulling and locking to an acceptable level are those of using body-shake dither (Bambini and Stenholm 1984) and the use of multioscillator techniques (using aplanarity, magnetic fields or some such effect to split the frequencies of the corotating beams of different polarization, and then sensing some difference of beat frequencies).

One approach to the removal of locking is the application of some bias to avoid the lock-in region near a null of rotation rate. The Zeeman laser is a standard case (Chow *et al* 1980); others include the use of optical biasing (Anderson *et al* 1980), and the use of intracavity phase-conjugate coupling (Dennis and Diels 1994). The use of femtosecond pulsed lasers, such as mode-locked dye lasers, also reduces the beam coupling (Lai *et al* 1992). Biasing gyros can introduce light-power-dependent noise (Doerr *et al* 1994). Bretenaker *et al* (1993a) showed how diffraction effects allowed control of the locking phenomenon. A number of other ingenious schemes have been proposed; as just one example, Konopsky (1996) has proposed a new type of optical gyro of quasiactive design, avoiding locking problems, using an electro-optic oscillator as a component.

3.9. Limitations on resolution from pulling, and scaling rules

Equations (12) and (11) show that the importance of the lock-in threshold frequency l (equation (14)) rests in its ratio Λ to the Sagnac frequency f. For example, weak pulling effects depend quadratically on this ratio (equation (12)). From equations (14) and (2) we find that

$$\Lambda = \frac{l}{f} = \frac{\Omega_\Lambda}{\Omega} \qquad \Omega_\Lambda \sim \frac{cs\lambda^2}{4\pi \, \mathrm{d}A'} \tag{23}$$

where Ω is the mechanical rotational frequency and A' the projected (latitude-reduced) ring area. The quantity Ω_Λ is thus a characteristic angular frequency for describing the effectiveness of lock-in in a ring laser, whose ratio to the applied rotational frequency sets the scale for pulling effects. Note that while the lock-in frequency decreases linearly with an increase in ring dimension (say P), this characteristic frequency Ω_Λ decreases quadratically as P increases, the Sagnac signal increasing linearly (see section 1.3). Pulling effects expressed as a fractional frequency shift depend quadratically on Ω_Λ. On this showing the accuracy of the Sagnac frequency increases as P^4 with scaling, further increasing the potential advantage in using large rings (see sections 1.3, 3.5, 5).

A dimensionless parameter κ for the accuracy of a ring-laser gyro (or lack of sensitivity to pulling) might be defined as the ratio of the Earth's rotation to this characteristic frequency:

$$\kappa = \frac{\Omega_E}{\Omega_\Lambda} \sim \frac{4 \times 10^{-3} A'}{s}. \tag{24}$$

For an avionics gyroscope, with $A' \sim 0.02$ m^2, even with $s \sim 10^{-3}\kappa < 1$, the accuracy is low, and the gyro would lock before detecting the Earth's rotation. To avoid this, dither (mechanical oscillatory rotational motion, applied piezoelectrically) is applied, so as to 'shake' the ring out of lock-in except for a small proportion of the total time; see for example Wilkinson (1987). The first Canterbury ring laser (section 5.2) made no provision for such complexities since with $A' \sim 0.5$ m^2, and taking the optimistic s value above, $\kappa > 1$ and it should prove possible for the laser to be unlocked by the Earth's rotation alone; this was indeed achieved.

One practical consideration reduces the quartic scaling advantage of large rings referred to above. The larger the ring, the less is the temperature or pressure change that will cause a given absolute amount of expansion of any subperimeter z_n (as compared to a wavelength) and so cause the backscatter pulling effects to cycle into and out of effect. We therefore reduce the advantage of a large ring laser on this score to a cubic advantage, i.e. an accuracy of fractional pulling scaling as P^3. Of course, this is still a considerable incentive for moving to larger rings.

4. Quantum shot noise

4.1. Introduction

The quantum nature of light introduces shot noise into any amplitude or phase measurement. The smaller the number of participating photons, the greater is the proportional difference made to each beam phase and so the Sagnac phase by the loss of any one photon from the beam. Reaching this quantum limit in a ring laser requires sufficient development to overcome other noise sources such as $1/f$ noise in comparison, and has been a historical challenge, the achievement being documented by Dorschner *et al* (1980). First we state the key formulae.

A sinusoidal oscillator with white frequency noise generates a Lorentzian line (Siegman *et al* 1967). We write the irreducible quantum noise contribution W to the full width-at-half-maximum power of the interferometric signal from a ring laser (assuming full inversion) as

$$W = \frac{2\pi h f_0^3}{Q^2 P_o}. \tag{25}$$

The corresponding one-sided power spectral density of the frequency fluctuations is white: $S_{\Delta f} = W/\pi$.

Associated with this is a precision for the detected Sagnac frequency (centre of the line) of

$$\Delta(\delta f) = \sqrt{\frac{h f_0^3}{Q^2 P_o T}}. \tag{26}$$

Note that the latter, and not the former, is reduced by taking longer runs. This in turn translates into a limit on its sensitivity to rotation of

$$\Omega_N = \frac{c P}{4 A Q} \sqrt{\frac{h f_0}{P_o T}}. \tag{27}$$

In these equations f_0 is the laser frequency, P_o the rate of power loss, Q the quality factor, P the perimeter, A the area, and T the observation time. All authors agree on these basic equations, modulo numerical factors (Sargent *et al* 1974, Statz *et al* 1985, Chow *et al* 1985, Wilkinson 1987, Stedman *et al* 1995c). The factors in the above equations apply to the noise in the beat frequency of ring lasers with full inversion and uncorrelated pumping, introducing a factor 2 or $\sqrt{2}$ in these equations because of the need to combine noise in two beams; they follow King *et al* (1996). See also Siegman *et al* (1967) and Cresser *et al* (1982a, b), Cresser (1982) (who for example proves the Lorentzian form of the spectrum) for derivations.

4.2. Expanded theory of quantum noise

As with the Sagnac effect itself, a wide variety of proofs now exist for these standard equations such as equation (25). Although the formulae are reasonably well established, quite different statements are made regarding the physical origin. They are not, therefore, inconsistent; a mere reordering of operators in a quantum calculation can convey a totally changed interpretation which is equally valid, and it is remarkable that an 'electrical engineering' approach with totally different appearance from the following gives the same answer (Haus 1995, Verdeyen 1995). Most derivations from quantum optics emphasize that within that context the effect is associated with the random phase of the spontaneously emitted photon, as opposed to the locked phase of the stimulated photons. In practice there are many contributions to P_o, including vignetting, mirror imperfections etc, and all losses should be included in P_o. All losses, however, have to be made up for by stimulated emission, and the inevitably accompanying spontaneous emission will perturb the phase of the phasor describing the net field into performing a random walk. It will also perturb the polarization, leading to a quantum diffusion of the polarization also (van Eijkelenborg *et al* 1995).

A simple demonstration of these equations is given by following Dorschner *et al* (1980). Let $\bar{n}$ be the mean number of photons in each counter-rotating mode (of nominal frequency f_0), and τ, or $Q/(2\pi f_0)$ (section 1.6) its lifetime. Then $\bar{n} = \tau P_o/hf_0$, where P_o is the power loss of the mode. The rms number fluctuation of a coherent state $\Delta n \equiv \{\overline{(n-\bar{n})^2}\}^{\frac{1}{2}} = \sqrt{\bar{n}}$, so that the minimum uncertainty number-phase Heisenberg relation $\Delta n \Delta \phi = \frac{1}{2}$ gives $\Delta \phi = 1/(2\sqrt{\bar{n}})$. This is the rms phase excursion for one mode over its natural lifetime (a few tens of microseconds in C-I). The phase performs a random walk of this magnitude on this timescale. In a measurement time T the number of steps of this walk will be $N = T/\tau$, and the magnitude of the random part will scale as $\sqrt{N}$: $\Delta \phi_T = \sqrt{N/4\bar{n}}$. The change in phase at the beginning and end of a run define the frequency of the run, and since the variances of Gaussian processes associated with these terminal measurements add, $\Delta \omega = \Delta(\phi_f - \phi_i)/T = \sqrt{2}\Delta \phi_T/T = 1/\sqrt{2\tau \bar{n}T}$. The Sagnac frequency δf accumulates the uncertainty in the frequency measurements for each counter-rotating mode, by another $\sqrt{2}$ factor when they are uncorrelated. Hence $\Delta(\delta f) = 1/(2\pi\sqrt{\tau \bar{n}T})$, giving equation (26). Equation (27) follows from this with equation (2). Note that lengthening the run increases the precision of these line-centre measurements for such white noise. The same is not true for $1/f$ noise, which, however, scales as Q^{-4} (Sayeh and Bilger 1985).

The (time-independent) width of the Sagnac line, as opposed to its rms frequency fluctuation, has a Schawlow–Townes form and may be defined as the full-width-at-half-maximum power $S_{\Delta f}$ of the power spectral density. Statz *et al* (1985) (see also Sargent *et al* 1974, Chow *et al* 1985) show that equations (25) and (26) are related by $S_{\Delta f} = T[\Delta(\delta f)]^2$, because the variance of δf is directly related to the decay constant of the autocorrelation function of the electric field phasor $\tilde{E} \propto \exp i\phi(t)$ and so to its Fourier transform, the spectrum. Walls and Milburn (1994) give a related calculation. The white noise is filtered by the square window of length T afforded by the run, whose modulation transfer function should be integrated with the power spectral density to give the variance in the frequency fluctuations.

The Lorentzian quantum-noise spectrum produced by discrete Fourier analysis of a periodically sampled signal should not be thought of as a smooth curve. King *et al* (1996) mention how in numerical Fourier analysis of a periodically sampled signal, the number x in each Fourier bin is a sample of a distribution $p(x) = x \exp(-x^2)$, but with a frequency-dependent scaling for the variable x so as to produce the line shape. The

Lorentzian curve of the quantum-noise spectrum is the mean height $\bar{x}$ of the bin entry in the Fourier spectral histogram, not an envelope, and the standard deviation of the values in each bin is $0.52\bar{x}$. For a signal to be visible demands more than that it should add a line to a smooth Lorentzian wing; it has to change $\bar{x}$ sufficiently to make the changed distribution experimentally distinguishable. The distribution width can be reduced as much as is necessary (a factor $1/\sqrt{N}$ say) by averaging N runs.

4.3. Limitations on resolution from quantum shot noise, and scaling rules

Limitations arising from the quantum shot noise limit, while of fundamental importance, are not absolute in the sense of being irreducible in magnitude. First, as with the Sagnac signal (section 1.3) and the fractional effects of pulling (section 3.9), their significance is greatly reduced by scaling the dimensions of the ring laser. Secondly, in contrast to these cases, they also are reduced as the mirror quality is improved; the cavity finesse (section 1.6) as much as the area is a crucial parameter for characterizing the sensitivity of a ring laser, which should be 'sharp' as well as 'big'. The quality factor Q entering the basic equations not only has this dependence on mirror quality, but also scales linearly with perimeter P (see section 1.6). Equations (25), (26) and (27) therefore scale as P^{-2}, P^{-1} and P^{-2} respectively, if the total power loss P_o does not change with the perimeter. Bilger *et al* (1996) suggest that $P_o \propto P^{-1}$, if single-mode performance is required, because of the reduction in free spectral range with increasing P and so the progressively increasing difficulty in maintaining monomode operation; in this case the scaling dependences become $P^{-3/2}$, $P^{-1/2}$ and $P^{-3/2}$.

To see a quantum shot noise linewidth in a HeNe laser greater than, say, 10 frequency bins of the Fourier analysis ($10/T$) requires $T \gtrsim 10^{-11} Q^2 P_o$. The right side scales as $P^{3/2}$, and present high-quality factors of supercavities make quantum noise less important in large rings. The same is even more true for $1/f$ noise. Nevertheless, this is certainly achievable for moderate run times.

4.4. Quantum optical modifications of standard quantum limits

It has been intriguing within the (explosively developing) discipline of quantum optics to search for ways of circumventing the 'fundamental quantum' limit of such equations. A ring laser certainly stands to benefit in principle from techniques which perforate the 'standard quantum limit' associated with quantum noise (or photon shot noise). A variety of ambitious schemes has already been proposed. Quantum non-demolition measurements are one option.

Two techniques deserve special mention. First, squeezed light may be employed. This may be done by introducing a nonlinear element into the cavity to induce squeezing in the observable of interest (Marte and Walls 1987). At the present time, the expected or achieved reductions in noise are hardly an order of magnitude, and in practice would be offset by the degradation of cavity quality if extra elements are required in the cavity. More plausible is the use of squeezed light by injection in a port (Haus *et al* 1991, Polzik *et al* 1992, Boivin 1995). Such attention to the effects of injecting squeezed light into one or more ports of an optical ring cavity or the effects of correlated beam pumping, in avoiding intracavity elements, may prove beneficial in larger and high-resolution rings.

Secondly, correlated excitation schemes for the two modes, with counterpropagating beams being pumped from two different transitions in a three-level scheme, have been proposed. These have the effect that the net quantum noise in the beat frequency signal is less than the uncorrelated combination of the rms fluctuations from each beam given above.

This has been pioneered by the work of Scully (1985) and Scully and Zubairy (1987); the application to a ring-laser gyroscope is proposed in Scully (1987) and to a maser gyroscope in Scully (1996); see also Orszag and Retamal (1991).

Schleich and Scully (1988) (see also Schleich *et al* 1988) show that this may be understood geometrically and in terms of equation (10) and section 3.7. The relative phase of the two counterpropagating modes, while varying linearly with time because of the Sagnac effect, is otherwise strictly locked, as in equation (10), despite the normally destabilizing (diffusional) effects of spontaneous emission. This is because, when the appropriately correlated pumping is employed, the fluctuations in the electric field phasors are so correlated as to preserve this relative phase.

In the meantime, working within the standard quantum limit and lowering its value by standard means, that is, by raising Q, and also P still permits much progress. This, together with parallel strategies for reducing backscatter-induced drifts etc, is the strategy explored in this article.

5. Precision rings

5.1. Introduction: large rings and scaling rules

As shown in sections 1.3, 3.9 and 4.3, the sensitivity of a He–Ne ring laser as a tool (e.g. a gyroscope) depends critically on its physical dimensions (perimeter, area) and the mirror quality (finesse). The advent of supermirrors, now to mirrors with total losses of 1 ppm, has made dramatic improvements as regards finesse. The present rate of progress is much slower than formerly but can be expected to continue since mirror quality is still well removed from fundamental constraints (Bilger *et al* 1994). The best option for short-term progress is that of scaling up the dimensions of the ring laser. While the formal benefits are obvious from sections 1.3, 3.9 and 4.3, and such scaling arguments have been important in the design of large perimeter rings (Bilger *et al* 1996) in practice other considerations are also important.

The ring laser as an active frequency generator lends itself to practical utility quite apart from scaling arguments (Anderson *et al* 1994). Early optical methods were replaced by electronic methods even for Sagnac interferometers, with consequential improvements in precision which anticipated the benefits of frequency measurement as opposed to phase measurement; nevertheless historically the introduction of the ring laser made a qualitative change. This is partly because obtaining the equivalent resolution in a passive cavity is technically more demanding and so was delayed, and partly because an active ring laser is a pair of oscillators in the optical regime, so that the ring can now be integrated into a servo-system in a straightforward and well defined manner by electronic control and processing systems. This aspect still awaits full development, and has major consequences for improving stability for big rings. Piezoelectric elements for path-length control coupled with frequency references such as the abundant I_2 molecular resonances can stabilize the average of the mode frequencies in the cavity, making their splitting much less dependent on changes in absorption/gain and so dispersion with mode frequency drift. Similarly, precise control of the oscillation amplitude, electronic and computational (Fourier transform and signal analysis) noise reduction through filtering techniques, sideband analysis techniques etc (the output being highly monochromatic) all give good promise of maintaining and improving performance as rings are scaled up in size.

It had been widely felt that larger rings do not achieve a worthwhile increase in sensitivity in view of their (undisputed) increased sensitivity to mechanical and thermal

instability. An analysis by Simpson at an AGARD meeting of the Royal Aeronautical Society of London in February 1987 led to an order-of-magnitude bound on the perimeter of $P < \Pi \sim 60$ cm on the basis of more fundamental quantum-noise considerations. However, this analysis is inadequate (Stedman *et al* 1995b), and has been revised somewhat by Bilger *et al* (1996), who take into account the need to servo the radio-frequency excitation power so as to avoid more than one longitudinal mode (as the perimeter is increased, the free spectral range decreases, constraining the margin of operation) and who state that the signal/noise ratio—expressed as the ratio of the Sagnac frequency to the quantum frequency noise (equations (2) and (27))—scales as $P^3(1 - \exp\{-[\Pi/P]^2\})^{1/2}$, i.e. as P^3 for $P < \Pi$ and as P^2 for $P > \Pi$. Though this revised argument still ignores a number of factors, such as the eventual limitation in detector noise, it has removed one discouragement to scaling.

Considerations of mechanical stability certainly have justified the cautions of Rodloff (1987), and have in the past imposed a practical limit on P of order Π. Recent progress in materials science has largely overcome this barrier. First, solid-state research has provided materials whose thermal expansion coefficients are two orders of magnitude less than that of fused silica, and has also provided the technological expertise of being able to produce homogeneous large plates (Anderson *et al* 1994). A significant step forward in ring-laser technology to 'supergyroscopes', larger than have heretofore been considered practical, is now underway (Rodloff 1994, Anderson *et al* 1994), marking the end of a reluctance to move to rings with perimeters P greater than a few tens of centimetres.

All proposals known to us consider square rings. The use of one extra mirror over the minimal triangle has advantages in reducing backscatter through the near-ideal incidence angle of $45°$, in permitting alternative choices of polarization, and in maximizing the signal/loss ratio A/PN, where N is the number of mirrors and, as before, A is the area and P the perimeter (Stedman *et al* 1993). In addition, the s reflectivity of a supermirror designed for normal incidence is in fact greater at $45°$ incidence than at either the design angle of $0°$ or the angle appropriate for a triangular ring ($30°$). A square ring has the disadvantage of being vulnerable to polarization changes and so various frequency drifts with changes in the degree of aplanarity.

Second, the quality factor of the cavity depends largely on the reflection losses of the mirrors (section 1.6), and the shot (quantum) noise is proportional in turn to the inverse square of the quality factor Q (section 4). Thanks to the initiative of the optical gyroscope industry, multidielectric SiO_2–TiO_2 layer mirrors have been developed in the visible region with total losses of 1 ppm, nor is this the ultimate (section 1.6). Rayleigh scattering in the gas sets a practical limit on the quality factor of a ring gas laser, but this limitation is not yet important.

The location of such big rings is critical. Buildings have substantial mechanical noise; even basements should be avoided, along with cultural (man-made) noise in cities and near traffic routes for example. Interactions between land and ocean—breakers on the beach—produce local microseismic fluctuations in the frequency range 0.1–1 Hz (Levine and Hall 1972, Aki and Richards 1980). Avoiding such frequency bands may bring something of a renaissance for low-frequency electronics, as frequency or amplitude modulation techniques may then be optimally applied in the microhertz regime.

5.2. C-I: design

The frequency difference between two laser modes in a (linear) cavity has been monitored to millihertz precision (Hall 1993). The Sagnac frequency difference lends itself to similarly precise measurement.

A recent facility is the C-I ring-laser system designed by Professor Hans R Bilger of Oklahoma State University, Stillwater, OK, USA and built at the University of Canterbury, Christchurch, New Zealand (Stedman *et al* 1993, Anderson *et al* 1994; figure 6(*a*)). This He–Ne ring laser system ($f_0 = 473.6$ THz, $\lambda = 633.0$ nm) is defined by a rectangle of four supermirrors, nominally 99.9985% reflectors and having measured total losses at manufacturing in the range 8–14 ppm, of which up to 10 ppm constitute the (designed) transmission loss, and 3–5 ppm are measured as scattering loss.

In what is of necessity a cheap construction, the mirror holders are placed directly on a 1.2 m × 1.2 m × 25 mm Zerodur plate, itself mounted on a 700 kg granite block. Stainless-steel boxes, which are sealed by Viton O-rings on the Zerodur, surround but do not touch these mirrors, and the connecting Pyrex tubes (id 10 mm) do not intersect the beam, which is always within the lasing gas. Part of this tube is a narrower fused silica tube (id 4 mm, length 200 mm) with a cylindrical radio-frequency exciter surrounding it. Since the beam never intersects a solid surface, maximal quality factors become feasible. Alignment of the mirrors is done in the open air with the cover plates removed and prior to pumpdown.

Its perimeter of 3.477 m was determined from rf measurements of the free spectral range, or longitudinal mode frequency separation $c/P = 86.345$ MHz, and its area of 0.7547 m^2 was derived from P and the measured linear dimensions. The quality factor Q has been based on two different measurement techniques, one involving a ringdown time when radio-frequency pumping is turned off, and the other involving the asymmetry in the cavity response to a swept frequency (Li *et al* 1991). Measurement of the ringdown time has given values up to $\tau = 25$ μs, and hence a quality factor Q up to 7.5×10^{10}.

The ring laser is operated in monomode with a radio-frequency pump power of order a few watts, a circulating power of order milliwatts, and an exit beam power of order nanowatts. Monomode operation is attained through the starvation of all but one longitudinal mode; the radio-frequency power is servoed against the mean intensity of one beam so as to stabilize the gain curve so that only one longitudinal mode lases. The choice of mirror radii ensures a reasonable frequency separation between longitudinal and the Hermite–Gaussian modes, although these can participate unless vignetted out by the 4 mm id fused silica gas tube in the excitation region. Transmitted components of the countercirculating beams are mixed at a beam-splitting prism external to the laser.

To provide maximal mechanical and thermal stability, C-I is mounted horizontally in an underground bunker (latitude $\Lambda = 43°\,34'\,37''$ S, which introduces a factor $\sin\Lambda$, and longitude $172°\,37'\,20''$), the pier being a cubic metre of concrete tied into the basaltic volcanic rock of Banks Peninsula. (A graphic description is given by Silverman 1992.) A sidereal day of 23 h 56 m 4.09 s corresponds to an angular velocity Ω_E of the Earth of magnitude $7.292\,12 \times 10^{-5}$ rad s^{-1}. Equation (2) gives an Earth-rate Sagnac frequency for a horizontal HeNe laser at this latitude of $\delta f_E = 317.6A/P$. The Sagnac effect from the Earth's rotation thus generates (from equation 2) a beat frequency $\delta f_E = 68.95$ Hz, which is highly amenable both to audio-frequency electronic processing and to monitoring by a speaker. A simple check that C-I is in the Southern Hemisphere is to press a corner of the table with the lightest of finger pressure: if the sense is clockwise, the pitch of the Sagnac signal audibly rises before it falls. The scale factor G of this instrument (the ratio of the angular frequency of the interferogram to the normal projection Ω' of the mechanical angular frequency) is 8.62×10^6. (In gyro-industry jargon, this is 6.65 counts per arcs.) As for mechanical stability, the proximity of a housing suburb and attendant traffic makes it less quiet than the more remote seismic stations; as for thermal stability, various improvements over the years have attained 1 mK h^{-1} over some hours.

A standard method in the optical-gyro industry of isolating the phase information is

to count zero crossings of the detector signal. An alternative technique is to use the full interferometric waveform to construct the analytic signal, so recovering pure phase information (Stedman *et al* 1995c). The real signal $X(t)$ is converted to the analytic signal $Z(t) = X(t) + iY(t)$, where $Y(t)$ is the Hilbert transform of $X(t)$. This is achieved most simply by noting that $\mathcal{Z}(\omega) = \mathcal{F}(Z(t))$, the Fourier transform of $Z(t)$, differs from $\mathcal{X}(\omega)$ principally by having all negative frequency components set to zero in the latter (what is a cosine in the real part is a sine in the Hilbert transform), and their negative frequency parts cancel on forming the analytic signal. This gives a minimum-phase estimate of the analytic signal, as is appropriate for a passive and causal physical system. The instantaneous phase $\Phi(t) = \arg(Z(t))$ may then be derived by unwrapping the principal-value phase. For signals whose harmonics form a geometric progression, the instantaneous phase ψ, however derived, has the same harmonic structure.

In practice the drifts associated with thermally induced variations in pulling (section 3.1) are a major problem. We apply subsequent numerical dedrifting, eliminating the low-frequency drift components in the instantaneous phase $\Phi_d(t)$ derived from the analytic signal, below a cut-off frequency f_{cut} of say 0.0005 Hz. Clearly one can track almost any carrier as closely as desired and so reduce its real frequency noise apparently to zero by taking a sufficiently high cut-off frequency f_{cut}, just as one can in principle electronically lock as close as desired to a drifting line by choosing an appropriate time constant for the electronic servo loop. In both the electronic and the numerical case there is the choice of cut-off frequency; all amplitude noise, and all frequency noise in the range f_{cut} to the Nyquist frequency is retained. Numerical dedrifting is effective and justifiable for clarifying sidebands whose frequency is significantly greater than f_{cut}, and this allows useful application for microseisms (section 7.4). However, it has not been consistent with a demonstration of quantum noise (section 5.3).

Short-term and crude adjustment of the net backscatter phase ζ to reduce pulling is achieved by moving weights on the Zerodur table. This flexes the table, changing the various partial perimeters z_n which appear in equation (19).

Until recently, piezo control of a mirror has not been of great practical value in this project. This has mainly been because of the much more rapid degradation of the vacuum with available piezoelectric devices (this has recently been largely overcome, though outgassing from the O-rings still limits data runs from C-I to a few weeks). It reflects also the fact that any piezoelectric element itself compromises thermal stability through its intrinsic thermal expansion coefficient. Finally, perimeter stabilization alone is ineffective in reducing pulled beat frequency drifts over time scales of order minutes, because stabilizing the free spectral range does not stabilize all the partial perimeters z_n.

5.3. C-I: observations

In practice the above strategy for achieving monomode operation proves to be very successful in C-I. The best ringdown measurement of cavity lifetime in C-I gave $\tau = 25\ \mu$s, which translates into a quality factor $Q = 2\pi f_0 \tau = 7.5 \times 10^{10}$. The associated finesse $F = \lambda Q/P = 14\,000$, less than the quality factor ($Q_{max} = 8.6 \times 10^{11}$) and finesse ($F_{max} = 160\,000$) commensurate with the mirror specifications at manufacture (total loss per mirror $1 - R$ of $\leqslant 10$ ppm) because of contamination and recleaning, the lesser figure corresponding in fact to a total loss per mirror of 115 ppm. The total power loss P_o is best estimated from the measured Q, the output beam power P_t at any port, and the known power transmittance of a mirror. In C-I P_o is typically in the range 10^{-7}–10^{-6} W (Stedman *et al* 1995b). For any given set-up P_o is determined to within an order of magnitude by the
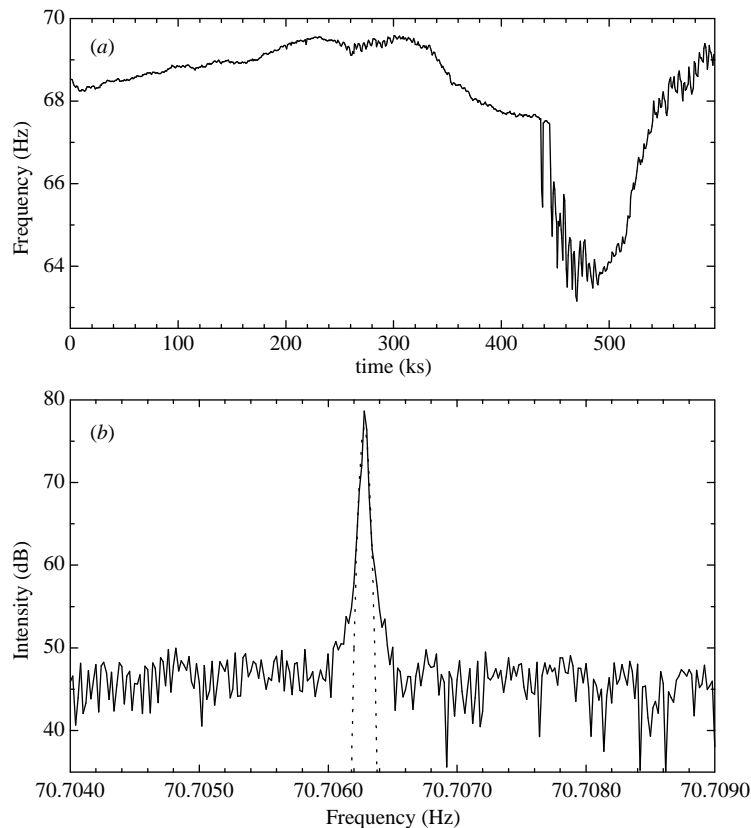
Figure 5. Results from an experimental run with C-I. (*a*) Frequency drift. (*b*) Dedrifted spectrum (Stedman *et al* 1995b).

requirement that all modes but one be starved, which essentially defines the available net gain and therefore (from Q) the circulating power and its loss.

With numerical dedrifting removing frequencies up to say 500 μHz, a narrow Sagnac line, of order microhertz in width, is found in the spectrum of the phase signal (figure 5). The white-noise baseline or 'grass' will be associated with the optical noise of all spontaneous emission in the gain curve at the detector and all mechanical noise from air-pressure variations, microseisms, etc. Even though C-I is sited 30 m beneath a Christchurch City Council park reserve, this background white noise is perceptibly affected by rush-hour suburban traffic in the general area.

It was a puzzle in earlier work that estimates of laser linewidth and quantum noise (from equation (25)) are larger than these widths, and are typically several tens or hundreds of microhertz (Stedman *et al* 1995b, c). This is because the dedrifting procedure adopted simply removed the dominant components in the Fourier spectrum of the quantum noise of the instantaneous phase. Although the frequencies removed are a very small fraction of the Nyquist frequency f_n this phase noise is not white, but varies approximately as

$1/f$ (more accurately as $1/\sin(2\pi f/f_n)$ (King *et al* 1996)). Hence the absolute frequency resolution was exaggerated in earlier reports on C-I. For the study of sidebands (section 6) including seismic studies in a reasonably narrow frequency band and more particularly field-modulation effects (sections 6.3 and 9), however, such dedrifting of those frequency bands in which no interesting signal is expected remains a practical way of reducing widths to microhertz levels.

The results quoted here derive from monitoring the intensity of a single beam, so that we depend on pulling effects to modulate the beam intensity and reveal the Sagnac fringes. Even so, signal/noise (defined as $20 \log_{10} V_s/V_n$) was of order 30 dB. In the interferogram, 65 dB signal/noise has been achieved. The full-width-at-half-maximum power of this Sagnac line is 6.2 μHz, and its position can be specified to 140 nHz, although the drifts numerically removed are typically of order hertz per hour or more.

The quantum shot noise limit of the sensitivity of C-I for measurement of an angular rotation (equation (27)) may be estimated from the above C-I parameters (P_o being 1 μW) as $\Omega_N T \sim 6 \times 10^{-9} \sqrt{T}$. This order of sensitivity has been achieved in practice (section 7.2). The observed white-noise floor for C-I in sensing local rotations is of order 150–300 prad. According to this quantum-noise formula, for $\Omega_N \sim 100$ prad s^{-1} or 20 microarcs s^{-1}, we need $T \sim 1$ h.

The basic results of the pulling theory of section 3 have been confirmed, including the geometric progression of harmonics (Stedman *et al* 1995b). Some deviations are under study; for example, asymmetric waveforms and pushing. The analytical solutions given earlier in this paper cover, at least approximately, a majority of the cases of interest and importance provided isotopically enriched neon is used and that l is not greater than f.

The harmonic structure of the interferogram and of the single-beam intensities, while also (if approximately) of the character of a geometrical progression with the pulled frequency as the fundamental, is in general less rich than that of the instantaneous phase, the amplitude variations taking strength from the higher harmonics. The phase relationships between these various signals, like the lock-in threshold, is a sensitive function of the net backscatter phase and so of the mirror separations. Removing the associated drift of the pulled frequency requires a different kind of stabilization method to the perimeter stabilization normally used to stabilize a mode in a cavity. Privatov and Filatov (1977) have described a method in which the relative phase of the intensity fluctuations in the single beams, which is backscatter-phase dependent (see section 3.6), is monitored and used to servo the phase of a reinjected beam to provide significant stabilization.

5.4. C-II

A ring laser, C-II, with greatly superior construction to C-I is being tested in location at Cashmere, Christchurch (figure 6(*b*)). As for C-I, the design is fundamentally that of Professor Hans R Bilger of Oklahoma State University without the very severe cost limitations that were essential for C-I. Major financial support, overall direction and the overseeing of manufacture has been provided by the Institut für Angewandte Geodäsie and the Forschungseinrichtung Satellitengeodäsie of the Technische Universität München (Professor M Schneider and Professor Dr U Schreiber). The University of Canterbury have collaborated with these groups in this enterprise in a variety of ways. The contract for construction was tendered to Carl Zeiss.

This system has much improved engineering in a variety of areas such as ultrahigh vacuum technology (e.g. the ultrahigh vacuum-compatible bonding of metal to Zerodur), a better definition of beam geometry and mechanical decoupling from the base. It also has
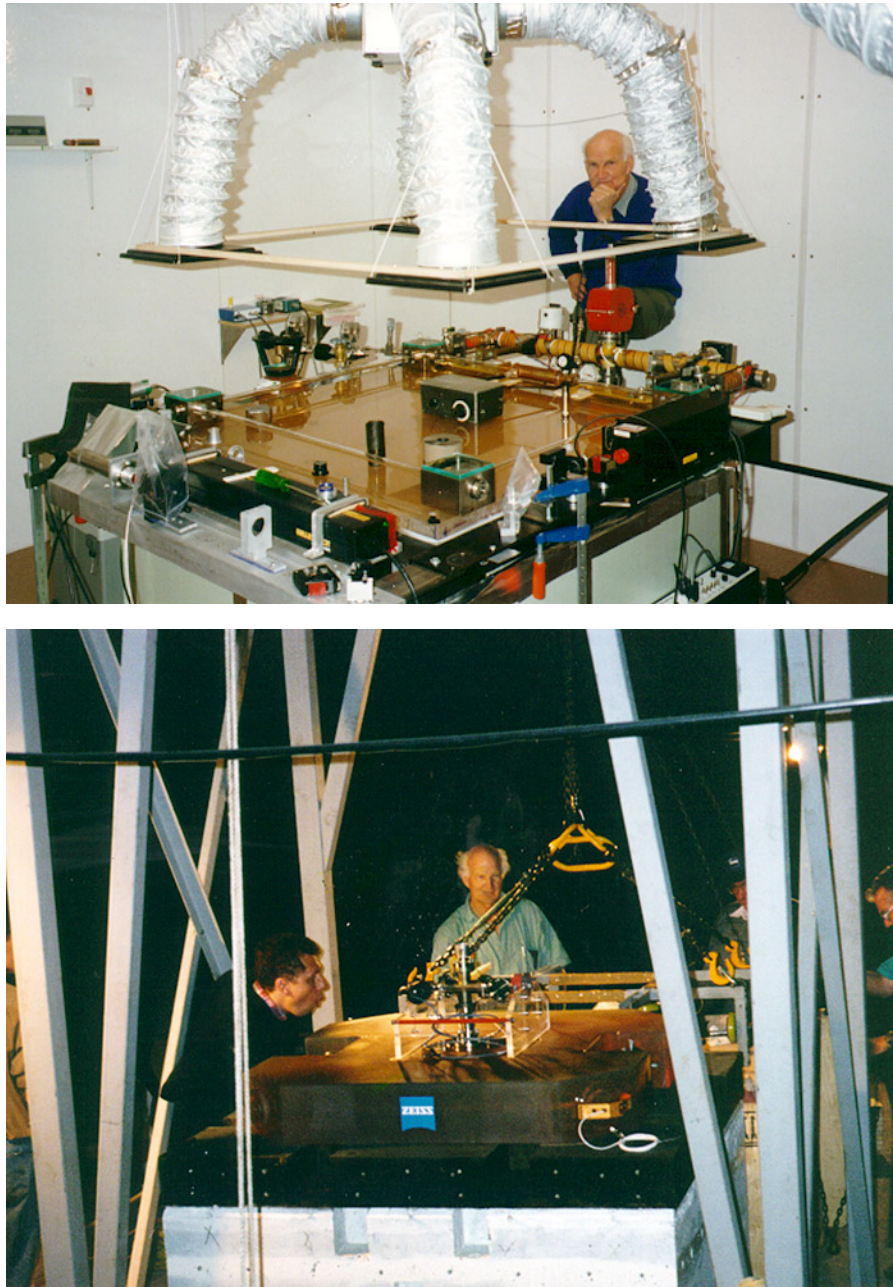
Figure 6. Large ring-laser gyroscopes at Cashmere, Christchurch, New Zealand. (*a*) C-I, with Clive Rowe. (*b*) C-II being installed, January 1997, with Ulrich Schrieber and Clive Rowe.

reduced thermal sensitivity. SiO_2–TaO_5 supermirrors were provided by Research Optics Ltd, Boulder, CO, with total losses of $\leqslant 1.2$ ppm. These losses include transmission, and

the detected beam has a typical power level from 60 to 400 pW. These mirrors give a greatly improved quality factor, the design value being $Q = 3 \times 10^{12}$. C-II avoids many of the problems of C-I by using the aircraft-gyro construction, by which the laser cavity is drilled out of a monolithic block of low-expansion ceramic, corners are precision-machined and mirrors are attached by molecular adhesion. Schott-Mainz provided and machined a monolithic piece of highest-quality Zerodur (with a measured linear expansion coefficient $\sim 5 \times 10^{-9}$ K^{-1}), itself 1.2 m × 1.2 m × 18 cm, and weighing ~ 0.65 t.

The lasing path is a square of side 1 m. At Christchurch this gives a predicted Sagnac frequency δf_E from the Earth's rotation of 79.40 Hz. Bore holes of diameter 2 cm follow the square lasing path and two diagonals. As for C-I, radio-frequency excitation is used. The two diagonally opposite mirrors are flat, one of these being adjustable by the use of a thermally compensated piezo system external to the ring which flexes the thinned plate mount of this mirror, and the other mirror giving ports to the main detectors. The other two mirrors have a 6 m radius of curvature. This gives elliptical spots at the two curved mirrors, with the larger vertical size of 790 μm. The mirror mounting flats are machined to a flatness of less than 1 μm, and the angle to the borehole axis is 45° to an accuracy of 10 arcs; a tolerance of 30 arcs guarantees adequate alignment for lasing, with beam displacement being everywhere within 1.8 mm of the design path. The single piezoelectric mirror driver is built with internal compensation for thermal expansion, greatly reducing the sensitivity of this component to temperature to a level approaching that of the Zerodur block (Bilger *et al* 1996).

The purpose of this machine is to anticipate and test construction techniques for a still larger planned ring, 'Grossring' (G), a device scaled up from C-II's 1 m square to 4 m square (section 5.5).

Initial informal results suggest that C-II is operating well within specification as regards quality factor and mirror loss. Extended results will be reported elsewhere by the team.

5.5. Proposed rings

Krainov and Zharov (1996) have reported the design for a square ring (presumably passive) resonator of side 3.1 m at the Sternberg State Astronomical Institute, Moscow, for monitoring the Earth's rotation. Since the proposed base is steel, it is planned to servo the ring parameters heavily so as to maintain beam alignment. I am unaware of further details of this project.

An even larger and more stable ring, and a laser as opposed to a resonator, is being proposed by the German Research Group for Space Geodesy (FGS), a cooperative effort of the Technische Universität München, the German Geodetic Research Institute with its two departments in Munich and Frankfurt (Institute of Applied Geodesy) and the University of Bonn (Geodetic Institute), pursuing space geodesy research and in particular fluctuations in the Earth's rotation via a wide variety of techniques including intercontinental very long baseline interferometry (VLBI, based on radar measurements on astronomical objects), satellite laser ranging, lunar laser ranging, GPS and seismometry. Under Professor M Schneider, this group is in collaboration with the Oklahoma State University, Stillwater and the University of Canterbury, New Zealand, and is planning a G with an area of 16 m^2 and utilizing state-of-the-art technology.

G is intended to measure the Earth's rotation rate with sufficient precision to gain relatively short-period (and not well known) fluctuations in the Earth's rotation rate, typically several milliseconds per day, i.e. at the level of 10^{-8} of the Earth's rotation rate Ω_E (section 7.7). Such an instrument will complement the present above-mentioned techniques

at the Fundamentalstation Wettzell (Bavaria, Germany), the measurement and research laboratory of the Institut für Angewandte Geodäsie. G will measure such rotations on relatively short time scales (hours to days), and much faster data analysis will be possible; VLBI data processing requires the physical transport of terabytes of information, since signals are hidden in noise, and so takes five days.

Such a system will help to fill a sizeable gap in our knowledge of the spectrum of fluctuations of the Earth's rotation, and will have immediate application in helping to relate the international terrestrial reference frame to the celestial reference frame. It will complement the use of precise (milliarcs) angular data from VLBI and optical interferometry and precise (cm) distance data from satellite and lunar laser ranging as input data to satellite geodesic models for such purposes, in a manner which is relatively rapid and totally independent of their systematics, thus enabling synoptic analysis and intercomparisons between the techniques.

Two aims of this ring-laser development are: the improvement in short-term noise by increasing the quality and size of the ring, and the increase in long-term stability to produce long time series in order to sense slow phenomena, kinematic or otherwise, in the Earth–Moon–Sun system (see section 7.7). The limits on an independent Sagnac experiment will then no longer be associated with the limitations of the experimenter's apparatus, but will be determined by the stability of the Earth itself. It is the Earth's noise—the local power spectral density of the mechanical movements of the Earth—which is the ultimate limit for large Earthbound 'Grossringe' (big rings).

6. Sideband detection

6.1. Introduction

Recording a ring-laser interferogram gives the time-domain representation of a novel spectroscopy. The standard method of readout for a ring gyroscope involves essentially the counting of the zero crossings of the interferometric output. However, much more information is capable of being extracted. With the advent of relatively large ring-laser systems, information in the spectrum other than the position and width of the dominant line is of interest.

Analysis of the sideband structure gives information on the fluctuations in the local rotation rate. Just as the information on the absolute average rotation rate is enshrined in the carrier, information about the absolute magnitude of subsidiary terms in the rotation rate are enshrined in its sidebands. AM and FM effects can be distinguished in practice by comparing the average phase of the upper and lower sidebands with that of the carrier. With systems such as C-I (section 5.2), this opens a previously inaccessible frequency range, from millihertz to microhertz, for laser spectroscopy. This range is of geophysical interest, for example in the studies of seismic events and tidal effects.

6.2. Basic sideband theory

When the applied rotational frequency f is constant, the instantaneous phase ψ of a ring-laser beat signal satisfies the Adler pulling equation, equation (10), where the lock-in threshold l is constant. Suppose now that a frequency-modulated rotation is applied:

$$f = f_e - Sf_m \sin 2\pi f_m t. \tag{28}$$

When integrated in time, this gives the phase

$$\psi_f(t) = 2\pi f_e t + S \cos 2\pi f_m t \tag{29}$$

where f_e is the Sagnac frequency from the Earth's rotation. The modulation index S is the amplitude in radians of the phase excursion induced by the frequency modulation (equation (29)).

First we neglect backscatter-induced pulling for simplicity. The solution of equation (10) when $l = 0$ and with this time-dependent forcing is simply $\psi = \psi_f(t)$ (equation (29)). In this case the ring-laser signal has the form:

$$V(t) = 1 + \mathcal{R}e\{\exp i(2\pi f_e t + S \cos 2\pi f_m t)\}$$

$$= 1 + \mathcal{R}e\left\{ \exp(2\pi i f_e t)\left(\mathcal{J}_0(S) + 2\sum_{n=1}^{\infty} i^n \mathcal{J}_n(S) \cos(2\pi n f_m t) \right)\right\}$$

where $\mathcal{J}_n(z)$ is the Bessel function of order n, and so has (the same) Fourier coefficient $i^n \mathcal{J}_n(S)$ for the (upper and lower) nth sideband at the frequency $f_e \pm n f_m$, $n = 1, 2, \ldots, \infty$. This result tells us that with single-frequency dithering, there will be an infinite series of satellites above and below the earth line, separated in frequency precisely by f_m, infinitely sharp (dithering does not affect linewidths) and with amplitudes controlled by the Bessel function. The relationship between the phases $\phi_{\pm k} = \phi_c \pm 2\pi k f_m t + k\pi/2$, $\phi_c = 2\pi f_e t$, for the upper and lower sideband phasors and for the carrier is time-dependent, but the average of the sideband phases at order k is $\phi_c + k\pi/2$. Hence for FM the average phase for the first-order sidebands is displaced 90° from the carrier. For AM this average phase is that of the carrier.

When S is small, i.e. the total phase excursion associated with the modulation is much less than a radian, the leading term in the series expansion of the Bessel's function

$$\mathcal{J}_n(S) = \left(\frac{S}{2}\right)^n \left(\frac{1}{n!} - \left(\frac{S}{2}\right)^2 \frac{1}{(n+1)!} + \left(\frac{S}{2}\right)^4 \frac{1}{2(n+2)!} - \cdots \right)$$

defines a Poisson distribution for the relative heights of the various orders of sideband: $\mathcal{J}_n(S) = S^n/(2^n n!)$. To the lowest two orders we have

$$\mathcal{J}_0(S) \approx 1 - \tfrac{1}{4}S^2 \qquad \mathcal{J}_1 \approx S(8 - S^2)/16 \qquad \mathcal{J}_2 \approx S^2(12 - S^2)/96. \tag{30}$$

Hence the heights of the lowest-order sidebands are B dB below that of the carrier, where

$$B = 20 \log_{10}\left(\frac{\mathcal{J}_0(S)}{\mathcal{J}_1(S)} \right) \approx 20 \log_{10}\left(\frac{2}{S}\left(1 - \frac{1}{8}S^2\right)\right) \approx 6 - 20 \log_{10} S \tag{31}$$

while the carrier amplitude itself is reduced by $-20 \log_{10} \mathcal{J}_0(S) \approx 2S^2$ dB. (The dB level is here defined by $20 \log_{10}(V/V_0)$.) Hence a modulation index of $S = 2.0 \times 10^{-n}$ generates a sideband with a height which is $20n$ dB below the carrier.

When the sideband arises from direct modulation of the mechanical rotation, the modulation index, being the phase excursion of the Sagnac signal, is related to the imposed mechanical rotation amplitude by the scale factor $G = 2P/\lambda$, the number of half wavelengths (or standing wave antinodes) in the perimeter (section 1.3). (Standard gyro jargon in fact uses the number of counts per arcs, the number of beads of length $\lambda/2$ in the necklace formed by the standing light wave in an inertial frame (see sections 1.3 and 3.2) which pass any point for 1 arcs of rotation; 1 bead corresponds to one full 360° rotation of the Lissajou pattern and to 0.118 arcs.) Hence a sideband line B dB below the carrier calibrates the mechanical rotation amplitude in radians as

$$\psi_0 = 2 \times 10^{-B/20}/G. \tag{32}$$

This translates into a maximum change in the rotation rate of $\delta\Omega = 2\pi\psi_0 f_m$. As a fraction η of the rotation rate Ω_E associated with the carrier (taken here as the Earth's rotation rate, $7.292\,12 \times 10^{-5}$ rad s^{-1}), this relative rate has the form

$$\eta = \frac{\delta\Omega}{\Omega_E} = \frac{4\pi f_m}{G\Omega_E} 10^{-B/20}. \tag{33}$$

6.3. Modulation spectroscopy

In several of the strategies mentioned in section 9, the frequency of the Sagnac signal is directly field dependent and may be modulated by an applied field. Frequency modulation can also be applied in any other situation via (for example) the sensitivity of the plasma to the ambient magnetic field. This permits the use of modulation spectroscopy and phase-sensitive detection techniques to extract a signal buried in noise.

   As a rule of thumb, modulation spectroscopy is typically capable of extracting a signal with sideband frequency γ_{sig} buried in a line of width Γ (i.e. $\gamma_{\text{sig}} \ll \Gamma$) if the signal-to-noise ratio is better than $\Gamma/\gamma_{\text{sig}}$. In practice, the frequency of a resonator mode has been monitored to better than $10^{-4}\Gamma$ (Levine and Hall 1972).

6.4. Limitations on detectability of sidebands, and scaling rules

Modulation deliberately imposed for phase-sensitive detection purposes will use sufficiently high frequencies f_m and amplitudes f_e to ensure that the sideband is separated cleanly from its carrier in frequency and from the noise floor in amplitude. However, with such observables as microseisms and lunar tides, these two separations are not under the control of the experimenter, and indeed amount to the wished-for data.

   A sideband with frequency (relative to the carrier) of f_m hertz will require at the very least an observation time $T \gg 1/f_m$ for the line to be removed by several Nyquist frequency bins in the Fourier spectrum. The next questions are whether it would be hidden in the residual linewidth or the noise floor.

   For quantum shot noise limited lines (section 4), the width $w = 2hf_0^3/Q^2 P_o$ (equation (25)) and the shape may be taken as Gaussian (section 4.2). Hence the line strength at a sideband frequency f_m, $\exp(-f_m^2/(w^2 \ln 2))$, will be B dB below its centre height where

$$B = \frac{5}{\ln 10} \frac{f_m^2 Q^2 P_o}{hf_0^3}. \tag{34}$$

   For a mechanically imposed sideband to be at least as strong, we require from equations (33) and (34) that the fractional excursion in rotation rate η satisfy

$$\log_{10} \frac{2\pi f_m \lambda}{\eta \Omega_E P} \lesssim \frac{1}{4 \ln 10} \frac{f_m^2 Q^2 P_o}{hf_0^3} \tag{35}$$

as a requirement for a minimally detectable signal.

   The above equations ignore the statistical nature of the lineshape (see section 4.2). King *et al* (1996) point out the need to ensure that the fluctuations in a numerically produced spectrum are taken into account when a sideband line is in the wings of a quantum noise limited line, and suggest accumulating data from repeated runs as necessary to overcome this.

Another such requirement is that the sideband be visible above the noise floor, itself at say N' dB below the carrier. This gives:

$$\log_{10} \frac{2\pi f_m \lambda}{\eta \Omega_E P} \lesssim \frac{N'}{20}. \tag{36}$$

Despite the rather idealized model assumptions, these estimates are pessimistic, in that they take no cognisance of the power of correlation techniques to extract a periodic signal buried in noise, and so are more suited to (relatively transient) microseisms than (relatively periodic) lunar tides; but they will serve to set a scale in subsequent discussion.

Again scaling rules clearly favour large rings, in this case dramatically, because of the exponential if complicated dependence on the quality factor in equation (35).

6.5. Effect of backscatter

Because backscatter-induced pulling has a dominant effect on frequency drift, it is important to check whether backscatter has a deleterious effect on the simple theory of section 6.2, by adding the pulling (l-dependent) term to equation (10) of Aronowitz (1971) and equations (3.1) and (3.3) of Wilkinson (1987). An analysis of equations (10) and (28) to first order in S (Stedman *et al* 1995c) shows that the Fourier spectrum of the instantaneous phase is the convolution of the Fourier spectra of a numerator and denominator factor

$$N \equiv -p \sin(2\pi pt + \chi) \cos 2\pi f_m t - f_m \cos(\pi pt + \chi) \sin 2\pi f_m t \tag{37}$$

$$D \equiv f + l \sin(2\pi pt + \chi) \tag{38}$$

with definitions as in section 3.4. Since N contains only the pure frequencies $p, \pm f_m$, sharp first-order sidebands displaced by $\pm f_m$ are formed around the pulled Earth line and equally around all its harmonics. The same behaviour can be anticipated to higher orders in S. Hence the sideband frequency separations are not themselves pulled; they move bodily with the carrier under pulling. Nor does pulling itself induce any width to the sidebands. Hence even severe pulling on sideband frequencies may be ignored, at least in this model. However, the amplitudes of the sideband lines can be affected significantly (Stedman *et al* 1995c).

6.6. Estimates for C-I

If we are discussing modulation effects with frequencies above say millihertz, the linewidth in C-I is negligibly small, and it is equation (36) which furnishes most practical limitations. In experimental records from C-I, the noise floor can be $N'_0 \sim 65$ dB below the carrier. For example in C-I, mechanical oscillations with the amplitude of 1 μrad, 1 nrad, and 1 prad will yield sidebands which are 13 dB above, 47 dB below and 107 dB below the carrier, respectively. The first two, but not the last, will appear above the noise floor, which itself corresponds to a noise term in the mechanical angular frequency whose amplitude is of order 150 prad. It is worth noting (as for the Sagnac effect itself) that this measurement is nominally an absolute measurement; it gives the angular amplitude of the harmonic excursion directly and irrespective of the sideband frequency. Just as the Sagnac measurement gives absolute rotation rate, so absolute rotation magnitude information is enshrined in even the relative sideband amplitudes. However, pulling can affect the second of these as well as the first (section 6.5).

We have no formal theory of the value N'_0 quoted above. It is not a fundamental limit. There are no vibration isolators on C-I; the noise floor can change markedly from this; and an independent check of the amplitudes of supporting table resonances at 28–32 Hz show

that they depend on local traffic conditions and fluctuate on a sub-minute scale. Such a noise floor is also likely to be correlated with external long-range sources: global seismic waves, air-pressure fluctuations (which are known to be a major contribution to seismic noise in conventional seismometers with periods greater than a few seconds, Sorrells and Goforth (1973), Sorrells and Douze (1974)) and fluctuations in solar surface heating of the hillside above the cave environment, with consequential local tilt. The mechanisms include that of first tilting the device and thus generating a horizontal component of the acceleration, and simply mass buoyancy.

7. Geophysics from large ring lasers

7.1. Introduction

All applications considered here involve sub-hertz modulation of the Sagnac signal. In most cases the frequencies are sub-millihertz; in a few, frequencies correspond to a few microhertz. The timescales considered below therefore span a frequency region which for the greater part was previously inaccessible to laser spectroscopy, and which nevertheless covers many decades. As such they furnish some vivid illustrations of the different potential applications of the formalisms of the previous section.

The very thorough development of a laser strain meter of length 30 m for the detection of seismic events, in this case the 'Boxcar' nuclear explosion at the Nevada test site on 26 April 1968, with the laser situated in the Poorman's Relief Mine, Boulder County, CO, and also the detection of the Earth's tides (section 7.5), is documented by Levine and Hall (1972).

In the case of seismic effects (section 7.2), the frequency scales of interest include 0.05 Hz for intercontinental mantle (Love) waves having covered intercontinental distances, from major (magnitude 7) earthquakes. They also include 0.1–0.5 Hz for the microseismic background motions from sea breakers. Down to these frequencies, quantum shot noise has a negligible effect and the noise floor of the device (itself partly seismic in origin) sets the sensitivity. Clearly each instrument will have its characteristic threshold and will be able to detect a corresponding proportion of seismic events.

In the case of lunar and solar Earth tides (section 7.5), the analysis shows that a typical relative rotation amplitude (equation (33)) is $\eta \sim 4 \times 10^{-8}$ (of the Earth's rotation). The modulation frequencies f_m (more than one, since there are diurnal, monthly and other effects in both lunar and solar tides) are also fixed, and are like sea tides dominated by a component at half the lunar day, or 25 μHz. These estimates meet the criterion of equation (36) (visibility above the noise floor) quite comfortably, but put the sideband in the wings of the main carrier line, whose width for relatively short runs can be expected to have a significant effect. For the present generation of ring-laser instruments the detection of these tides is a credible task.

7.2. Detection of seismic rotation

The rotational part of seismic motion, which may be defined in terms of the curl of the velocity field v:

$$\mathbf{\Omega} = \tfrac{1}{2}\mathbf{\nabla} \times \mathbf{v} \tag{39}$$

has some intrinsic interest. Its direct measurement has been difficult, since it has been a differential measurement; conventional seismometers invariably detect linear motion only

(Usher *et al* 1979, Riedesel *et al* 1990). The detection of rotational motion has been discussed by seismologists in several contexts (Smith and Kasahara 1969, Bouchon and Aki 1982, Nigbor 1994, Takeo and Ito 1997), the last of these contemplating an array of relatively cheap and insensitive rotation sensors near a fracture site to assist in the location of fault lines. The establishment of a network of rotation sensors to complement the existing networks of linear seismometers has been recommended (Aki and Richards 1980). Torsional seismometry is in principle complementary to linear seismometry, although we expect the same sources to activate both types of detector, given the regular conversion between linear and circular polarization at media boundaries. Because of this, and because of its differential nature, rotational measurements are even more dependent than linear seismometry on local conditions, including tunnelling effects, rock fracture zones, free surface reflections, etc. Hence, while a local measurement is less-closely related to large-scale tectonic effects, by the same token, the results could be of direct interest in assessing the exposure and vulnerability of a given site to rotational motion through local resonances, etc. While the linear components of motion from major seismic events are the most destructive, buildings are particularly vulnerable to rotational motion.

A ring laser is an ideal tool to complement linear seismometers in this manner. It is insensitive to linear acceleration (section 2.3). It can in principle discriminate between P and S waves, detecting only the latter, though local mode conversion will complicate this.

Stedman *et al* (1995c) presented a model of relevant rotational effects associated with SH waves. The theoretical model was restricted to an elementary analysis of the apparent rotation as true in-plane rotation. This should be generalized to include tilt effects.

We write equation (2) as

$$\delta f = \frac{4\mathbf{A} \cdot (\mathbf{\Omega}_E + \mathbf{\Omega})}{\lambda P} \tag{40}$$

where $\mathbf{\Omega}_E$ is the Earth's rotation rate, on which $\mathbf{\Omega}$ (equation (39)) is a perturbation.

The seismic motions may be adequately quantified for our purposes by a locally uniform and time-dependent strain tensor ε; $u_i(\mathbf{r}, t) = \varepsilon_{ij}(t)r_j$. Then seismic activity can affect δf only differentially, and in three ways.

First, it is a rotation sensor; δf depends on local fluctuations $\mathbf{\Omega}$ in rotation rate (we call this vorticity, as opposed to tilt, as in section 7.6). These relate to the antisymmetric parts of the strain tensor: $\Omega_x = \frac{1}{2}(\dot\varepsilon_{zy} - \dot\varepsilon_{yz})$, etc. It suggests that, apart from local mode conversions, a ring laser can discriminate between the longitudinal P waves and the transverse S waves, detecting only the latter, because only those velocity fields have a finite curl (equation (39)).

Secondly, if the ring is bonded at more than one point to the local terrain it is a strain gauge, the beat frequency varying with the ratio A/P of ring area to perimeter. Seismic motion (including the compressional waves) may alter A and P. However, even the large and heavy ring-laser systems considered here mechanically float on a flat table, with little friction in the support, so that local Earth strain, as opposed to rotation (above) or orientation (below), is poorly communicated. There is no intrinsic strain of the ring, as there is in lunar-tide theory (section 7.5).

Thirdly, the ring laser acts as a tiltmeter through its dependence on the projection $\hat{\mathbf{A}} \cdot \mathbf{\Omega}_E$ of the unit normal of the ring on the vector angular velocity of the Earth's rotation. For a horizontal ring at mid-latitudes the projection factor is optimally sensitive to perturbation, and in a horizontal ring-laser tiltmeter effect dominates in the detection of lunar and solar tidal effects, because gravitationally induced vorticity then does not affect δf (section 7.6). This component of a seismic signal in a ring laser will not diminish with frequency as rapidly as the other components. However, it will be shown elsewhere using an argument

similar to the scaling arguments of this paper that the ratio of tilt effects on the Sagnac frequency to rotation effects is of the order of the ratio of the frequencies of Earth rotation and the seismic wave, so that tilt as well as strain may safely be neglected. Rotations with the axis parallel to the area vector will not affect $\hat{A}$ or the projection $\hat{A} \cdot \mathbf{\Omega}_E$.

7.3. Magnitude of rotations from seismic waves

If $\mathbf{u}$ represents the local displacement field, the angular rotation vector is

$$\delta\mathbf{\Omega} = \frac{1}{2} \nabla \times \frac{\mathrm{d}\mathbf{u}}{\mathrm{d}t}.$$

From the theory of seismic waves (Ewing and Press 1956, Bullen and Bolt 1985, Bath 1979) S waves all have non-zero curl. We choose axes with z locally vertical, and consider first an S wave polarized in the y direction and propagating parallel to x:

$$\mathbf{u} = a\hat{\mathbf{y}} f(y, z) \sin \kappa (x - c_s t)$$

where c_s is the wave velocity, $\kappa = 2\pi f_m/c_s$ and is the wave vector and the functional form of f is determined by boundary conditions.

In the simplest case of a regular shear wave—a plane wave with constant f—the equivalent instantaneous rotation rate is readily seen to be

$$\delta\Omega = \tfrac{1}{2}u(t)c_s\kappa^2 \tag{41}$$

where u is the instantaneous amplitude. More complicated waves lead to similar formulae, with a different numerical coefficient, also of order unity.

Microseisms (both the 0.1–0.5 Hz approximately periodic waves from sea breakers, and the superimposed higher-frequency transients) are a constant background, readily detectable with standard instruments.

Intercontinental signals from earthquakes of magnitude 6–7 on the Richter scale travel in the mantle waveguide and magnitude 7 quakes are more pronounced than microseisms for intercontinental distances. The Love waves for example have horizontal polarization like SH waves but are waveguide trapped in say 30 km of crust (with speeds $c_s \sim 6.5$ km s^{-1}) so that the whole mantle responds quickly and rings like a bell. These waves induce a locally vertical component of angular rotation, detectable by a horizontal ring laser.

From equation (41), the effect is strongest for oscillations of highest wavevector, since the differential motion is then strongest. It is not so much a question of minimizing the radial distance from the epicentre, but of minimizing the wavelength as well. A wave sustained by waveguide action in the mantle can induce rotations which perhaps decay only linearly with distance, but which fall quadratically with frequency. The frequency dependence in equation (35) adds strongly to this fall, because the dominant effect is to require the sideband to stand out from the main line the closer it comes. In effect, one must have systems whose quantum shot noise widths are much less than the frequencies of interest. In equation (36), quantifying the need for the sideband to be visible above the noise floor, the situation is the opposite; one factor of frequency (from the definition of the modulation index) is cancelled in forming an estimate of signal height. A ring laser then has a response curve which, like many other seismic detectors, falls with frequency below say 1 Hz. However, by the same token its sensitivity increases with frequency above this level, and remains sensitive to all rotational frequencies up to the reciprocal cavity decay time, of order 100 kHz.

7.4. Seism detection in C-I

Combining equations (36) and (41) gives a practical limit on the detection of seismic rotation rates by C-I of $\delta\Omega_0 \sim 0.1 f_m$ nrad s^{-1}, and so a linear displacement amplitude of $u_0 \sim c\delta\Omega_0/(2\pi^2 f_m^2) \sim 30/f_m$ nm.

C-I is mounted on bedrock (volcanic basalt) in a cave 30 m underground and is therefore shielded from undue temperature fluctuations, and also from unduly localized seismic effects. It is, however, within the suburbs of a city, and is 5.8 km from the Pacific Ocean; microseismic noise in the range 0.1–0.5-Hz has the reasonably high linear motion amplitude of 4–10 μm, measured using a New Zealand standard EARSS seismometer. It is 131 km from the Pacific–Indian tectonic plate boundary, and its output can be compared with that from New Zealand's extensive seismic network (Adams 1979). The square design also makes it more sensitive to seismic effects.

As an example, for C-I a magnitude 3 earthquake at a distance of 40 km would generate a local displacement of amplitude 54 μm, and given a period of say 0.2 s and wave velocity c_s of 3.5 km s^{-1}, give an estimate for the induced rotation rate of $\delta\Omega = 1.5$ mrad s^{-1}, or 5 arcmin s^{-1}, well in excess of the appropriate limit $\delta\Omega_0$.

For a controlled test of sideband sensitivity, a synchronous motor with period 0.625 00 Hz mounted on a wall was attached via a thin elastic line (of length $\sim$ 3 m) to one corner of the granite table and in a tangential sense. Estimates of the applied torque, the modulus of rigidity of the support system, give the non-resonant amplitude of the angular excursion applied by the elastic band to be $\Psi = 2.0$ nrad, and the sideband is predicted to be 48 dB below the carrier. This is confirmed by observation (Stedman *et al* 1995c).

C-I certainly detected the Richter 6.3 Arthurs Pass–Coleridge seismic event of 18 June 1994. Figure 7 plots the instantaneous phase of the ring laser against the response of a seismograph 15 km away (McQueens Valley, MQZ) (Stedman *et al* 1995c).

Joint records have been taken with a conventional seismograph and C-I in the cavern site from late 1996. In particular, seismic data from a shallow magnitude 5.2 earthquake on 5 September 1996, located 90 km east of Kaikoura, and only 230 km from the ring site were recorded on both the ring laser and seismograph. This will be reported elsewhere. Microseismic activity is also currently becoming visible as sidebands in the region 0.1–0.5 Hz.

7.5. Lunar and solar tides: introduction

For brevity we refer in the following to lunar tides only, with the substantial but secondary component from solar tides being included in the numerical results reviewed here. The displacements associated with the tides in solid earth are substantially less than the metre or more characteristic of ocean tides at the shoreline, but are not negligible, and can be 30 cm (Wahr 1985). Their effects, highly conspicuous in satellite laser ranging, have been detected in several other ways, including fluid tiltmeters and also a high-quality laser strainmeter (Levine and Hall 1972); see section 7.1.

Such tides also affect large precision ring interferometers noticeably. Its effect in the CERN particle storage ring LEP came as a surprise. These effects arise from a 12-h modulation of the circumference of the LEP ring, itself 26.7 km, by about 1 mm, or a fraction 4×10^{-8}. They became noticeable as a modulation of beam energy of order 10 MeV, itself the source of the biggest component of error in the initially reported mass of the Z particle discovered in 1983 (Chown 1992, Arnaudon *et al* 1995).

The Earth's rotation is of paramount interest for understanding the system dynamics on

time scales from less than hours up to millenia (section 7.7). At the high-frequency end, the detection and measurement of the effect of free oscillations on the Earth's rotation would increase our understanding of these eigenmodes. Further examples are Earth tides in polar motion and the length of day, which contribute to our understanding of the rheology of the Earth's mantle, and further constrain our models. The Nearly Diurnal Free Wobble and the Chandler Wobble as well as other rotational eigenmodes due, for example, to the presence of the inner core are the concern of several research groups. Most theoretical questions related to such matters can be solved only on the basis of more precise observations.

The main limitation on ring-laser measurements (sections 5.5 and 7.7) will most likely be due to local effects. Yet, particularly in the context of space geodesy, the study of local effects is of increasing importance.

Tidally induced Sagnac effects have several origins. As the CERN experience shows, one may expect areal strain and perimeter variations, i.e. changes δA, δP in the scalar parameters A, P associated with ring geometry. If the ring is decoupled from its supports (as are C-I and C-II) these will be strongly dependent on the elastic constants of the ring material (Zerodur in these cases). If the effect of tidal distortions on A/P (and so equation (2)) is reasonably approximated by scaling one dimension, the changes in δA and δP will cancel in this ratio. Rautenberg *et al* (1997) have considered changes $\delta \hat{A}$ in the direction of the area vector of the lasing path (tilt), and the vorticity of the Earth's tidal deformations (local variations $\delta \Omega$ in the Earth's rotation rate Ω_E), the other factors which influence the observed Sagnac frequency of equation (2). At mid-latitudes the magnitude of the vorticity $\delta \Omega$ is of order $8 \times 10^{-8} \Omega_E$, but within the spherically symmetric Earth
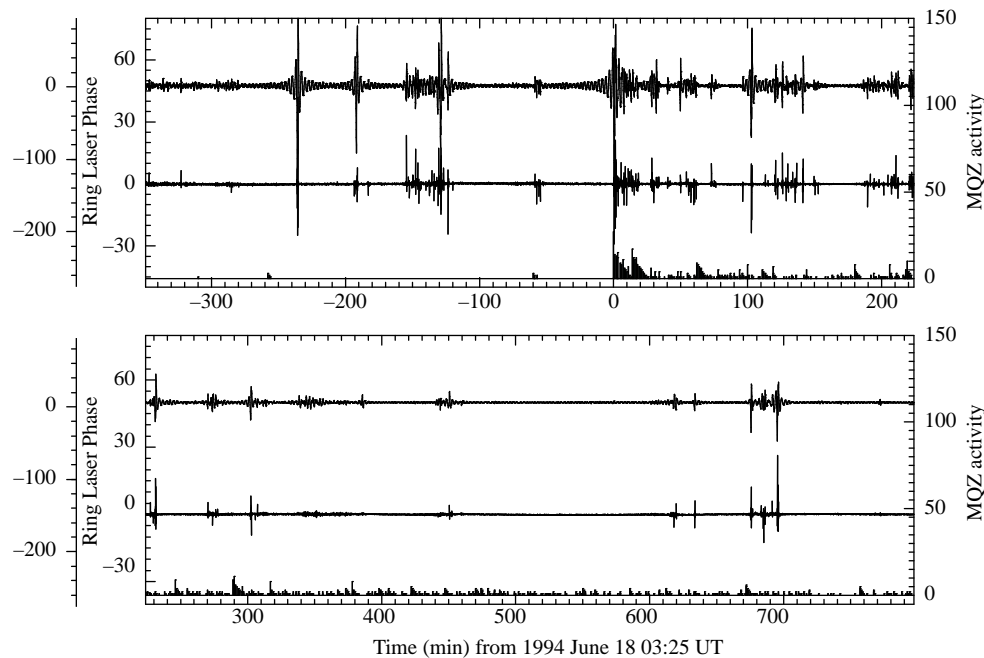

Figure 7. Comparative results from C-I and a standard seismograph during the Arthurs Pass–Coleridge seismic event of June 1994 (Stedman *et al* 1995c). The upper traces are from C-I with different dedrifting parameters. The lowest is a histogram indication of the activity on the standard seismograph.

model with its radially variable visco-elastic parameters, $\delta\mathbf{\Omega}$ is in the local horizontal plane. Hence it is not detectable by a horizontal ring such as C-I and C-II ($\mathbf{A} \cdot \mathbf{\Omega} = 0$). At mid-latitudes even in a horizontal ring the tilt effect gives a fractional change in the Sagnac beat frequency (which may, like the fractional change in the Earth's rotation of equation (33), be parametrized as η) of order 4×10^{-8}. In terms of FM generation of sidebands (see section 6.2), the modulation depth associated with lunar tides is $S = 0.035$ (King *et al* 1996).

This satisfies the constraint of equation (36) in C-I; the constraint of equation (35) is more problematical (King *et al* 1996). Direct cross-correlation techniques are likely to give much better results than Fourier analysis, giving reason for the hope of detecting lunar tides in C-II.

7.6. Extended theory of tidal effects

We summarize the analysis and results of Rautenberg *et al* (1997). In principle, deformations of the Earth's surface alter the local vertical and so the direction of the normal vector of the ring laser and hence the projection of $\mathbf{\Omega}$ on the ring area $\mathbf{A}_0 = A_0\mathbf{n}_0$. In addition, the vorticity of the deformations is superimposed on any Earth's rotation observation by a ring laser and appears as a disturbing signal to such measurements. Assuming for each of the quantities $\mathbf{\Omega}$, $\mathbf{n}_0$, A_0, and P a perturbation (e.g., $\mathbf{\Omega} = \mathbf{\Omega}_E + \delta\mathbf{\Omega}$), the relative variation in the beat frequency is given to first order by

$$\frac{\delta f_{\text{tide}}}{\delta f} = \delta f_\Omega + \delta f_n \tag{42}$$

$$\delta f_\Omega = \frac{\delta\mathbf{\Omega} \cdot \mathbf{n}_0}{\mathbf{\Omega}_E \cdot \mathbf{n}_0} \qquad \delta f_n = \frac{\mathbf{\Omega}_E \cdot \delta\mathbf{n}}{\mathbf{\Omega}_E \cdot \mathbf{n}_0}. \tag{43}$$

The vorticity term δf_Ω and tilt term δf_n may then be estimated using an appropriate model of Earth tides. A distortion field $\mathbf{u}(\mathbf{r}, t)$ of the Earth generates a first-order change $\delta\mathbf{A}_S$ in an area $\mathbf{A}_S = A_S\mathbf{n}_S$ at the Earth's surface or inside the Earth of

$$\delta\mathbf{A}_S = (\nabla \times \mathbf{u}) \times \mathbf{A}_S - \nabla \times (\mathbf{u} \times \mathbf{A}_S) \tag{44}$$

which may be decomposed into an areal variation $\delta A_S = A_S\mathbf{n}_S \cdot (\nabla \times (\mathbf{n}_S \times \mathbf{u}))$ and the variation of the normal vector $\delta\mathbf{n}_S = \mathbf{n}_S \times (\mathbf{n}_S \times \nabla(\mathbf{n}_S \cdot \mathbf{u}))$. A ring laser on the Earth's surface rotates according to the Earth's rotation and local vorticity and changes its normal according to the change in the normal vector of the Earth's surface. Thus, for a ring laser with normal $\mathbf{n}_0$ mounted on the Earth's surface with the local normal $\mathbf{n}_S$

$$\delta\mathbf{\Omega} = \tfrac{1}{2}\nabla \times \dot{\mathbf{u}} \qquad \delta\mathbf{n} = \mathbf{n}_0 \times (\mathbf{n}_S \times \nabla(\mathbf{n}_S \cdot \mathbf{u})). \tag{45}$$

δA is equal to δA_S only if the ring laser is perfectly coupled and parallel to the local Earth's surface.

Deformations of the Earth's surface are due to exogenic and endogenic causes. Endogenic deformations are generally small (of order mm yr^{-1} with rotations of order a degree per 10^6 yr) or episodic in time and local in space (e.g., earthquakes). Seismic oscillations have periods of less than 1 h and are not considered here. Exogenic deformations result from tidal forces and surface loading and traction, and on time scales of days to years, the primary exogenic deformations of the Earth's surface are due to the Earth's body tides and to tidal and non-tidal (oceanic, hydrological and atmospheric) loading. Tidal effects dominate at the level of $\geq 10^{-8}\Omega_E$; other geophysical sources of vorticity are at the level of 10^{-8}–$10^{-9}\Omega_E$ (Bilger 1984). Effects of the order of general relativistic corrections, such

as gravitomagnetic or frame-dragging effects which themselves have been considered for experimental study using ring lasers (Scully *et al* 1981), are of order $10^{-10}\Omega_E$.

The computation of exogenic deformations of the Earth due to, for example, tidal forcing or atmospheric loading are based on the momentum balance of an elastic or viscoelastic continuum, taking into account the gravitational effects of the deformations (Wilhelm 1986). For spherically symmetric, non-rotating, elastic, isotropic Earth models, the resulting equations of motion can be solved separately for spheroidal and toroidal forcing. The Earth's tidal potential described next is purely spheroidal and for spherically symmetric models results in purely spheroidal deformations. Similarly, surface loads produce spheroidal deformations, only. Toroidal deformations of spherically symmetric models are solely forced by the toroidal parts of the horizontal component of an external force, such as the stress due to winds or oceanic currents. For Earth-body tides, the coupling of spheriodal and toroidal solutions for laterally heterogeneous or rotating models are small however (Wang 1991). The following computation of $\delta\Omega$ and $\delta\boldsymbol{n}$ is based on Love numbers (Wilhelm 1986).

The tidal acceleration is written as the gradient of a scalar potential, called the tide generating potential (TGP) $\phi(\boldsymbol{r},t)$. This is expanded harmonically in partial tides: $\phi(\boldsymbol{r},t) = \sum_{mnk} \phi_{nmk}(\boldsymbol{r},t)$ (with $-n \leqslant m \leqslant n$). The labels are harmonic degrees n ($n \geqslant 2$) and orders m ($0 \leqslant m \leqslant n$), the latter indicating the tidal band of a partial tide ($0 =$ long period, $1 =$ diurnal, $2 =$ semidiurnal, etc), with each band having a large number of partial tides with slightly different frequencies. The kth partial tide of the (n,m) group is given by

$$\phi_{nmk}(\boldsymbol{r},t) = DC_{nmk}\left(\frac{r}{R_t}\right)^n Y_{nm}(\vartheta,\lambda)\exp\mathrm{i}(\omega_{nmk}t - \delta_{nmk}) \tag{46}$$

where the position $\boldsymbol{r}$ is given in geocentric spherical coordinates (radius r, colatitude ϑ, and longitude λ), D is the Doodson constant ($2.627\,713$ m^2 s^{-2}), R_t the radius of reference of the TGP model, C_{nmk} the amplitude, ω_{nmk} the circular frequency and δ_{nmk} the phase.

The response $\boldsymbol{u}(\boldsymbol{r},t) = \sum_{nmk} \boldsymbol{u}_{nmk}(\boldsymbol{r},t)$ of a spherically symmetric, non-rotating, elastic, isotropic Earth model with radius R_e to periodic forcing by partial tides may be expressed by the dimensionless, radius-dependent Love–Shida numbers $h_n(r)$ for radial and $\ell_n(r)$ for horizontal displacements (Wilhelm 1986) with

$$\boldsymbol{u}_{nmk}(\boldsymbol{r},t) = \frac{1}{g}[h_n(r)\boldsymbol{e}_r + \ell_n(r)\nabla_\circ]\phi_{nmk}(R_e,\vartheta,\lambda,t) \tag{47}$$

where g is the gravitational acceleration at the Earth's surface, $\boldsymbol{e}_r$ the radial unit vector, and $\nabla_\circ$ the spherical nabla operator (a tangential derivative), $\nabla_\circ \equiv r[\nabla - \boldsymbol{e}_r(\boldsymbol{e}_r \cdot \nabla)]$. Due to inertial forces, the Love–Shida numbers actually are frequency dependent, however, at tidal frequencies this dependence may be neglected. Hence

$$\nabla \times \boldsymbol{u}_{nmk}(\boldsymbol{r},t)|_{r=R_e} = \frac{2}{g}\frac{\ell_n - h_n}{R_e}\boldsymbol{e}_r \times \nabla_\circ\phi_{nmk}(R_e,\vartheta,\lambda,t) \tag{48}$$

where we have used the fact that the surface of the Earth remains free of horizontal stress for deformations due to body tide or surface loading, which leads to

$$\left.\frac{\mathrm{d}\ell_n}{\mathrm{d}r}\right|_{r=R_e} = \frac{\ell_n(R_e) - h_n(R_e)}{R_e}. \tag{49}$$

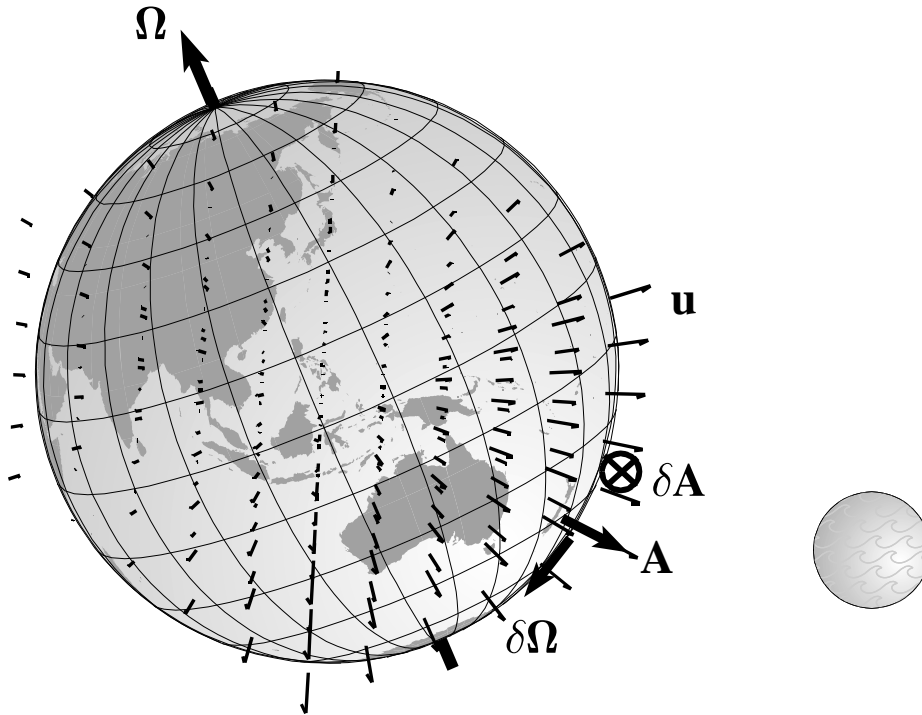**Figure 8.** Schematic of the effect of the Moon on solid Earth tides. An induced deformation field u is indicated; its curl gives a vector $\delta\Omega$ which has no projection on the area vector A of a locally horizontal ring in the model used here. However, the associated tilt δA in this area does have finite projection on the Earth's rotation vector Ω, leading to tidal signals in a horizontal ring laser.

As a result, the vorticity and the variation of the normal as given in equation (45) have the form

$$\delta\Omega = \frac{1}{g} \sum_{nmk} \frac{\ell_n - h_n}{R_e} e_r \times \nabla_\circ \dot{\phi}_{nmk} \tag{50}$$

$$\delta n = \frac{1}{g} \sum_{nmk} n_0 \times (n_S \times \nabla[h_n(n_S \cdot e_r) + \ell_n(n_S \cdot \nabla_\circ)]\phi_{nmk}. \tag{51}$$

As a consequence of the spheroidal forcing $\delta\Omega$ is perpendicular to e_r, therefore, a horizontal ring laser will not sense this signal. In a far-cruder model where detailed viscoelastic models were not included, u would be the gradient of the Newtonian potential, and its curl would vanish identically. Stresses in the present model avoid this extreme result, but the spheroidal symmetry (for example, ℓ_n and h_n depending on R_e only) forces the curl to be locally horizontal (figure 8). In the case of $n_0 \parallel \Omega$, the tilt term vanishes independent of n_S. On the other hand, δn is perpendicular to n_0 and a ring laser with a normal not aligned with Ω_E will be sensitive to tilt.

This surviving tilt term δf_n is proportional to δn (equation (51)). For a horizontal laser $(n_0 = n_S = e_r)$ at Christchurch, it is of order 4×10^{-8} and 4×10^{-9} for the semi-diurnal and diurnal tides, respectively, and of order 6×10^{-9} for the zonal tides ($m = 0$) mainly from the fortnightly tide Mf. Hence within this model a *horizontal* ring laser acts as a tiltmeter, detecting the effects of Earth tides on its attitude.

A ring laser mounted vertically with its area vector A parallel to e_ϑ would detect the vorticity signal given in figure 1 with maximal sensitivity, and it would also be sensitive to the tilt term. A tilted ring laser with *equatorial* mounting, $n_0 \parallel \Omega$, would be insensitive to the tilt term, and hence to the associated cavity effects. This would be the cleanest configuration for detecting the Earth's rotation fluctuation or tidal vorticity effect. It is under consideration for G.

7.7. Fluctuations of length of day

The tidal effects discussed in the preceding subsections discuss the direct induction of vorticity and tilt on a local scale, as if the rotating Earth were an unperturbed reference. However, in changing mass distributions, ocean and body (solid Earth) tidal effects change the inertia tensor. The rotation of the solid Earth therefore exhibits changes in the orientation of the axis, or polar motion, and angular speed, or length-of-day (LOD) fluctuations directly from lunar and solar tides. Dissipation makes the tidal distortions lag the Moon or Sun so as to create an asymmetry of the force that lengthens the day. Geographical inhomogeneities similarly give polar motion (Gross *et al* 1996). Annual changes in the atmospheric wind patterns also affect the moment of inertia of the Earth. Seismic events can perturb both LOD and polar motion (Chao *et al* 1996).

These effects are also typically a fraction 10^{-8}, i.e. up to tens of milliseconds in one day. Decade fluctuations and effects from the last ice age are among those measurable; Babylonian records of a total solar eclipse during 136 BC demonstrate an increase in the LOD over historic times whose integrated effect amounts to a change of $48.8°$ in longitude—the eclipse would otherwise have been visible near Marrakech, not Babylon (Morrison and Stephenson 1997).

The deformability of the Earth at this level, central to the previous subsections, clearly complicates the choice of reference system. The Earth's figure axis is arguably more relevant than its angular momentum axis to surface observations, and as of 1980 the International Astronomical Union's theory of nutation refers to the location of the celestial ephemeris pole—an axis which corresponds to neither of these axes exactly, but which shows no nearly diurnal motion—with respect to some rotating, body-fixed terrestrial reference frame (Gross 1992). Combinations of Earth orientation measurements are required (Gross 1996). Astrometric measurements especially those based on VLBI have proved very sensitive, determining angular positions to milliarcs. Laser ranging to the Moon and to the LAGEOS satellite have also assisted geodesic modelling by giving precision ranges (Wahr 1985).

However, there remains a significant dearth of information about short-period LOD variations. Ring lasers eventually may provide accurate determinations of geophysical rotations with high temporal resolution. This would have particular interest for the rotational dynamics of the Earth. Alternative techniques are space-geodetic methods, the most promising in terms of temporal resolution and accuracy being VLBI. Atmospheric angular momentum effects have been traced to periods as short as eight days (Freedman *et al* 1994). GPS measurements give sub-daily resolution, with periods down to 2 h (Lichten *et al* 1992). However, VLBI measurements take several days to process (section 5.5), and VLBI is a rather complex method requiring very considerable resources and international cooperation to achieve the highest possible accuracies. Also the VLBI community has sustained budget cuts particularly at NASA. To have an alternative technique with its own advantages and disadvantages would be an asset. It is at the short end of the spectrum of LOD variations that ring-laser measurements could contribute to relating the International Terrestrial Reference Frame to the Celestial Reference Frame, and so assist in the measurement of UT1 and

polar motion (Soffel *et al* 1986). The G proposal (section 5.5) is an outgrowth of these considerations.

7.8. Unusual applications

Rudenko and Kravchuk (1996) have considered the possibility that global seismic effects generated by gravitational waves in the range 0.01–0.1 Hz, commensurate with the fundamental frequencies of spheroidal Earth oscillations, might be detectable. Such waves from pulsars produce seismic effects about five orders of magnitude below natural seismic noise levels. The detection of gravity waves favours nearby binary stars; the frequencies are comparable. An experimental search showed that ground motion amplitudes were less than 10 pm.

8. Tests of relativity

Einstein's theory of gravity and in particular Einstein's equivalence principle incorporates the concept of a local inertial frame at any point. In such a frame, the results of special relativity are assured. In particular, clocks may be synchronized to give c as the speed of light regardless of direction. It follows that the Sagnac effect vanishes in a local inertial frame. The latter must then be something more than a free-fall frame; it has also to be non-rotating in some sense. In the absence of gravity this implies that a local Lorentz frame has no relative rotation (and only a uniform relative velocity) with respect to a resting frame, whose Machian definition is the frame with no linear or angular momentum relative to the (inertial) mass distribution of the universe. This Machian perspective is of little practical value in the sense that when components of the Universe have differential rotation, local inertial frames at different positions may themselves be in relative rotation as a result of the Lense–Thirring effect (section 8.1). The simplest definition of non-rotation in relativity is therefore the requirement of a null Sagnac effect. So in a relativistic formulation, the 'absolute' character of a Sagnac measurement of rotation rate gives direct insight into the local Lorentz frame, the frame with zero Sagnac effect. The Sagnac effect is the fundamental signature of the rotation rate relative to the local Lorentz frame in which special relativity— including the isotropy of the apparent speed of light—holds.

The precision with which non-inertial electromagnetic effects such as the Sagnac effect may be monitored raise the question as to what is learned about (as well as within) the theory of relativity from searches for (say) a diurnal component of the Sagnac signal.

Relativity can simplify a discussion. For example, a static gravitational field will not influence the ring-laser beat frequency (Kuriyagawa *et al* 1975). Another example is that the phase shift in the Sagnac effect is a relativistic invariant, but not a Newtonian invariant (Anandan 1981).

8.1. Frame dragging

Rotating matter drags the local inertial frames in the surrounding space in a sympathetic rotation. Ether-theoretic ideas led to some vigorous experimental searches near the turn of the century (Anderson *et al* 1994, Ciufolini and Wheeler 1995). However, Lense and Thirring (see Mashhoon *et al* 1984) gave a definitive if miniscule answer from general relativity. They showed that, near a sphere of moment of inertia I and angular frequency

Ω, and at a distance R from its centre, this had the magnitude

$$\Omega' = \frac{GI}{c^2 R^3}\left[\frac{3R}{R^2}(\Omega \cdot R) - \Omega\right]. \tag{52}$$

It has been dubbed frame dragging (a rotating ball in a viscous fluid stirs up eddies nearby, and short sticks in the fluid rotate sympathetically) and a particularly direct manifestation of a gravitomagnetic effect (a rotating magnet will couple to a neighbouring magnet). Such descriptions as a gravitational analogue of Larmor's theorem (Mashhoon 1993) and the gravitational analogue of the Aharonov–Bohm effect (Harris 1996) introduce more complexities than is often realized. The term goes back at least to Dowker (1967) and lends itself to a rich variety of interpretations.

As with any general relativistic effect associated with the Earth (for example the ratio of the mass of the Earth to that of a black hole with the same radius) the frequency ratio is of order $GM/c^2 \sim 10^{-10}$. Schleich and Scully (1984), quoting a review by Ginzburg, recount how, on an evening in 1918 when Thirring was telling Einstein about his work with Lense, Einstein complained that the effect was so small for the Moon: 'it is a pity that we don't have an earth-moon just moving outside of the Earth's atmosphere'. Nowadays we have many such moons, and much effort has been put into testing this prediction of general relativity.

At the start of the satellite era, in the early 1960s, Schiff and colleagues proposed the placing and self-monitoring of precise mechanical gyroscopes in Earth orbit in order to detect the frame-dragging effect. This was later developed as the Stanford Gyro Project, and more recently (following the many delays including the Challenger Space Shuttle disaster) as the Gravity Probe B experiment. Various complementary proposals have been made to study Lense–Thirring frame dragging. The Foucault effect on a pendulum at the South Pole has been proposed (Braginsky *et al* 1984), but is not yet practical (Pippard 1988). The spin dynamics of the LAGEOS satellites is being improved with the goal of performing this measurement (Habib *et al* 1994), as is the comparison of different LAGEOS satellites (Ciufolini *et al* 1996). Proposals are being developed for measuring the gravitomagnetic effect on the output of orbiting the 3-axis superconducting gravity gradiometers; see for example Chan *et al* (1987). Rosenblum and Treber (1988) have suggested that a clock stability of 1 part in 10^{18} over 2 years will permit the gravitomagnetic effect on the differential, Sagnac-compensated, synchronization gap in orbiting satellites ($\sim 6 \times 10^{-16}$ s), along with the geodetic effect, to be determined. Lunar laser ranging has detected the geodetic effect, if slightly indirectly (Williams *et al* 1996).

The first person to contemplate measurement of the gravitomagnetic field, or frame dragging, using a ring laser appears to be Dehnen (1967). He showed that optical consequences of frame dragging were visible in principle, but that the very small values involved made a ring laser the best tool for its measurement, calculating a fractional beat frequency shift of 7.2×10^{-23} at a latitude of $45°$ for a square ring with area 0.01 m². A considerably greater area (50 m²) was considered by Scully *et al* (1981) for a similar experiment in which, could the laser be constructed, the signal would be more easily detected, though such a laser would more easily limit the preferred-frame parameter α of the PPN formalism. Soffel *et al* (1986) (see also Soffel 1989) have promoted Sagnac devices for measuring geodetic and Lense–Thirring precession. Schleich (1991) has considered the value of reducing quantum noise limits for Sagnac interferometric tests for preferred frame effects.

8.2. *Tests of local Lorentz invariance*

Several different strategies have been proposed for testing for possible deviations from general and from special relativity. All metric theories of gravity are based on the Einstein equivalence principle, which assumes both the weak equivalence principle and local Lorentz invariance. A metric theory possesses a symmetric, locally Lorentzian metric, with test particles following geodesics of that metric and with non-gravitational laws of physics being those of special relativity in local Lorentz frames.

Another structure is needed to impart the full character of the corresponding space-time. Tests which honour special relativity (or local Lorentz invariance) within an alternative to general relativity (or Einstein's theory of gravity), are often performed in the context of the well established PPN framework of metric-test theories (Misner *et al* 1973, Will 1992). In this, just such other structural features, e.g. a revised role of the stress-energy tensor, different constants for the bending of space-time by matter and their possible dependence on a preferred frame, are used. In testing local Lorentz invariance, we are discussing a more radical departure in which preferred-frame effects may show up even within non-gravitational experiments and which therefore require a non-metric theory.

A given test of local Lorentz invariance often limits a particular kind of violation, and has a dual nature characteristic of the test, making an experiment of unique interest. For example, Bell and Damour (1996) cite tests in binary pulsars of the PPN parameter α_3 which parametrizes violation of momentum conservation as well as the existence of a preferred frame; in bounding α_3 below parts in 10^{-20} theirs is one of the most precise null experiments in physics, far beyond the accuracy being considered in section 8.3. Berglund *et al* (1995) discuss literature in which a preferred metric may affect the form of the weak interaction. In their case the possible coupling between magnetic field and particle momentum (expressed in a preferred-frame basis) is considered as it affects the precessional frequency of atoms in a magnetometer. The proposal discussed in section 8.3 has been of interest only in so far as it gives a different perspective on the manner in which local Lorentz invariance may be violated.

The most prominent tests of local Lorentz invariance are those in the tradition of, for example, Gabriel and Haugan (1990), Chupp *et al* (1989), Audretsch *et al* (1993), Haugan and Kauffmann (1995). Until recently (e.g. Phillips 1987, Lamoreaux *et al* 1986) such experiments were cited as testing the isotropy of space, by which was meant testing for a preferred-frame directionality on atomic properties. This has now been more helpfully re-presented as testing local Lorentz invariance.

The strategy currently employed now has only a small choice of procedures. Either the Lagrangian is adapted, or a preferred-frame metric (or generic distance measurement) is proposed, on the basis of some non-metric test theory whose parameters enter the problem through this choice of dynamics or reference space. A fundamental equation of atomic physics such as the Dirac equation, written in a covariant formulation, is then solved using this Lagrangian and/or metric. The parameters of the test theory appear in its observables and therefore can be bounded by experiment.

By now, there are several choices of test theories to some extent chosen or adapted with an eye to the nature of the experimental test in hand. The TH$\epsilon\mu$ theory postulates that the limiting speed of matter is not that of light, and adapts the material Lagrangian accordingly. Gabriel and Haugan (1990) and Haugan and Kauffmann (1995) give a mature discussion as to how Moffat's non-symmetric gravitation theory is a member of Ni's non-metric $\chi-g$ family of theories in which gravitational effects make space optically birefringent.

Tests of the principle of equivalence essentially require a non-metric theory as a test

theory. For example, Opat and Unruh (1991) suggest the comparison of atomic clocks at sea level at different latitudes; this compares the effect of gravity on clock atoms and seawater to 1 part in 10^{18}. They suggest that a search for solar and lunar modulation of the frequencies may also be worthwhile. Such an experiment seems basically electromagnetic; pulses from each clock are sent to the other, and the relative lag is monitored.

8.3. A preferred frame-test theory for a rotating observer

The Mansouri–Sexl test theory was formulated for inertial frames only. Generalizations by Abolghasem *et al* (1988, 1989) for the analysis of non-inertial observers merely applied a coordinate transformation for constant rotational (Earth) motion. Golestanian *et al* (1995) considered minimal deviations from the geometry of standard relativity.

We summarize the strategy of Vetharaniam and Stedman (1994) (amplified in the further analysis of Anderson *et al* 1997) for conducting a ring laser test of local Lorentz invariance for an accelerated observer with a more fundamental perspective. A geometrical foundation from which a family of coordinate transformations is derived, as opposed to simply being postulated. It proves to be complementary to the traditional approach in the Mansouri–Sexl formalism. The assumption of flat space-time is unnecessary, since the affine structure is quite adequate to include curvature. Beil (1995) quotes this as one illustration of non-metric-preserving transport, and shows how it is merely one class of a very much larger set of possible theories.

When special relativity is formulated on a four-dimensional manifold, its characteristic kinematics derives from the existence of two geometric structures on the manifold: an affine connection or law of vector transport corresponding in this case to a flat space-time, and a Lorentzian metric of signature $(1, 3)$ which is compatible with the connection and with invariance of the interval. If an affine connection is torsion-free, there always exist coordinates centred on any event such that at that event the connection coefficients (but not necessarily their derivatives) are all zero and then a $(1, 3)$ metric compatible with that connection is Lorentzian at that event. These properties hold, for example, for all PPN test theories for general relativity.

To test local Lorentz invariance, one must go outside the restrictions of such theories, removing structure which corresponds to local Lorentz invariance, and operate in a framework of more general theories. Since kinematical analysis requires the comparison of vectors propagated along curves, an affine structure is needed, and so it is natural rather to choose to remove the metric as a geometric structure in order to produce a test theory.

The omission of a metric as a geometric structure on the manifold is not in conflict with relativistic kinematics, nor is it a denial of the existence of a space-time metric. Rather, it allows the test theory to examine both those theories which have a metric and those which do not, with the aim that experimental tests be used to restrict these theories and to determine the validity of local Lorentz invariance at a given level of precision or confidence.

Vetharaniam and Stedman (1994) therefore proposed a family of test theories in which the general affine structure is restricted by postulating extra geometric structure (a preferred vector field) corresponding to a preferred frame. A natural candidate for the preferred frame is the cosmic background radiation. In a suitable axis choice, their postulate produces the following form for the transformation, from the preferred frame Σ with coordinates $(c\tau, \boldsymbol{\xi})$ to a frame S with coordinates $(ct, \boldsymbol{x})$:

$$\mathrm{d}t = a\frac{\mathrm{d}\tau - \mathrm{d}\boldsymbol{\xi} \cdot \boldsymbol{v}/c^2}{(1 + x\chi)(1 - v^2/c^2)} \tag{53}$$

$$\mathrm{d}\boldsymbol{x} - \boldsymbol{V}\,\mathrm{d}t = \left(\beta\frac{\mathrm{d}\boldsymbol{\xi}\cdot\boldsymbol{v}}{v^2} - \mathrm{d}\tau\right)\boldsymbol{v} + \delta\left(\frac{\boldsymbol{v}\times\mathrm{d}\boldsymbol{\xi}}{v^2}\right)\times\boldsymbol{v}. \tag{54}$$

The parameters include a (a time dilation parameter), β, δ (length contraction factors), and are functions of the relative velocity $\boldsymbol{v}$. χ is the observer's self-measured acceleration, and $\boldsymbol{V} = \boldsymbol{x}\times\boldsymbol{\Omega}$, the velocity of a point at $\boldsymbol{x}$ in S with respect to the instantaneously comoving non-rotating frame.

The one-way speed of light c_p (c in the preferred frame Σ) in a direction $\hat{\boldsymbol{p}}$ of frame S is then given by

$$\frac{c_p^2}{c^2}\left(1 + \frac{(\boldsymbol{p}\cdot\boldsymbol{v})^2 Q}{v^2}\right) - 2\frac{c_p}{c}\left(\frac{\boldsymbol{p}\cdot\boldsymbol{V}}{c} + \frac{(\boldsymbol{p}\cdot\boldsymbol{v})(\boldsymbol{V}\cdot\boldsymbol{v})Q}{cv^2}\right)$$
$$= \frac{(1 + x\chi)^2\delta^2}{a^2\gamma_v^2} - \frac{V^2}{c^2} - \frac{(\boldsymbol{V}\cdot\boldsymbol{v})^2 Q}{c^2 v^2} \tag{55}$$

where

$$\gamma_v^{-2} = 1 - v^2/c^2 \qquad Q \equiv \delta^2\gamma_v^2/\beta^2 - 1. \tag{56}$$

Within this test theory, an analysis of the Sagnac effect in a ring laser predicts sidereal, $\boldsymbol{v}$-dependent variations in the measured beat frequency. Following Scorgie (1990a), let c_+ and c_- be the (position- and direction-dependent) speed of light in each sense around the laser path. From equation (55) and Stokes' theorem the difference in transit time for the two directions $\delta t = \oint_C(1/c_+ - 1/c_-)\,\mathrm{d}l$ and has the form:

$$\delta t = \frac{2a^2\gamma_v^2}{\delta^2 c^2}\left[(2 + Q)\boldsymbol{\Omega}\cdot\boldsymbol{A} - Q\frac{(\boldsymbol{\Omega}\cdot\boldsymbol{v})(\boldsymbol{v}\cdot\boldsymbol{A})}{v^2}\right]. \tag{57}$$

When a, β and δ take on the special relativistic values ($1/\gamma_v$, γ_v and 1, respectively), $Q = 0$ and equation (57) reduces to equation (1).

The parameters a, β, and δ may be expanded in terms of v^2 (Mansouri and Sexl 1977); we note that this requires that we work within the Einstein synchrony choice, so that contrary to Mansouri and Sexl no one-way or first-order tests are possible. To second order $a = 1 + a_2 v^2/c^2$, $\beta = 1 + \beta_2 v^2/c^2$, $\delta = 1 + \delta_2 v^2/c^2$ (in special relativity $a_2 = -\frac{1}{2}$, $\beta_2 = \frac{1}{2}$, $\delta_2 = 0$). Hence

$$\delta t = 4\left[1 + \left[\frac{3}{2} + 2a_2 - \delta_2 - \beta_2\right]\frac{v^2}{c^2}\right]\frac{\boldsymbol{\Omega}\cdot\boldsymbol{A}}{c^2} - 4\left[\frac{1}{2} + \delta_2 - \beta_2\right]\frac{(\boldsymbol{\Omega}\cdot\boldsymbol{v})(\boldsymbol{v}\cdot\boldsymbol{A})}{c^4}. \tag{58}$$

When $v = 0$, this reduces again to equation (1). Let $\boldsymbol{v} = \boldsymbol{v}_0 + \delta\boldsymbol{v}$ where $\boldsymbol{v}_0$ is the velocity of the (centre of the) Earth with respect to the preferred frame defined by the cosmic microwave background (CMB) and $\delta\boldsymbol{v} = \boldsymbol{\Omega}\times\boldsymbol{R}$ and is that due to Earth's rotation relative to the centre of the Earth. $\boldsymbol{R}$ is the position of the ring laser relative to the centre of the Earth (figure 9).

The CMB dipole has parameters (Bennett *et al* 1994) $v_0/c = 1.22\times 10^{-3}$, a declination and right ascension of $\delta = -6.82\pm 0.12$, $\alpha = 167.52\pm 0.09 = 11^h.17$. This is on the boundary of the constellations Leo and Crater (the microwave photons seem hotter when coming from this direction), and approximately $10°$ S of the Ecliptic. The declination δ of the CMB as seen from Earth is the angle between $\boldsymbol{v}_0$ and the equatorial plane.

The term $Y_0 = (\boldsymbol{\Omega}\cdot\boldsymbol{v}_0)(\boldsymbol{v}_0\cdot\boldsymbol{A})$ in the numerator of the second term in equation (58) dominates. It has a diurnal variation in principle; the direction $\hat{\boldsymbol{A}}$ of $\boldsymbol{A}$ varies as the Earth rotates. This gives a beat frequency contribution $\delta f'$ which, relative to that surviving in special relativity, i.e. the Sagnac effect from Earth's rotation, has the form:

$$\eta_2 = \left[\frac{\delta f'}{\delta f_E}\right]_2 = -\left[\frac{1}{2} + \delta_2 - \beta_2\right]\frac{(\boldsymbol{v}_0\cdot\hat{\boldsymbol{\Omega}})(\boldsymbol{v}_0\cdot\hat{\boldsymbol{A}})}{c^2\sin\lambda}.$$
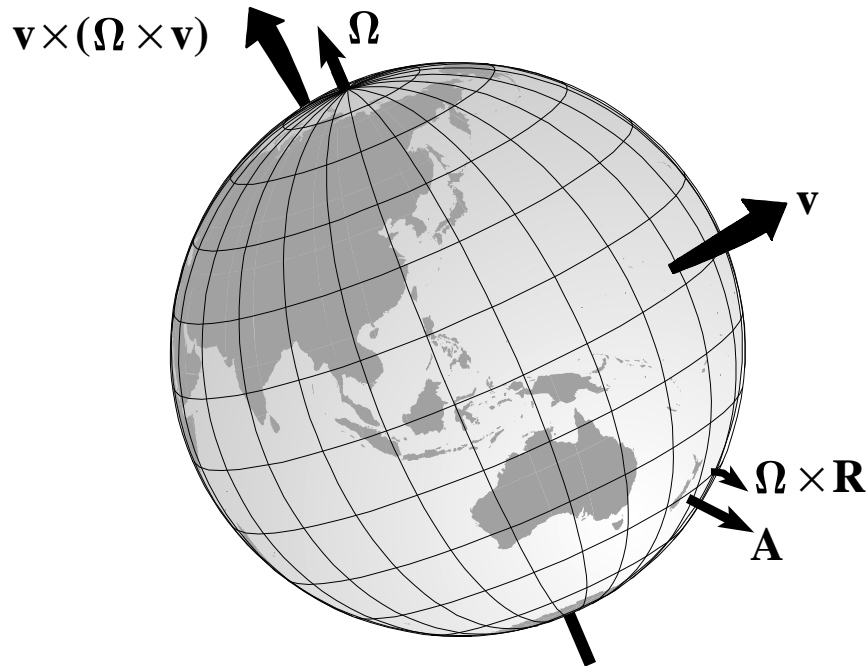
Figure 9. Schematic of the effect of the possible effect within a class of preferred-frame theories of an Earth velocity v relative to the cosmic microwave background on the ring laser signal. The observable is the projection of $v \times (\Omega \times v)$ on the area vector A, and this projection has a diurnal fluctuation.

This term is not, like others ignored here, limited by the rotation-induced speed $\delta v \leqslant$ 465 m s^{-1} of the Earth's surface at the ring-laser laboratory. Physically then, this term reflects an anistropy $\delta_2 - \beta_2$ of length contraction (parallel and perpendicular to the relative velocity) additional to that $(\delta_0 - \beta_0)$ defined by the Lorentz transformation, but formally permitted within this generalized Mansouri–Sexl test theory.

With a suitable choice of time origin $v_0 \cdot \hat{A} = v_0 \cos(\delta + \lambda) \cos \Omega t$, $v_0 \cdot \hat{\Omega} = v_0 \sin \delta$, and

$$\eta_2^{\text{max}} = \left[\frac{1}{2} + \delta_2 - \beta_2 \right] \left(\frac{v_0^2}{c^2} \right) \frac{\cos(\delta + \lambda) \sin \delta}{\sin \lambda} = 9.2 \times 10^{-8} \left[\frac{1}{2} + \delta_2 - \beta_2 \right].$$

The small size of the coefficient coupled with the attainable values of η, even with G, shows that if this application is regarded as a standard example of the Mansouri–Sexl methodology it is many orders of magnitude removed from fundamental interest. Other experiments (see Müller and Soffel 1995) have already determined $\delta_2 - \beta_2$ at the 10^{-9} level, and Robinson (1985) makes this even more precise in the light of studies of atomic or nuclear frequencies. The speed v_0 is unremarkable in that a sodium ion attains this speed under 28 kV, and as with seismic studies the ring laser is a differential device. This application is then merely a case study exploring the possible usefulness of ring lasers in relativity tests.

However, the requirement for a non-inertial frame in order to generate the Sagnac effect, including its possible preferred-frame dependence, might be regarded as giving a unique status to this application among other Mansouri–Sexl types of test. Its genesis, after all, is from a more fundamental perspective. An experimental check for diurnal variations with a period half the sidereal day and the appropriate phase relation to the CMB could be regarded

as a test of the development which leads to equation (55), with its relative novelty over the expression standard for Mansouri–Sexl theory in inertial frames (Müller and Soffel 1995).

8.4. Gravitational waves

All present and planned gravitational wave detectors search for the quadrupole distortion of space (or tidal forces) caused by a gravitational wave. Laser interferometric detectors search directly for this in a Michelson-like arrangement wherein the simultaneous shrinking of one arm, and expansion of the other, in an L-shaped interferometer is the observable. Incidentally, ring interferometers have been tested as part of the arsenal of optical processing and recycling devices so as to enhance the observed effect and to remove some systematic errors.

The order of magnitude sensitivities of these devices are approaching the strain level of sensitivity (10^{-22} or better) where one may expect to detect events on the timescale of a year or less. The requirements for a ring laser capable of sensing such strains was discussed by Scully *et al* (1981), with the suggestion that an area of order 50 m^2 would be needed. Equations (35) and (36) show that the techniques discussed here are many orders of magnitude removed from practicality even for ring lasers of this area. As mentioned in section 1.7, an orbiting ring laser (Chaboyer and Hendriksen 1988) has been proposed. The continuing development of ring lasers such as C-II and G will help refine such arguments.

Anandan and Chiao (1982) have considered the possibility of detecting gravitational waves by their associated Sagnac effect in a figure-eight-shaped ring interferometer. This detects the components R_{0xxz} of the Riemann tensor associated with the gravitational wave, whereas the conventional detectors detect the tidal components R_{0i0j}. Anandan and Chiao considered a superfluid detector, and now that this is a reality (see section 1.4) such matter interferometers may prove greatly superior. In the meantime the present advanced ring-laser technology still is competitive.

9. Tests of fundamental symmetries

9.1. General theory

This review has so far concentrated on the Sagnac effect *per se*—the effect of physical rotation (seismic, for example) relative to the local inertial frame on the phase shift in a ring interferometer and the frequency shift seen in a ring laser from interference between counterrotating beams. However, Sagnac interferometers can be, and have been, used to measure other physical effects than rotation.

The basic observable is the non-reciprocal part of the refractive index of the medium in the frame of the interferometer. It is this which differentiates the optical path lengths and so the cavity frequencies for the counterrotating beams. It follows directly that any contribution to this non-reciprocity, however caused (say by some magneto-optical or nonlinear optical effect), will contribute to the beat frequency in an active ring (or fringe shift in a passive ring). A Sagnac device therefore has a much greater potential than merely that of rotation measurement, important though that has been.

As is characteristic in physics, this potential is firmly targeted, in this case to the detection of violation of certain fundamental symmetries of physical theory. In standard geometries, a ring-laser beat frequency necessarily senses a time-reversal (T) violating effect, for which a rotational frequency is merely the obvious exemplar. For some less-usual geometries, the beat frequency denotes a parity-violating signal. Given the ultrahigh

sensitivity of a ring-laser gyro, one might hope for a considerable improvement in sensing time-reversal violation in nature by using a ring laser to reveal ultrasmall symmetry-violating effects.

As is often the case, the first mention of the idea is elusive. While a reasonably general theorem to this effect was enunciated recently (Stedman *et al* 1995a) several partial anticipations may be noted in the literature (Markelov *et al* 1977, Zhang *et al* 1992, Kapitulnik *et al* 1994, Weber *et al* 1994) and an early discussion of the capabilities of ring devices given by Alekseev *et al* (1976) includes a proof that the splitting of the resonant frequencies of beams with different helicity in a ring resonator is P-odd (anticipating the discussion of equations (62) and (63) below). T violation in high-T_c superconductors has already been tested using a fibre-optic gyroscope (Spielman *et al* 1990). Kapitulnik *et al* (1994) clearly connected the Sagnac interferometer with the breakdown of T symmetry. This allowed the measurement of magneto-optical effects and the search for T violation in high-temperature superconductors (Spielman *et al* 1990) and of Faraday and Kerr effects (Kapitulnik *et al* 1994) with a sensitivity of 2 μrad Hz$^{-1/2}$. Incidentally, the association of magneto-optical effects with the spin–orbit interaction is not universally applicable, and its over-emphasis has led to some claims that the spin–orbit interaction induces violation of T invariance, claims which are unjustified (Etchegoin *et al* 1994).

The links between T violation, the Sagnac effect and an associated Berry phase form a triangle of connections (Hendriks and Nienhuis 1990, Hasselbach and Nicklaus 1993, Ihm 1991, 1993).

The theorem (section 9.2) from Stedman *et al* (1995b) shows, amongst other things, that any supposed electric counterparts of these effects, being time even, can never give independent beat-frequency contributions in ring lasers with standard geometries. It has as a corollary that previous searches using ring lasers (see for example Elliott and Small 1984) for parity (P) violation in the electroweak interaction were doomed: such P-violating but T-even couplings as $\sigma_e \cdot p_e$ are invisible in such geometries, and must be detected otherwise (Alekseev *et al* 1976, Kriplovich 1993, Warrington *et al* 1995). Even if a segment of a ring in *s* polarization is bounded by $\lambda/4$ plates whose optic axes are crossed and at 45° to the *s* direction, any beat frequency induced by a specimen in this segment must involve T (and not necessarily TP) violation (Spielman *et al* 1990, Stedman and Bilger 1987). This makes ring-laser beat frequencies a sensitive discriminator of a wide variety of observables of interest in fundamental physics; see section 9.6.

While, as in conventional ring-laser gyroscopes, the spectral line referred to above is induced by the Sagnac effect of Earth's rotation, a ring laser is much more than a gyroscope. Its beat frequency detects any effect contributing differently to the average refractive index between CCW $(+)$ and CW $(-)$ beams (we write their polarizations as e_+, e_- respectively). We show that independent contributions to the beat frequency originate in a violation within the electronic and radiation subsystem of either time-reversal invariance or of both P and TP symmetry: only then can such a non-reciprocity in the relevant refractive indices arise. For example, a finite angular velocity Ω of rotation, and the finite beat frequency associated with its Sagnac effect, as a motional quantity is reversed with time. In a Hamiltonian formalism in the rotating frame, the Sagnac effect is associated with a T-odd angular momentum operator L in the Coriolis coupling $\Omega \cdot L$. Formally, it is the presence of this electronic and T-odd operator which is the signal of T violation within the quantum-mechanical theory of the electronic subsystem. If the theory possesses global T invariance, the associated operator— in this case Ω—for the remaining subsystem, such as the radiation field, is invariably also T-odd. Similarly magnetic effects in magnetic mirrors (Martin 1984) or the Zeeman laser (Statz *et al* 1985) also involve L or S, reverse with all motions, and induce a beat

frequency. Spin–orbit coupling has a T-even electronic operator $(S \cdot L)$, does not reverse with motions and does not itself induce a beat frequency. Such T signatures for electronic operators are known to generate important selection rules in solid-state and nonlinear optics (Naguleswaran and Stedman 1996).

9.2. Time-reversal and parity-violation theorem

The non-reciprocity in the optical path length $P_\pm = \int n_\pm \, \mathrm{d}x \ (\approx P)$ gives the beat frequency $\delta f / f_0 = (P_+ - P_-)/P$ which is non-zero if there is a term δn in the refractive indexes $n_\pm$ of the medium satisfying:

$$\delta n(e_+, k, e_-) = -\delta n(e_-, -k, e_+). \tag{59}$$

By an analogue of Lloyd's theorem, each term δn is either symmetric or—as above— antisymmetric (Stedman 1990b). The first arguments of δn (for example e_+, k) refer to the polarization and wavevector of the beam which experiences the refractive index change δn; the reference to the polarization of the other beam (for example e_-) allows for two-beam effects on this δn. Take the case that the counter-rotating beams have the same ellipticity:

$$e_+ = e_-^* \tag{60}$$

as for linear polarization in a plane ring (which naturally chooses s polarization), or when the left circularly polarized (LCP) CW, LCP-CCW modes are degenerate and are jointly split from the right-circularly polarized (RCP) CW, RCP-CCW modes. This condition is the reciprocity condition for conventional fibre interferometric gyros, and is essential for fibre ring-laser gyros, for example (Kim *et al* 1994). In this case we show equation (60) forces δn to originate in T violation.

It is helpful to note as illustrations the contrast between reciprocal and non-reciprocal polarization rotators. A reciprocal polarization rotator, namely a chiral or P violating material such as a naturally optically active system, is defined by having a refractive index contribution δn which depends on handedness: $\delta n(e, k) = \delta n(e^*, -k) \neq \delta n(e, -k)$. Such a system cannot satisfy equations (60) and (59). A non-reciprocal polarization rotator gives a refractive index change which depends on the polarization vector: $\delta n(e, k) = \delta n(e, -k) \neq \delta n(e^*, k)$, for example a Faraday cell. This may satisfy equations (60) and (59), and its optical properties originate in T violation such as a magnetic field. Purely electric effects, including standard pulling and pushing effects, only modify a pre-existing beat frequency. These well known cases illustrate the fact that T violation is equivalent to requiring a term in δn satisfying

$$\delta n(e_+, k, e_-) = -\delta n(e_+^*, -k, e_-^*) \tag{61}$$

itself essential for a beat frequency if equation (60) holds.

Within an extended golden rule approach (Stedman 1990b, 1993), applying T to all electronic states and operators which appear in the various matrix elements (contributing to any term in any refractive index change δn) gives simply an overall sign. The operators are each T-even or T-odd. Since T-conjugate states are degenerate, the state change gives merely a relabelling in the state summations. Since the interaction is globally T symmetric, this sign is identical to that obtained from applying T in the optical subsystem. The latter sign is found by time-reversing the optical states (an equivalent argument is implied by Halperin 1990), and therefore involves the operations $e \rightleftharpoons e^*$, $k \rightleftharpoons -k$ for each participating photon. Hence this sign is negative if and only if an odd number of external electronic interaction operators O are T-odd ($\bar{O}^\dagger = -O$). If, then, equation (60) holds, equations (59) and (61)

are identical, and a beat frequency can originate in a T-odd (but not a T-even) sequence of electronic interactions.

The alternative to this result, and to equation (60), arises when the modes have the same polarization vector but not the same handedness. The only instance we have found is that of a non-planar and P-violating ring geometry (Bilger *et al* 1990), when the LCP-CW and RCP-CCW modes are degenerate and split from the degenerate pair RCP-CW, LCP-CCW:

$$e_+ = e_- \neq e_-^*. \tag{62}$$

P violation similarly requires:

$$\delta n(e_+, k, e_-) = -\delta n(e_+, -k, e_-). \tag{63}$$

This yields equation (59) when equation (62) holds; conversely equations (59) and (62) imply equation (63) and so P violation. As noted in section 9.1, Alekseev *et al* (1976) obtained this result. TP symmetry would similarly enforce $\delta n(e_+, k, e_-) = \delta n(e_+^*, k, e_-^*)$, i.e. the degeneracy of LCP, RCP beams in each direction. Hence P and TP violation, but not T violation, is required and adequate. When neither equations (60) and (62), are satisfied, as in the multioscillator gyroscope (Statz *et al* 1985), both reciprocal and non-reciprocal polarization rotation occur, implying breakdown of both P and T invariance.

9.3. Tests of quantum field theory

The advantages of working with radiation in a vacuum for high-accuracy interferometry have been attractive for several workers. Iacopini and Zavattini (1979) and Ni *et al* (1991) have considered the possibility of making optical interferometric tests of quantum electrodynamics, and in particular the detection of photon–photon coupling via vacuum birefringence which with allied topics such as Delbruck scattering has been a Holy Grail for many experimental proposals. In laboratory conditions, the field-dependent changes in the refractive index of the vacuum are of order 10^{-21}. The experimental schemes use the properties that the birefringence will induce ellipticity in a linearly polarized laser beam (Iacopini and Zavattini 1979) or be detectable in a double (field and polarization) modulation experiment (Ni *et al* 1991). This level of precision is comparable with that for gravitational wave detection, where strain amplitudes of order 10^{-21} or less will also induce comparable changes in optical path length. These proposals assume fairly conventional interferometry, but with high-quality optics and with multipass interference so as to enhance the effect towards observability.

Originally the Oklahoma–Canterbury collaboration was stimulated to work on a ring-laser project as an essay into fundamental science, exploiting the great advances in supermirrors for pure scientific rather than military uses. This expectation began with the joint realisation that a ring interferometric system could have a unique significance and sensitivity for tests of relativity (Stedman 1973), and was fostered by an expectation that purely electromagnetic effects characteristic of some aspect of advanced quantum field theory might be uniquely detectable in a sufficiently sensitive ring laser. Considerable debate has followed, of which little has been reported, and the situation is still open-ended. Our initial optimistic reading of one proposal by Widom *et al* (1985) (with other such papers) was tempered when we found (Stedman and Bilger 1987) that the 'QED chiral anomaly' effects discussed were the effects of the Maxwell displacement current (and which incidentally respects parity, unlike the anomaly). It was further tempered by a proof by Ross and Stedman (1988) that CPT symmetry forbids vacuum optical activity from the supposed spin waves generated by the 'chiral anomaly' in the Dirac sea. There can be no

link between spin current and the chiral current which are vector and scalar respectively under rotations in space. However, it is conceivable, if not very credible, that the Ross and Stedman theorem could be invalidated by the novel effects of boundary conditions in Chern–Simons or quantum Hall systems in a Fadeev-type model.

Regardless of such fine-spun speculations, the interesting possibility that ring lasers amongst other devices could check for nonlinear optical properties of the vacuum with fields justifies as thorough an experimental study as possible. Although by particle physics standards the energies involved are unremarkable, the photon luminosities of such laser experiments are high, and may give such approaches special interest. For example, QED photon–photon coupling, and the Aharonov–Bohm effect for photons (Silverman 1991) all involve virtual particles and motivate a search for a beat frequency contribution when a magnetic field is applied to the beam path *in vacuo*. One collaboration (Bakalov *et al* 1994) has been concerned with detection by standard optical methods of nearly massless weakly interacting particles.

9.4. Limitations on resolution of refractive index and scaling rules

The emphasis in this section is on the detection of a non-reciprocal contribution to a refractive index δn in the medium forming part of a ring-laser optical path. If the sample length is L, which in all estimates we take to be 10% of the perimeter P, the resulting Sagnac frequency (Rosenthal 1962) in the absence of external rotation, and the equivalent angular rotation rate (from equation (2)), is

$$\delta f = \frac{Lf_0}{P}\delta n \qquad \delta\Omega = \frac{\lambda L f_0}{4A'}\delta n. \tag{64}$$

Equation (27) with $Q = FP/\lambda$ (section 1.6) then gives a quantum shot noise limit on the determination of a refractive index, of the form

$$\delta n_0 = \frac{\lambda}{LF}\sqrt{\frac{hf_0}{P_oT}}. \tag{65}$$

This is proportional to P^{-1} if the sample length L so scales, though against this (when ensuring single-mode excitation through gain starvation, section 5.3) possibly with smaller power losses P_o. δn changes markedly with finesse F, and with the C-I estimate of P_o equation (65) gives $\delta n_0 \sim 3 \times 10^{-12}/(PF\sqrt{T})$. For a cavity with mirrors of total loss 1 ppm ($F = 1.7 \times 10^6$) and run time 1 h, $\delta n_0 \sim 3 \times 10^{-20}/P$. The corresponding quantum shot limit on the phase shift is independent of L and is of the form $\delta\phi_0 = 2\pi L\delta n_0/\lambda \sim 4.6 \times 10^{-7}/(F\sqrt{T})$which for the above mirrors and run time gives $\delta\phi_0 \sim 4 \times 10^{-15}$ rad.

These figures are comparable with those for some alternative experimental techniques mentioned in section 9.3 (Iacopini and Zavattini 1979, Ni *et al* 1991). However, in order to detect QED vacuum birefringence, from the estimate $\delta n \sim 10^{-21}$ (section 9.3) and equation (64), a beat-frequency resolution of order 47 nHz is required, regardless of size. For a square ring this is a fraction $\eta \sim 1.6 \times 10^{-9}/P$ of δf_E, the Sagnac frequency of the Earth's rotation. This result suggests that larger rings, though possessing greatly enhanced frequency resolution, are not automatically better, unless the sample length L scales (by multipass, perhaps) more rapidly than perimeter P.

9.5. Axion detection

A ring-laser experiment to detect axion- and QED-induced vacuum birefringence was proposed by Cooper and Stedman (1995). It uses a slowly modulated magnetic field and a

novel polarization geometry. Both axion coupling and vacuum birefringence modulate the Sagnac beat frequency. A null result would bound the axion mass and two-photon coupling.

Originally introduced to explain the absence of CP violation in QCD (Peccei and Quinn 1977), axions have since become candidates for dark matter and have also arisen in supersymmetric and superstring theories. The axion, however, remains elusive: laboratory experiments and a host of astrophysical arguments (Kolb and Turner 1990, Raffelt 1996) constrain the axion mass to between 10^{-6} and 10^{-3} eV. A number of optical experiments, which exploit the coupling of axions to two photons via the triangle anomaly, have further constrained the axion mass and coupling to two photons (Lazarus *et al* 1992, Cameron *et al* 1993, Wuensch *et al* 1989, Hagmann *et al* 1990, 1996, Matsuki 1996). Cooper and Stedman (1995) adapted the ideas of Maiani *et al* (1986) to propose and examine the feasibility for a ring-laser experiment suitable for detecting axion-and QED-induced vacuum birefringence.

The connotation of CP violation (and therefore T violation) in axion physics suggests that a standard ring geometry should be appropriate. However, a different ring-laser polarization geometry which may well not be optimal will serve as an illustration of this approach. In this geometry, Faraday rotators whose optic axes are opposed in the direction of beam propagation, and whose rotation angle is $\theta = 45°$, are placed at each end of the sample section so as to rotate the linear polarizations of the counter-rotating beams, elsewhere identical, into perpendicularly polarized beams within the sample section. Note that this is neither the standard nor the alternative geometry of section 9.2, which clearly are far from exhaustive.

The coupling of axions to two photons via the triangle anomaly is described by the effective Lagrangian

$$\mathcal{L} = g_{\gamma\gamma a}(\boldsymbol{E} \cdot \boldsymbol{B}_{\text{ext}})a \tag{66}$$

where $\boldsymbol{E}$ is the electric-field vector of a laser beam propagating through an applied (static)
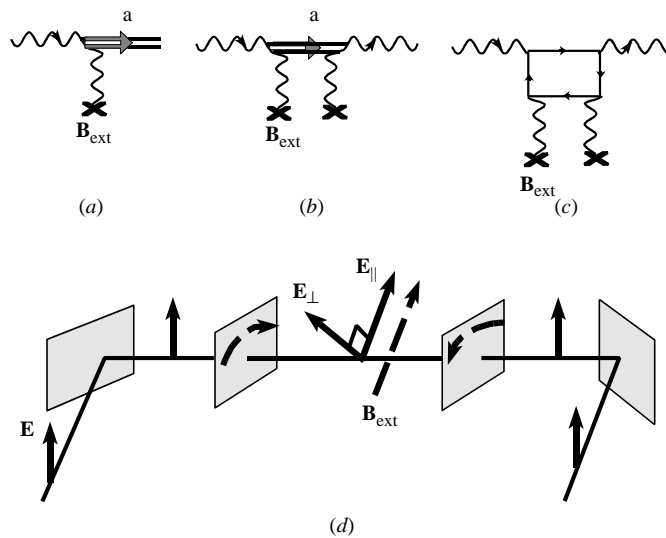

Figure 10. Possible axion-photon coupling in a ring laser (see Cooper and Stedman 1995). (*a*) The creation of axions from a laser photon and a near-static magnetic field. (*b*) Virtual production of axions. (*c*) Second-order coupling. (*d*) A possible polarization geometry which could be relevant to case (*b*).

magnetic field B_{ext}, a is the pseudoscalar axion field, and $g_{\gamma\gamma a}$ is the coupling constant. Virtual axions may be produced from the beam which has its electric field parallel to the imposed magnetic field (figure 10); the other beam is unaffected. The oscillation to a massive axion for part of its travel retards this beam compared with the orthogonal component. This magnetically induced birefringence between the two beams results in a difference δn in the refractive indices, measureable in good conditions down to the order of 10^{-14} rad (section 9.4). For photon energies $\hbar\omega < 2m_e c^2$, the birefringence between $E_{\parallel}$ and $E_{\perp}$ due to QED vacuum polarization is (Adler 1971):

$$\phi_{\text{QED}} = \frac{\alpha^2\hbar^2}{15c^7}\frac{B_{\text{ext}}^2}{m_e^4}\omega L \tag{67}$$

where m_e is the electron mass, α is the fine structure constant and L is the length of the beam path over which the magnetic field is applied. This gives $\phi_{\text{QED}}(0.1P) \sim 1.4 \times 10^{-17} P B_{\text{ext}}^2$. This estimate is significantly below the limit of 10^{-14} (equation (65)). In addition, the suggested geometry requires non-reciprocal optical devices (Krasinski and Pearson 1994); presently available TGG Faraday rotators have $\sim$99.9% transmission at 633.0 nm, and would impose a loss of order 1000 ppm, degrading the cavity quality factor by a factor of up to 500, and from equation (65) reducing sensitivity by more than two orders of magnitude. We shall suppose that these may be reconciled by the use of techniques not considered here, such as improved Faraday rotators, multipass geometry and modulation spectroscopy (section 6.3).

If the external magnetic field were modulated at low frequency, then the selective attenuation and retardation of one of the ring-laser beams will induce AM and FM sideband peaks to the Earth's-rotation-induced Sagnac beat frequency (section 6). The amplitude, phase and harmonic content of the sideband spectrum should give sufficient data to shed light on the mass, coupling and parity of the axion. The end result of a calculation on these lines (Cooper and Stedman 1995) is illustrated in figure 11, which gives bounds on the coupling constant as a function of axion mass for a 1 T magnetic field applied across a 10 cm section of the beam paths. The figure includes various experimental and theoretical bounds on the axion (see Cameron *et al* 1993). The shaded region indicates the results of the Brookhaven–Fermilab–Rochester (BFR) multipass cavity experiment, which searched for an axion-induced ellipticity and optical rotation in a laser beam propagating through a magnetic field. For $m_a < 10^{-3}$ eV, the BFR optical-rotation bound is an order-of-magnitude better than what could be achieved by a ring-laser experiment with the frequency resolution suggested above. This is despite the fact that the ring-laser experiment could detect phase shifts some four orders better than BFR, because the magnitude of the induced effects depend critically upon the external magnetic field and the measured rotation and ellipticity are cumulative upon reflection, allowing multiple passes of the beam. In the single-pass geometry considered here, the ring-laser beat frequency is determined by the non-reciprocal change in the optical path length for just one complete circuit of the ring. The ring laser would, however, perform better for relatively large axion masses.

A purpose-built ring-laser experiment (much in the style of C-II, section 5.4, but with the above special adaptation of the beams in the research-station area) to place sensitive new bounds on the axion, by searching for axions in the mass range 10^{-6}–10^{-3} eV which couple to two photons up to an effective energy of 2×10^7 GeV, is worthy of fuller consideration.
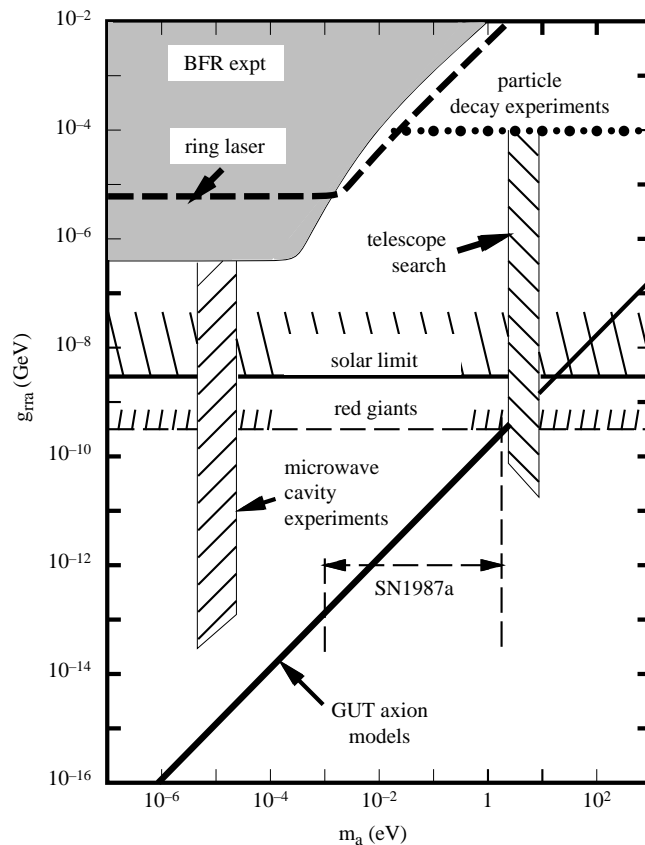
Figure 11. Comparison of some axion searches (see Cooper and Stedman 1995).

9.6. Testing fundamental symmetries

P-odd T-even, P-odd T-odd, and P-even T-odd effects have very different physical origins, and are differentiated in different ways in different experiments. For example parity non-conservation in atoms is a P-odd T-even effect, and electric dipole moments represent a P-odd T-odd effect (Kriplovich 1992); P-even T-odd effects may be seen directly by certain beats in oppositely cycled pumping of three-level systems, for example, and in certain polarization effects in the stimulated Raman effect (Sandars and Stephens 1996) as well as by the method discussed below. The NMR-induced frequency shift of a laser beam detects P-odd effects, whether T-even or T-odd (Sushkov 1993). For the bounds that already exist for such terms independently, see Conti and Kriplovich (1992) for the T-odd P-even case, and Barr (1992) and Baryshevsky and Baryshevsky (1994) for the T-odd P-odd case.

A quasi-Sagnac beat frequency in a ring laser with standard geometry detects T-odd effects only (section 9.2), and so the last two of these three cases. In particular, it would not detect parity non-conservation in atomic spectroscopy. However, the allowed detection of P-even T-odd terms such as $\mathbf{k} \cdot \mathbf{E}$ (Sandars 1987, Barr 1993) where $\mathbf{k}$ is a (T-odd) photon wavevector in a standard ring interferometer (or laser) has already been suggested by Kozlov and Porsev (1989) for a search for T violation in atomic physics. This has considerable interest; an experimental feasibility study with a fibre ring interferometer is being undertaken

at Clarendon Laboratory, Oxford, UK (Sandars and Stephens 1996). While the mechanism of parity violation in atomic spectroscopy is now well understood, the mechanism of time-reversal violation is not, though experiments with atoms and molecules have ruled out many theoretical models, and no good experimental limit currently exists for the magnitude of a T-violating term in the Hamiltonian proportional to $\boldsymbol{k} \cdot \boldsymbol{E}$. Kozlov and Porsev (1989) proposed a ring interferometer with the beam through a heavy-atom vapour (such as thallium) with an axial electric field. The optical density of the thallium vapour assumed in their work (a sample length L twice the absorption length) was chosen to maximize signal/noise in an interferometer, but are inappropriate for the quality factor of a laser cavity. In setting this density estimate, Kozlov and Porsev worked with a phase sensitivity $\delta\phi \sim 10^{-10}$ appropriate for such an interferometer. However, the estimated shot noise limit ($\delta\phi_0 \sim 4 \times 10^{-15}$ rad) of section 9.4 allows a proportionately lower optical density to be employed. This translates into an attenuation factor of $\exp(-10^{-4})$, or a fractional loss of 100 ppm. While this is two orders greater than present supermirror losses (section 1.6), and so would still have the dominant effect on cavity quality, it deserves consideration for an experimental design in which (as for axion searches) the advantages of modulation spectroscopy (section 6.3) could offset this.

10. Conclusions and prospects

Large ring lasers with correspondingly increased resolving powers have been a pipedream for decades, but have been widely dismissed as impractical, partly for reasons of mechanical instability. Indeed large ring interferometers have been a pipedream for a century (Anderson *et al* 1994). However, remarkably early on, significant progress was made by Michelson, Gale and Pearson in turning that pipedream into reality with their 1927-vintage yet practical 0.21 km^2 ring interferometer. Within the last two decades, very considerable progress has been made with the quality of mirrors, and in this decade some progress is being made with the construction of working devices whose dimensions and sensitivities are significantly scaled up from those of the standard aircraft gyro.

This has a wide variety of consequences, depending on the application, and the scaling arguments dispersed through this review will not be summarized here in detail. The geophysical applications seem to be the most promising, with the clear target of determining fluctuations in the real or apparent rotation rate of the Earth, however caused, at the level of 10^{-8} of the Earth's rotation rate. There is now a significant momentum in this as an international project, thanks to the instigation by the Institut für Angewandte Geodäsie, Frankfurt and Technische Universität München of the C-II project, with the ring laser installed in early 1997. By contrast, more fundamental tests of physics (relativity, CP violation, axion detection) seem more difficult, yet some are sufficiently close to feasibility as to be well worthy of a more full study than they have received till now.

I would like to encourage particle physicists and quantum field theorists to search for more ingenious ideas than the somewhat pedestrian ones explored in this review, ideas that undoubtedly await discovery and analysis. I would like to encourage experimeters to review the scaling and sensitivity constraints given here in the light of their experience of more sophisticated techniques in signal recovery. In this encouraging progress to the joint scaling up of ring-laser area and finesse, physics has acquired a new sensitivity for an old tool, in some applications by several orders of magnitude. This has helped to open up the sub-millihertz regime to laser spectroscopy. An old knife has been sharpened, and in effect a novel window on the world has been opened. Much of the present work is concerned to characterize large rings as potential tools, and while obvious geophysical applications

exist, justifying the present endeavour, their promise may be realised more fully when (as for experimental particle physics) these high-precision optical beams are employed within other (nonlinear, even non-classical) optical experimental techniques.

Acknowledgments

References

Abolghasem G H, Khadjehpoor M R H and Mansouri R 1988 *Phys. Lett.* A **132** 310–12
——1989 *J. Phys. A: Math. Gen.* **22** 1589–97
Adams R D 1979 *Phys. Earth Planet Interiors* **18** 114–20
Adler R 1973 *Proc. IEEE* **61** 1380–5
Adler S L 1971 *Ann. Phys.* **67** 599–647
Aki K and Richards P G 1980 *Quantitative Seismology Theory and Methods* (San Francisco, CA: Freeman)
Alekseev V A Ya, Zel'dovich B and Sobel'man I I 1976 *Sov. Phys.–Usp.* **19** 207–19
Allan D W, Weiss M A and Ashby N 1985 *Science* **228** 69–70
Anandan J 1981 *Phys. Rev.* D **24** 338–46
——1984 *Phys. Rev.* D **30** 1615–24
——1992 *Phys. Rev. Lett.* **68** 3809–10
Anandan J and Chiao R Y 1982 *Gen. Rel. Grav.* **14** 515–21
Anderson R, Bilger H R and Stedman G E 1994 *Am. J. Phys.* **62** 975–85
Anderson D Z, Chow W W, Scully M O and Sanders V E 1980 *Opt. Lett.* **5** 413–15
Anderson R and Stedman G E 1992 *Found. Phys. Lett.* **5** 199–220
——1994 *Found. Phys. Lett.* **7** 273–83
Anderson R, Vetharaniam I and Stedman G E 1997 *Phys. Rep.* to be published
Andrews D A and King T A 1996 *IEEE J. Quantum Electron.* **QE-32** 543–8
Aono O and Sugihara R 1987 *J. Phys. Soc. Japan* **56** 2004–6
Arif M, Kaiser H, Clothier R, Werner S A, Berliner R, Hamilton W A, Cimmino A and Klein A G 1988 *Physica* **151B** 63–7
Arif M, Kaiser H, Clothier R, Werner S A, Hamilton W A, Cimmino A and Klein A G 1989 *Phys. Rev.* A **39** 931–7
Arif M, Kaiser H, Werner S A, Cimmino A, Hamilton W A, Klein A G and Opat G I 1985 *Phys. Rev.* A **31** 1203–5

Arnaudon L *et al* 1995 *Nucl. Instrum. Methods Phys. Res.* A **357** 249

Aronowitz F 1971 *Laser Applications* vol 1, ed M Ross (New York: Academic) pp 133–200

Aronowitz F and Collins R J 1970 *J. Appl. Phys.* **41** 130–41

Ashby N and Shahid-Saless B 1990 *Phys. Rev.* D **42** 1118–22

Ashtekar A and Magnon A 1975 *J. Math. Phys.* **16** 341–4

Audretsch J, Bleyer U and Lämmerzahl C 1993 *Phys. Rev.* A **47** 4632–40

Avenel O, Hakonen P and Varoquaux E 1997 *Phys. Rev. Lett.* **78** 3602–6

Avenel O and Varoquaux E 1996 *Czech. J. Phys. Suppl.* **46** 3319–20

Bakalov D *et al* 1994 *Nucl. Phys. (Proc. Suppl.)* B **35** 180–2

Bambini A and Stenholm S 1984 *Opt. Commun.* **49** 269–74

Barr S M 1992 *Phys. Rev.* D **45** 4148–55

——1993 *Int. J. Mod. Phys.* A **8** 209–36

Baryshevsky V G and Baryshevsky D V 1994 *J. Phys. B: At. Mol. Opt. Phys.* **27** 4421–31

Bath M 1979 *Introduction to Seismology* 2nd edn (Basel: Birkhauser)

Beil R G 1995 *Found. Phys.* **25** 717–42

Bell J F and Damour T 1996 *Class. Quantum Grav.* **13** 3121–7

Bennett C L *et al* 1994 *Astrophys. J.* **436** 423–42

Berglund C J, Hunter L R, Krause D, Prigge E O, Ronfeldt M S and Lamoreaux S K 1995 *Phys. Rev. Lett.* **75** 1879–82

Bilger H R 1984 *Proc. SPIE* **487** 42–8

Bilger H R, Schreiber U and Stedman G E 1996 Design and application of large perimeter ring lasers *Symposium Gyro Technology (Stuttgart)* pp 0–24

Bilger H R, Stedman G E, Li Ziyuan Schreiber U, and Schneider M 1995 *IEEE Trans. Instrum. Meas.* **44** 468–70

Bilger H R, Stedman G E and Wells P V 1990 *Opt. Commun.* **80** 133–7

Bilger H R and Stowell W K 1977 *Phys. Rev.* A **16** 313–19

Bilger H R and Zavodny A T 1972 *Phys. Rev.* A **5** 591–9

Bilger H R, Wells P V and Stedman G E 1994 *Appl. Opt.* **33** 7390–6

Boivin L 1995 *Phys. Rev.* A **52** 754–66

Bonse U and Rumpf A 1986 *Phys. Rev. Lett.* **56** 2441–4

Bouchon M and Aki K 1982 *Bull. Seism. Soc. Am.* **72** 1727–38

Braginsky V B, Polnarev A G and Thorne K S 1984 *Phys. Rev. Lett.* **53** 863–6

Bretenaker F, Lepine B, Le Calvez A, Adam O, Taché J-P and Le Floch A 1993b *Phys. Rev.* A **47** 543–51

Bretenaker F, Taché J-P and Le Floch A 1993a *Europhys. Lett.* **21** 291–7

Bullen K E and Bolt B A 1985 *An Introduction to the Theory of Seismology* 4th edn (Cambridge: Cambridge University Press)

Cameron R *et al* 1993 *Phys. Rev.* D **47** 3707–25

Chaboyer B and Henriksen R N 1988 *Phys. Lett.* A **132** 391–8

Chan H A, Moody M V and Paik H J 1987 *Phys. Rev.* D **35** 3572–97

Chao B F, Gross R S and Hans Y-B 1996 *PAGEOPH* **146** 407–19

Chow W W, Gea-Banacloche J, Pedrotti L M, Sanders V E, Schleich W and Scully M O 1985 *Rev. Mod. Phys.* **57** 61–104

Chow W W, Hambenne J B, Hutchings T J, Sanders V E, Sargent M and Scully M O 1980 *IEEE J. Quantum Electron.* **QE-16** 918–36

Chown M 1992 *New Scientist* 5 December, p 8

Christian W R and Mandel L 1986 *Phys. Rev.* A **34** 3932–9

——1988 *J. Opt. Soc. Am.* B **7** 1406–11

Chupp T E, Hoare R J, Loveman R A, Oteizam E R, Richardson J M, Wagshul M E and Thompson A K 1989 *Phys. Rev. Lett.* **63** 1541–5

Ciufolini I, Lucchesi D, Vespe F and Mandiello A 1996 *Nuovo Cimento* A **109** 575–89

Ciufolini I and Wheeler J A 1995 *Gravitation and Inertia* (Princeton, NJ: Princeton University Press)

Clauser J F 1988 *Physica* **151B** 262–72

Conti R S and Kriplovich I B 1992 *Phys. Rev. Lett.* **68** 3262–5

Cook R J, Fearn H and Milonni P W 1995 *Am. J. Phys.* **63** 705–10

Cooper L and Stedman G E 1995 *Phys. Lett.* B **357** 464–8

Corum J F 1977 *J. Math. Phys.* **18** 770–6

——1980 *J. Math. Phys.* **21** 2360–4

Cresser J D 1982 *Phys. Rev.* A **26** 398–409

Cresser J D Hammonds D Louisell W H Meystre P and Risken H 1982b *Phys. Rev.* A **25** 2226–34

Cresser J D, Louisell W H, Meystre P, Schleich W and Scully M O 1982a *Phys. Rev.* A **25** 2214–25
Dehnen H 1967 *Z. Natforsch.* a **22** 816–21
Dennis M L and Diels J-C 1994 *Appl. Opt.* **33** 1659–72
Dieks D 1991a *Eur. J. Phys.* **12** 253–9
——1991b *Proc. 8th General Conf. of the European Physical Society (EPS-8 Trends in Physics)* part III, ed J Kaczér
	(Prague: Prometheus) pp 969–82
Dieks D and Nienhuis G 1990 *Am. J. Phys.* **58** 650–5
Doerr C R, Tamura K, Shirasaki M, Haus H A and Ippen E P 1994 *Appl. Opt.* **33** 8062–8
Dorschner T A, Haus H A, Holz I M, Smith I W and Statz H 1980 *IEEE J. Quantum Electron.* **QE-16** 1376–9
Dowker J S 1967 *Nuovo Cimento* **52** 129–35
Dresden M and Yang C N 1979 *Phys. Rev.* D **20** 1846–8
Eddington A S 1924 *The Mathematical Theory of Relativity* 2nd edn (Cambridge: Cambridge University Press)
Elliott C J and Small J G 1984 *Proc. SPIE* **487** 128–37
Etchegoin P, Fainstein A, Santos P, Lew Yan Voon L C, and Cardona M 1994 *Solid State Commun.* **92** 505–10
Etrich C, Mandel P, Centeno Neelen R, Spreeuw R J C and Woerdman J P 1992 *Phys. Rev.* A **46** 525–36
Ewing M and Press F 1956 *Surface Waves and Guided Waves (Encyclopaedia of Physics 47) (Geophysics I)* (Berlin:
	Springer) pp 119–39
Feynman R P 1989 *Surely You're Joking Mr Feynman!* (New York: Bantam Books)
Feynman R P, Leighton R B and Sands M L 1968 *The Feynman Lectures in Physics* vol 3 (Reading, MA:
	Addison-Wesley)
Fizeau A H L 1851 *Comptes Rendus* **33** 349–55
Forder P W 1984 *J. Phys. A: Math. Gen.* **17** 1343–55
——1985 *J. Phys. A: Math. Gen.* **18** 3343–50
——1986 *Class. Quantum Grav.* **3** 1125–31
Freedman A P, Steppe J A, Dickey J O, Eubanks T M and Sung L-Y 1994 *J. Geophys. Res.* **99** 6981–96
Fresnel A J 1818 *Ann. Chim. Phys.* **9** 57–66
Gabriel M D and Haugan M P 1990 *Phys. Rev.* D **41** 2943–55
Gea-Banacloche J 1987 *Phys. Rev.* A **35** 2518–22
Goldstein H 1950 *Classical Mechanics* (Reading, MA: Addison-Wesley) p 163
Golestanian R, Khajehpour M R H and Mansouri R 1995 *Class. Quantum Grav.* **12** 273–8
Grøn Ø 1975 *Am. J. Phys.* **43** 869–76
——1977 *Int. J. Theor. Phys.* **16** 603–14
——1979 *Found. Phys.* **9** 353–69
——1984 *Int. J. Theor. Phys.* **23** 441–8
Gross R S 1992 *Geophys. J. Int.* **109** 162–70
——1996 *J. Geophys. Res.* **101** 8729–40
Gross R S, Hamdan K H and Boggs D H 1996 *Geophys. Res. Lett.* **23** 1809–12
Gustavson T L, Bouyer P and Kasevich M A 1997 *Phys. Rev. Lett.* **78** 2046–9
Habib S, Holz D E, Kheyfets A, Matzner R A, Miller W A and Tolman B W 1994 *Phys. Rev.* D **50** 6068–79
Hafele J C and Keating R E 1972 *Science* **177** 166–8
Hagmann C *et al* 1996 *Nucl. Phys. (Proc. Suppl.)* B **51** 209–12
Hagmann C, Sikivie P, Sullivan N S and Tanner D B 1990 *Phys. Rev.* D **42** 1297–300
Hall J L 1993 *Proc. SPIE* 1837
Halperin B I 1990 *Proc. Int. Seminar on High Temperature Superconductivity (Dubna)* ed V L Aksenov,
	N M Plakida and Y Yu Yuschkhai (JINR) p 83
Hamilton J D 1981 *Can. J. Phys.* **59** 213–24
Hannam M D 1997 Spin-rotation coupling *MSc Thesis* University of Canterbury
Harris E G 1996 *Am. J. Phys.* **64** 378–84
Hasselbach F and Nicklaus M 1993 *Phys. Rev.* A **48** 143–51
Haugan M P and Kauffmann T F 1995 *Phys. Rev.* D **52** 3168–75
Haus H A 1995 *J. Opt. Soc. Am.* B **12** 2019–36
Haus H A, Bergman K and Lai Y 1991 *J. Opt. Soc. Am.* B **8** 1952–7
Haus H A, Statz H and Smith I W 1985 *IEEE J. Quantum Electron.* **QE-21** 78–85
Hecht J 1992 *Laser Focus World* November, p 99
Heer C V 1984 *Proc. SPIE* **487** 2–12
Hehl F W and Ni W-T 1990 *Phys. Rev.* D **42** 2045–8
Hendriks B H W and Nienhuis G 1990 *Quantum Opt.* **2** 13–21
Hestenes D 1990 *New Formulations for Classical Mechanics* (Dordrecht: Kluwer) p 489

Hirshfeld A C and Metzger F 1986 *Am. J. Phys.* **54** 550–2

Holton G 1969 *Isis* **60** 133–97

Horne M A, Zeilinger A, Klein A G and Opat G I 1983 *Phys. Rev.* A **28** 1–6

Iacopini E and Zavattini E 1979 *Phys. Lett.* **85B** 151–4

Ihm J 1991 *Phys. Rev. Lett.* **67** 251–4

——1993 *Int. J. Mod. Phys.* B **7** 2109–46

Jacob D, Vallet M, Bretenakaer F, le Floch A and Oger M 1995 *Opt. Lett.* 671–3

Kapitulnik A, Dodge J S and Fejer M M 1994 *J. Appl. Phys.* **75** 6872–7

Kersey A D and Burns V K 1993 *Photonics Spectra* **27** 72–6

Kichenassamy S and Krikorian R A 1994 *J. Math. Phys.* **35** 5728–33

Kim B Y and Shaw H J 1986 *IEEE Spectrum* 54–60

Kim S K, Kim H K and Kim B Y 1994 *Opt. Lett.* **19** 1810–12

King B T, Stedman G E and Bilger H R 1996 *OSA Technical Digest Series* (Washington, DC: Optical Society of America) p 181

Klein A G, Opat G I, Cimmino A, Zeilinger A, Treimer W and Gähler R 1981 *Phys. Rev. Lett.* **46** 1551–4

Knopf O 1920 *Ann. Phys. Vierte Folge* **62** 389–447

Kolb E W and Turner M S 1990 *The Early Universe* (Reading, MA: Addison-Wesley)

Konopsky V N 1996 *Opt. Commun.* **126** 236–9

Kowalski F V, Murray J and Head A C 1993a *Phys. Rev.* A **48** 1082–8

——1993b *Phys. Lett.* A **174** 190–5

Kozlov M G and Porsev S G 1989 *Phys. Lett.* A **142** 233–6

Krainov V A and Zharov K E 1996 *Proc. EGS General Assembly (The Hague, May 6–10)*

Krasinski J S and Pearson G W 1994 *Acta Phys. Polon.* A **86** 245–55

Kriplovich I B 1990 *Sov. Phys.–Usp.* **31** 558–60

——1993 *Phys. Scr.* T **46** 90–1

Kuriyagawa A, Ihara M and Mori S 1975 *Phys. Rev.* D **12** 2955–8

Kuriyagawa A and Mori S 1979 *Phys. Rev.* D **20** 1290–3

Lai M, Diels J-C and Dennis M L 1992 *Opt. Lett.* **17** 1535–7

Lalak Z, Pokorski S and Wess J 1995 *Phys. Lett.* B **355** 453–60

Lamoreaux S K, Jacobs J P, Heckel B R, Raab F J and Fortson E N 1986 *Phys. Rev. Lett.* **57** 3125–8

Landsberg P T 1961 *Nature* **189** 654

Landau L D and Liftshitz E M 1987 *The Classical Theory of Fields* (New York: Pergamon)

Laub J 1908 *Ann. Phys., Lpz.* **25** 175–84

Lazarus D M, Smith G C, Cameron R, Melissinos A C, Ruoso G, Semertzidis Y K and Nezrick F A 1992 *Phys. Rev. Lett.* **69** 2333

Lemon H B 1936 *Am. Phys Teacher* **4** 1–11

Lenef A, Hammond T D, Smith E T, Chapman M S, Rubenstein R A and Pritchard D E 1997 *Phys. Rev. Lett.* **78** 760–3

Levine J and Hall J L 1972 *J. Geophys. Res.* **77** 2595–609

Li Z, Bennett R G T and Stedman G E 1991 *Opt. Commun.* **86** 51–7

Lichten S M, Marcus S L and Dickey J O 1992 *Geophys. Res. Lett.* **19** 537–40

Ljubičić A and Logan B A 1992 *Phys. Lett.* A **172** 3–5

Lorentz H A 1895 *Versuch einer Theorie der Electrischen und Optischen Erscheinungen in Bewegten Körpern* (Brill: Leiden)

Macek W M, Schneider J R and Salamon R M 1964 *J. Appl. Phys.* **35** 2556–7

MacKenzie D 1993 *Technol. Culture* **34** 475–515

Maiani L, Petronzio R and Zavattini E 1986 *Phys. Lett.* **175B** 359–63

Mainwaring S R and Stedman G E 1993 *Phys. Rev.* A **47** 3611–20

Mansouri R and Sexl R U 1977 *Gen. Rel. Grav.* **8** 497–524

Markelov V A, Novikov M A and Turkin A A 1977 *Sov. Phys.—JETP Lett.* **25** 378–80

Marte M A M and Walls D F 1987 *J. Opt. Soc. Am.* B **4** 1849–52

Martin G J 1984 *Proc. SPIE* **487** 94–109

Martinez J C 1992 *Eur. J. Phys.* **13** 142–4

Mashhoon B 1993 *Phys. Lett.* A **173** 347–54

——1995 *Phys. Lett.* A **198** 9–12

Mashhoon B, Hehl F W and Theiss D S 1984 *Gen. Rel. Grav.* **16** 711–50

Matsuki S, Ogawa I, Nakamura S, Tada N, Yamamoto K and Masaike A 1996 *Nucl. Phys. (Proc. Suppl.)* B **51** 213

Michelson A A 1904 *Phil. Mag.* **8** 716–19

Michelson A A, Gale H G and Pearson F 1925 *Astrophys. J.* **61** 137–45

Michelson A A and Morley E W 1886 *Am. J. Sci.* **31** 377–86

——1887 *Am. J. Sci.* **34** 333–45

Misner C W, Thorne K S and Wheeler J A 1973 *Gravitation* (San Francisco, CA: Freeman)

Møller C 1972 *The Theory of Relativity* 2nd edn (Delhi: Clarendon)

Morrison L V and Stephenson F R 1997 *Contemp. Phys.* **38** 13–23

Müller J and Soffel MH 1995 *Phys. Lett.* A **198** 71–3

Naguleswaran S and Stedman G E 1996 *J. Phys. A: Math. Gen.* **29** 4027–40

Neutze R J 1995 *Phys. Rev.* A **51** 5039–42

Neutze R J and Hasselbach F 1997 in preparation

Neutze R J, Stedman G E and Bilger H R 1996 *J. Opt. Soc. Am.* B **13** 2065–74

Ni Wei-Tou, Tsubono K, Mio N, Narihara K, Chen S-C, King S-K and Pan S-S 1991 *Mod. Phys. Lett.* A **6** 3671–8

Nigbor R L 1994 *Bull. Seism. Soc. Am.* **84** 1665–9

Opat G I 1990 *Am. J. Phys.* **58** 1173–6

——1991 *Am. J. Phys.* **59** 822–3

——1995 *Advances in Quantum Phenomena (Nato ASI Series B Physics 347)* ed E G Beltrametti and J-M Levy-
    Leblond (New York: Plenum)

Opat G I and Unruh W G 1991 *Phys. Rev.* D **44** 3342–4

Orszag M and Retamal J C 1991 *Phys. Rev.* A **43** 6209–16

Papini G 1967 *Phys. Lett.* **24A** 32–3

Parks W F and Dowell J T 1974 *Phys. Rev.* A **9** 565–7

Peccei R D and Quinn H R 1977 *Phys. Rev. Lett.* **38** 1440–3

Percival I C and Strunz W T 1997 *Proc. R. Soc.* A **453** 431–46

Peres A 1978 *Phys. Rev.* D **18** 2173–4

Phillips P R 1987 *Phys. Rev. Lett.* **59** 1784–7

Pippard A B 1988 *Proc. R. Soc.* A **420** 81–91

Poirson J, Bretenaker F, Vallet M and Le Floch A 1996 Analytical and experimental study of ringing effects in a
    Fabry Perot cavity *J. Opt. Soc. Am.* B to be published

Polzik E S, Carri J and Kimble H J 1992 *Phys. Rev. Lett.* **68** 3020–3

Post E J 1967 *Rev. Mod. Phys.* **39** 475–93

——1972a *Ann. Phys., NY* **70** 507–15

——1972b *J. Opt. Soc. Am.* **62** 234–9

Prade B and Vinet J-Y 1988 *Nuovo Cimento* B **101** 323–31

Privatov V E and Filatov Yu V 1977 *Sov. J. Quantum Electron.* **7** 802–6

Raffelt G G 1996 *Stars as Laboratories for Fundamental Physics* (Chicago, IL: University of Chicago Press)

Ranganathan D 1992 *J. Mod. Opt.* **39** 1791–8

Rautenberg V, Plag H-P, Burns M, Stedman G E and Jüttner H-U 1997 *Geophys. Res. Lett.* **24** 893–6

Riedesel M A, Moore R D and Orcutt J A 1990 *Bull. Seism. Soc. Am.* **80** 1725–52

Riehle F, Kisters Th, Witte A, Helmcke J and Borde Ch J 1991 *Phys. Rev. Lett.* **67** 177–80

Rindler W 1972 *Essential Relativity: Special, General and Cosmological* 2nd edn (New York: Springer)

Robinson A L 1985 *Science* **229** 745

Rodloff R 1994 *Z. Flugwiss Weltraumforsch* **18** 2–15

——1987 *IEEE J. Quantum Electron.* **QE-23** 438–45

Rosenblum A and Treber M 1988 *Int. J. Theor. Phys.* **27** 921–4

Rosenthal A H 1962 *J. Opt. Soc. Am.* **52** 1143–8

Ross H J and Stedman G E 1988 *Phys. Lett.* **132A** 229–32

Rozanov N N 1970 *Opt Spectrosc.* **28** 398–400

Rudenko V N and Kravchuk V K 1996 *Gravitational Wave Background from Low Frequency Seismic Data*
    (Moscow: Sternberg Astr. Inst.)

Sagnac G 1913 *Comptes Rendus* **157** 708–10

——1914 *J. Physique* **4** 177–95

Sakurai J J 1980 *Phys. Rev.* D **21** 2993–4

Sandars P G H 1987 *Phys. Scr.* **36** 904–10

Sandars P G H and Stephens E C 1996 *J. Phys. B: At. Mol. Opt. Phys.* **29** 5597–606

Sanders G A and Ezekiel S 1988 *J. Opt. Soc. Am.* B **5** 674–8

Sargent M, Scully M O and Lamb W E 1974 *Laser Physics* (Reading, MA: Addison-Wesley)

Sayeh M R and Bilger H R 1985 *Phys. Rev. Lett.* **55** 700–2

Schlegel R 1973 *Nature* **242** 180

Schleich W 1991 *Phys. Bl.* **47** 595–601

Schleich W, Dobiasch P, Sanders V E and Scully M O 1984 *NATO Adv. Study Inst. Series B Physics* vol 135, ed G T Moore and M O Scully pp 385–408

Schleich W and Scully M O 1984 *New Trends in Atomic Physics (Les Houches Session XXXVIII)* ed G Grynberg and R Stora (Amsterdam: Elsevier)

——1988 *Phys. Rev.* A **37** 1261–9

Schleich W, Scully M O and von Garssen H-G 1988 *Phys. Rev.* A **37** 3010–17

Schulz-Dubois E O 1987 *IEEE J. Quantum Electron.* **QE-2** 299–305

Schwab K, Bruckner R and Packard R E 1997 *Nature* **386** 585–7

Schwider J 1992 *Appl. Opt.* **31** 6107–10

Scorgie G C 1990a *Eur. J. Phys.* **11** 142–8

——1990b *J. Phys. A: Math. Gen.* **23** 5169–84

——1991 *Eur. J. Phys.* **12** 64–5

——1993a *J. Phys. A: Math. Gen.* **26** 3291–9

——1993b *J. Phys. A: Math. Gen.* **26** 5181–4

Scully M O 1985 *Phys. Rev. Lett.* **55** 2802–5

——1987 *Phys. Rev.* A **35** 452–5

——1996 *Amazing Light* ed R Y Chiao (Heidelberg: Springer) p 573

Scully M O and Zubairy M S 1987 *Phys. Rev.* A **35** 752–8

Scully M O, Zubairy M S and Haugan M P 1981 *Phys. Rev.* A **24** 2009–16

Shankland R S 1974 *Phys. Today* **27** 36–43

Siegman A E, Daino B and Manes K R 1967 *IEEE J. Quantum Electron.* **QE-3** 180–9

Silberstein L 1921 *J. Opt. Soc. Am.* **5** 291–307

Silverman M P 1991 *Phys. Lett.* A **156** 131–3

——1992 *And Yet it Moves: Strange Systems and Subtle Questions in Physics* (Cambridge: Cambridge University Press) ch 5

Smith S W and Kasahara K 1969 *Bull. Earthquake Res. Inst.* **47** 831–48

Soares I D and Tiomno J 1996 *Phys. Rev.* D **54** 2808–13

Soffel M H 1989 *Relativity in Astrometry, Celestial Mechanics and Geodesy* (Berlin: Springer)

Soffel M H, Herold H, Ruder H and Schneider M 1986 Reference frames in relativistic space-time *Veröff d Bayer Komm f d Int. Erdm, Astron. Geod. Arb. (Munich)* **48** 237–70

Sorrells G G and Douze E J 1974 *J. Geophys. Res.* **79** 4908–17

Sorrells G G and Goforth T T 1973 *Bull. Seis. Soc. Am.* **63** 1583–601

Spielman S, Fesler K, Eom C B, Geballe T H, Fejer M M and Kapitulnik A 1990 *Phys. Rev. Lett.* **65** 123–6

Statz H, Dorschner T A, Holtz M and Smith I W 1985 *Laser Handbook* vol 4, ed M L Stitch and M Bass (Amsterdam: North-Holland) pp 229–332

Stedman G E 1973 *Am. J. Phys.* **41** 1300–2

——1985 *Contemp. Phys.* **26** 311–32

——1986 *Quantum Optics* vol IV, ed J D Harvey and D F Walls (Berlin Springer) pp 259–66

——1990a *Physics World* **3** 23–5

——1990b *Diagram Techniques in Group Theory* (Cambridge University Press Cambridge U K) Ch 7

——1993 *Modern Nonlinear Optics (Adv. Chem. Phys. 85)* ed S Kielich and M W Evans (New York: Wiley) pp 489–544

Stedman G E and Bilger H R 1987 *Phys. Lett.* **122A** 289–92

Stedman G E, Bilger H R, Li Z, Poulton M P, Rowe C H, Vetharaniam I and Wells P V 1993 *Aust. J. Phys.* **46** 87–101

Stedman G E, Johnsson M T, Li Z, Rowe C H, and Bilger H R 1995a *Opt. Lett.* **20** 324–6

Stedman G E, Li Z and Bilger H R 1995c *Appl. Opt.* **34** 7390–6

Stedman G E, Li Z, Rowe C H, McGregor A D and Bilger H R 1995b *Phys. Rev.* A **51** 4944–58

Sushkov O P 1993 *Phys. Scr.* T **46** 193–7

Taeko M and Ito H M What can be learned from rotational motions excited by earthquakes? *Geophys. J.* submitted

Telegdi V L 1990 Mind over matter the intellectual content of experimental physics *CERN Report* 90-09 Geneva

Tobin W and Pippard B 1994 *Interdiscipl Sci. Rev.* **19** 326–37

Tyler R H and Mysak L A 1995 *Can. J. Phys.* **73** 393–402

Usher M J, Burch R F and Guralp C 1979 *Phys. Earth Planet Interiors* **18** 38–50

van Eijkelenborg M A, Schrama C A and Woerdman J P 1995 *Opt. Commun.* **119** 97–103

Venema B J, Majumder P K, Lamoreaux S K, Heckel B R and Fortson E N 1992 *Phys. Rev. Lett.* **68** 135–8

Verdeyen J T 1995 *Laser Electronics* 3rd edn (Englewoods Cliffs, NJ: Prentice-Hall)

Vetharaniam I and Stedman G E 1993 *Phys. Lett.* A **183** 349–54

——1994 *Class. Quantum Grav.* **11** 1069–82

Wahr J 1985 *Am. Scientist* **73** 41

Walls D F and Milburn G J 1994 *Quantum Optics* (Berlin Springer)

Wang R 1991 *Tidal Deformations on a Rotating Spherically Asymmetric Visco-elastic and Laterally Heterogeneous Earth (European University Studies Series XVII Earth Sciences)* vol 5 (Frankfurt: Peter Lang)

Warrington R B, Lucas D M, Stacey D N and Thompson C D 1995 *Phys. Scr.* T **59** 424–8

Weber H-J, Burau A and Blechschmidt J 1994 *Phys. Rev.* B **49** 6991–7003

Werner S A 1994 *Class. Quantum Grav.* **11** A207–26

Werner S A, Staudenmann J-L and Colella R 1979 *Phys. Rev. Lett.* **42** 1103–6

Wilhelm H 1986 *J. Geodyn.* **59** 16–22

Wilkinson J R 1987 *Prog. Quantum Electron.* **11** 1–103

Widom A, Friedman M H, Srivastava Y and Feinberg A 1985 *Phys. Lett.* **108A** 377–8

Will C M 1992 *Theory and Experiment in Gravitational Physics* (Cambridge: Cambridge University Press) revised edition

Williams J G, Newhall X X and Dickey J O 1996 *Phys. Rev.* D **53** 6730–9

Winkler W, Rüdiger A, Schilling R, Strain K A and Danzmann K 1994 *Opt. Commun.* **112** 245–52

Woerdman J P, Nienhuis G and Kuscer I P 1992 *Opt. Commun.* **93** 135–44

Wuensch W U, DePanfilis-Wuensch S, Semertzidis Y K, Rogers J T, Melissinos A C, Halama H J, Moskowitz B E, Prodell A G, Fowler W B and Nezrick F A 1989 *Phys. Rev.* D **40** 3153–67

Zeeman P 1916 *Proc. R. Acad. Sci., Amsterdam* **18** 398–408

Zeeman P, de Groot W, Snethlage A and Diebetz G C 1920a *Proc. R. Acad. Sci., Amsterdam* **22** 462–70

——1920b *Proc. R. Acad. Sci., Amsterdam* **22** 512–22

——1922a *Proc. R. Acad. Sci., Amsterdam* **23** 1402–11

——1922b *Proc. R. Acad. Sci., Amsterdam* **24** 206–8

Zeeman P and Snethlage A 1920 *Proc. R. Acad. Sci., Amsterdam* **22** 512–22

Zernike F 1947 *Physica* **13** 279–88

Zhang J, Feng T, Zhang S and Jin G 1992 *Appl. Opt.* **31** 6459–62

Zimmerman J E and Mercereau J E 1965 *Phys. Rev. Lett.* **14** 887–90